A solution and solid state study of niobium complexes

by

Leandra Herbst

A dissertation submitted to meet the requirements for the degree of

Magister Scientiae

in the

Department of Chemistry
Faculty of Natural- and Agricultural Sciences

at the

University of the Free State

Supervisor: Prof. Andreas Roodt
Co-Supervisor: Prof. Hendrik G. Visser

January 2012

Acknowledgements

First and foremost, I thank God Almighty for the countless blessings he has given me.

Thank you to Prof. Roodt for all the opportunities, patience and endless enthusiasm for chemistry, inspiring me to learn as much as I can. It is truly an honour to be known as one of your students.

To Prof. Deon Visser, thank you for all your guidance and encouragement. Your neverending patience and willingness to give advice is what kept me motivated throughout my studies.

To Dr. Linette Bennie, thank you for your guidance with the niobium NMR throughout this project.

Thank you to all my colleagues in the Inorganic group for all the laughter and jokes. Thank you for sharing your knowledge and for your patience when having to explain something several times. Every one of you contributed to this study in some way and for that I thank you.

To my father, Lucas Herbst, my sister, Shané Herbst, and my grandmother, Nellie Grobler, without your love, support, faith, sacrifices, understanding and continuous encouragement this would not be possible.

Financial assistance from the Advanced Metals Initiative (AMI) of the Department of Science and Technology (DST) of South Africa, through The New Metals Development Network (NMDN) coordinated by the South African Nuclear Energy Corporation Limited (Necsa), and the University of the Free State are gratefully acknowledged.

Table of contents

Abbreviations and Symbols

Abbreviation	Meaning
thd^-	Tetramethylheptanedionate
acacH	Acetylacetone
phacacH	1-phenyl-1,3-butanedione
tBu_2(acacH)	Di-tertiarybutylacetylacetone
$ttbd^-$	1,1,1-trifluoro-4-thenoyl-2,4-butanedionate
hfacacH	Hexafluoroacetylacetone
tropH	Tropolone
dbm	Dibenzoylmethanato
IR	Infra red
UV/Vis	Ultraviolet/visible
NMR	Nuclear magnetic resonance
XRD	X-ray diffraction
Z	Number of formula units in a unit cell
A	Absorbance (theoretical)
*A*obs	Observed absorbance
(L,L')	Bidentate ligand
k_x	Rate constant for a forward equilibrium reaction
k_{-x}	Rate constant for a backward equilibrium reaction
K_x	Equilibrium constant for an equilibrium reaction
k_{obs}	Observed rate constant
ppm	(Unit of chemical shift) parts per million
DMF	Dimethyl formamide
THF	Tetrahydrofuran
C_6D_6	Deuterated benzene
CD_3OD	Deuterated methanol
v	IR stretching frequency
λ	UV/Vis wavelength
$\Delta H^{\neq}$	Enthalpy of activation
$\Delta S^{\neq}$	Entropy of activation
mg	Milligram
mmol	Millimol
M	$mol.dm^{-3}$

Abstract

This research project focused on the investigation and identification of various niobium(V) complexes containing selected O,O'-bidentate ligands that could potentially be used for the selective separation of niobium from tantalum. Emphasis was placed on acetylacetone (acacH) type of ligands due to the ease of varying their electronic and steric properties.

The crystallographic characterization of three novel complexes, (acetylacetonato-κ^2-O,O')chloridotrimethoxidoniobium(V) (**1**), the "cage"-like structure of tetrakis-(acetylacetonato-κ^2-O,O')octakis(etoxy)tetrakis(μ^2-oxo)tetraniobium(V) (**2**) and the two structures that were obtained from the same crystal, (1-phenyl-1,3-butanedionato-κ^2-O,O')chloridotrimethoxidoniobium(V) (**3a**) and (1-phenyl-1,3-butanedionato-κ^2-O,O')dichloridodimethoxidoniobium(V) (**3b**), is discussed and compared to literature. Complex **1** crystallized in an orthorhombic crystal system and space group *Pbca*, while complexes **2**, **3a** and **3b** all crystallized in a monoclinic crystal system and a space group $P2_1/c$, for all. In general it was observed that these mono substituted β-diketonato complexes of niobium(V) crystallized in a distorted octahedral coordination polyhedron. The average O-Nb-O bite angle and Nb-O bond distance for these complexes were determined as 80.5 (1) ° and 2.108 (2) Å, respectively.

A kinetic investigation was conducted to follow the formation of the (acetylacetonato-κ^2-O,O')chloridotrimethoxidoniobium(V) complex in methanol. The coordination mechanism is postulated for the two observed steps of acacH coordination, of which the initial coordination of the ligand takes place in the first step. The equilibrium constant, K_1, was determined as 1975 (201) M^{-1} at 25.0 ℃. The second, rate determining step is representative of the total reaction and includes the ring-closure of the acac ligand and yields K_1 as 1403 (379) M^{-1}. Within experimental error, this value is in good agreement with that of the first step. When comparing the rate constants, k_1 and k_2, it is found that the first reaction is roughly six orders of magnitude (10^6) faster than the slower, second reaction step.

Abstract

^{93}Nb NMR was successfully used in characterising the niobium(V) products synthesised and played an important role in the kinetic study of the project. With regards to the kinetic study; solvent coordination proceeded rapidly upon solvation of the dimeric starting material, $[NbCl_5]_2$, in methanol and the niobium(V) starting reagent was correctly determined as $[NbCl_2(OMe)_3(MeOH)]$ through ^{93}Nb NMR.

Opsomming

Hierdie navorsingsprojek fokus op die ondersoek en identifikasie van verskeie niobium(V)komplekse wat uitgesoekte O,O'-bidentateligande bevat wat moontlik gebruik kan word vir die selektiewe skeiding van niobium en tantalum. Klem is gelê op asetielasetoon (acacH) tipe ligande as gevolg van die maklike manier waarop hulle elektroniese en steriese eienskappe verander kan word.

Die kristallografiese karakterisering van drie nuwe komplekse, (asetielasetonato-κ^2-O,O')chloridotrimetoksidoniobium(V) (**1**), die "hok"-agtige struktuur tetrakis-(asetielasetonato-κ^2-O,O')oktakis(etoksi)tetrakis(μ^2-okso)tetraniobium(V) (**2**) en die twee strukture wat verkry is vanuit dieselfde kristal, (1-feniel-1,3-butaandionato-κ^2-O,O')chloridotrimetoksidoniobium(V) (**3a**) en (1-feniel-1,3-butaandionato-κ^2-O,O')di-chloridodimetoksidoniobium(V) (**3b**), word bespreek en vergelyk met literatuur. Kompleks **1** kristalliseer in `n ortorombiese kristalstelsel en ruimtegroep *Pbca*, terwyl komplekse **2**, **3a** en **3b** almal in `n monokliniese kristalstelsel en ruimtegroep $P2_1/c$, kristalliseer. Oor die algemeen is dit waargeneem dat hierdie mono-gesubstitueerde β-diketonato komplekse van niobium(V) in `n verwronge oktahedriese koördinasie polyheder kristalliseer. Die gemiddelde O-Nb-O bythoek en Nb-O bindingsafstand vir hierdie komplekse is onderskeidelik as 80.5 (1) ° en 2.108 (2) Å bepaal.

`n Kinetiese ondersoek is uitgevoer om die vorming van die (asetielasetonato-κ^2-O,O')chloridotrimetoksidoniobium(V)kompleks in methanol te volg. Die koördinasie-meganisme is gepostuleer vir die twee waargenome stappe van acacH koördinasie, waarvan die aanvanklike koördinasie van die ligand in die eerste stap plaasvind. Die ewewigskonstante, K_1, is as 1975 (201) M^{-1} teen 25.0 °C bepaal. Die tweede, tempo-bepalende stap is verteenwoordigend van die totale reaksie en sluit die ring-sluiting van die acac ligand in, en lewer K_1 as 1403 (379) M^{-1} op. Binne eksperimentele fout stem hierdie waarde goed ooreen met die waarde van die eerste stap. Wanneer die tempokonstantes, k_1 en k_2, vergelyk word is, gevind dat die eerste reaksie ongeveer ses ordegroottes (10^6) vinniger as die stadiger, tweede reaksie stap is.

Opsomming

^{93}Nb KMR is met sukses gebruik in die karakterisering van die bereide niobium(V) produkte en speel `n belangrike rol in die kinetiese studie van die projek. Met betrekking tot die kinetiese studie vind oplosmiddel-koördinasie vinnig plaas met oplossing van die dimeriese reagens, $[NbCl_5]_2$, in methanol en die niobium(V) reagens is korrek vasgestel as $[NbCl_2(OMe)_3(MeOH)]$ deur middel van ^{93}Nb KMR.

1. Introduction

Synopsis...

A brief introduction on the discovery of niobium is given. Focus is placed on the major contributors in the discovery and initial chemistry of the metal. The controversy surrounding the name of the metal is discussed. A proposal of the project aims are also included.

oooooooooooooo

1.1 History of Niobium

Niobium and tantalum were discovered early in the nineteenth century, barely a year apart, and since then great difficulty has been experienced in separating them. The chemical properties of niobium are very similar to those of tantalum, an element in the third row of the periodic table which completes the vanadium triad, and the two are always found together.

In 1801[1] Charles Hatchett, a British chemist, analysed a mineral he called columbite, after the location where it had been found near New London in Connecticut, North America. He described the mineral as "...a heavy black stone with golden streaks...". Charles Hatchett determined that the mineral contained tantalic, titanic and tungstic acids as well as thoria, zirconia, ceria and yttria and a new element that he named Columbium. The mineral sample was stored in the British Museum in London since 1753. It was acquired from the collection of John Winthrop, the first governor of Connecticut, who was a physician, an alchemist and a keen rock collector.[2]

Tantalum was discovered by Anders Gustaf Ekeberg in 1802. Both columbite and tantalite were analysed by William Hyde Wollaston, a British chemist, in 1809. He incorrectly concluded that columbium and tantalum were the same element. Wollaston was confused by the similar chemical and physical properties of the two

[1] P. Enghag, *Encyclopedia of the Elements: Technical Data, History, Processing, Applications*, Wiley and Sons, New York, 549, 2004.
[2] C. Hatchett, *Phil. Trans. Royal Society,* **92**, 49, 1802.

metals.[3] Due to Wollaston's influence, Hatchett's name for the new element was disregarded until 1844. In 1844 Heinrich Rose, a German chemist, distinguished the two elements by differences in their valence states. Tantalum only existed in the pentavalent state where columbium exhibited both the pentavalent and trivalent states. He changed Hatchett's name for the element from columbium to niobium; according to Greek mythology Niobe was the daughter of Tantalus, in recognizing the close relationship between the two elements.

Jean Charles Galissard de Marignac[4], a Swiss chemist, finally confirmed Rose's findings in 1864. He was the first to prepare the metal by reducing niobium pentachloride through heating it in a hydrogen atmosphere. He was able to produce tantalum-free niobium by 1866, when he developed a process for the separation of niobium from tantalum. He was also able to determine the atomic weights of both metals.

For about a century both the names columbium and niobium were used to describe the same element. In 1947 the International Union of Applied Chemistry (IUPAC) officially stated niobium as the name for the element. Some metallurgists and chemists however still use the name columbium.

1.2 The Aim of this Study

This MSc project is aimed at the investigation and identification of various niobium(V) complexes containing selected O,O'-bidentate ligands that could potentially be utilized for the selective separation of niobium from tantalum. If the relative niobium and tantalum complexes display differences in their chelating behaviour, either by solubility, density, coordination modes, etc., it could potentially be exploited as a new separation method for the two metals.

O,O'-bidentate ligands are selected due to their availability and the ease of varying their electronic and steric properties, and since niobium, being a hard metal centre, is known to prefer oxygen type of ligands.

[3] W. H. Wollaston, *Phil. Trans. Royal Society,* **99**, 246, 1809.
[4] M. Elvira, *Journal of Chemical Education,* **9**, 10, 1751, 1932.

The proposed aims for the study can be briefly summarized as follows:

1. The synthesis of niobium(V) complexes by coordinating it to different O,O'-bidentate ligands. Two ligands are proposed, exploring symmetric and non-symmetric coordination modes:

a **b**

Figure 1.1: Proposed O,O'-bidentate ligands for the study; (**a**) acetylacetone (acacH) and (**b**) 1-phenyl-1,3-butanedione (phacacH).

2. The characterization of new niobium complexes by utilizing their solid state and solution properties. Specific emphasis will be placed on X-Ray Crystallography as well as Infrared-, Ultraviolet/Visible- and Nuclear Magnetic Resonance Spectroscopy.

3. Determination of the nature of the niobium halido starting reagent, as solvent coordination proceeds rapidly in alcohol solutions to form the corresponding alkoxides. Different alkoxide species may form and it is essential to know which take part in the reaction, especially when studying the detailed reaction mechanism by time revealed spectroscopic kinetic studies. ^{93}Nb NMR will be used to identify the relevant species.

4. A mechanistic investigation of the formation of $[NbCl(acac)(OMe)_3]$.

5. Analysis of results and comparison with the corresponding tantalum study[5].

[5] R. Koen, *M.Sc Thesis*, University of the Free State, 2012.

2. Literature Review of Niobium

Synopsis...

Background information on the occurrence, properties and chemistry of niobium is briefly discussed. A more detailed review on the coordination of niobium to acetylacetone and its derivatives is also included.

oooooooooooooo

2.1 Introduction

Niobium and tantalum are always found associated with each other in their minerals and niobium is 10 to 12 times more abundant in the earth's crust than tantalum. It never occurs as the free metal and is usually combined with oxygen and other metals forming a niobate. Most niobium deposits occur as carbonatites (carbon-silicate rocks).[1] Primary niobium containing minerals can be divided into two groups; the tantalo- and titano-niobates.

Tantalo-niobates consist of tantalic and niobic acid salts. The general formula for this group is $(Fe,Mn)M_2O_6$ (M = Nb, Ta) and the mineral is known as niobate or tantalite, depending on which metal dominates.[2] These minerals consist of isomorphic mixtures of the four possible salts and generally contain tin, tungsten, titanium and other impurities.

Titano-niobates comprise of the salts of niobic and titanic acids. The most important mineral in this group is pyrochlore. The main sources of pyrochlore are from Brazil and Canada and the general formula for the mineral varies depending on the source. The general formula for a typical Brazilian pyrochlore is $(Na,Ca)_2M_2O_6$ (M = Nb, Ti) and for that of a Canadian one is $(Ba, Ca)_2M_2O_6$ (M = Nb, Ti, Ce).[3]

[1] C. W. Balke, *Ind. Eng. Chem.*, **27**, 1166, 1935.
[2] N. N. Greenwood, A. Earnshaw, *Chemistry of the Elements,* Butterworths/Heinemann, Oxford, 977, 1997.
[3] G. L. Miller, *Metallurgy of the Rarer Metals*, Butterworths Scientific Publications, London, **6**, 548, 1959.

Significant difficulty is experienced in the industrial separation of niobium and tantalum due to their similar chemical properties. The processes involved in the separation of the two metals are varied and complicated, and significant efforts to find methods which are both cost effective and deliver high purity products, have been made.

2.1.1 Properties of Niobium

Niobium is a steel-gray metal and when pure, it is a soft and ductile metal, but impurities usually have a hardening and embrittling effect. Some of the more important properties of niobium and tantalum (group V metals) are summarized in Table **2.1**. From the table it is apparent that there are a great number of similarities between the two metals. Niobium and tantalum are virtually identical in size as a consequence of the lanthanide contraction. The lanthanide contraction is the decrease in ionic radii of the elements in the lanthanide series from atomic number 58 to 71. This results in smaller than expected ionic radii for the subsequent elements, starting with an atomic number of 72 (hafnium). The effect results from poor shielding of nuclear charge by 4f electrons.

Table 2.1: Properties of niobium and tantalum.[4]

Property	Niobium	Tantalum
Atomic number	41	73
Natural occuring isotopes	1	2
Atomic weight [g/mol]	92.906	180.948
Electronegativity	1.6	1.5
Electronic configuration	$[Kr]4d^3 5s^2$	$[Xe]4f^{14}5d^3 6s^2$
Metal radius (12-coordinate) [pm]	146	146
Ionic radius (V) (6-coordinate) [pm]	64	64
Melting point [℃]	2468	2980
Boiling point [℃]	4758	5534
Density (20℃) [g/cm³]	8.57	16.65
Thermal-neutron-capture cross section [barns]	1.15	21

[4] F. A. Cotton, G. Wilkinson, C. A. Murillo, M. Bochmann, *Advanced Inorganic Chemistry,* Wiley and Sons, New York, **6**, 895, 1999.

Niobium resembles tantalum closely in its properties and it is slightly more reactive chemically. It has a lower electron work function than tantalum and is unreactive to most gases below 200 ℃. At 350 ℃ niobium is air o xidized, developing an oxide film. The adsorption of hydrogen occurs at 250 ℃ a nd that of nitrogen at 300 ℃. Niobium is attacked by gaseous hydrogen fluoride and fluorine at room temperature, but it is stable to mineral acids and aqua regia at ordinary temperatures, except hydrofluoric acid. Concentrated sulphuric and hydrochloric acid dissolve niobium at elevated temperatures (170 ℃) and hot alkali carbo nates and hydroxides causes embrittlement of niobium.[2]

At only 8.57 grams per cubic centimetre, niobium's density is just about half of that of tantalum making it one of the lightest of the refractory metals. It has a higher strength-to-weight ratio than titanium, nickel, zirconium and vanadium. This is an important industrial property where the weight is of concern.

Niobium and tantalum have formal oxidation states from +5 down to -3 and they display very little cationic behaviour. The most common oxidation state of niobium is +5. Metal-metal bonds are fairly common for oxidation states +2 and +3. The most common oxidation states and stereochemistry of niobium is presented in Table **2.2**.

Table 2.2: Stereochemistries and oxidation states of niobium.[2,4]

Oxidation state	Coordination number	Geometry	Complex
Nb^{-3} (d^8)	5	Trigonal bipyramidal	$[Nb(CO)_5]^{3-}$
Nb^{-1} (d^6)	6	Octahedral	$[Nb(CO)_6]^{-}$
Nb^{0} (d^5)	6	π Complex	$Nb(\eta^6\text{-mes})_2$
Nb^{+1} (d^4)	7	π Complex	$(C_5H_5)Nb(CO)_4$
Nb^{+2} (d^3)	4	Square planar	NbO
	6	Trigonal prismatic	NbS
	6	Octahedral	$NbCl_2(py)_4$
Nb^{+3} (d^2)	6	Trigonal prismatic	$LiNbO_2$
	6	Octahedral	$Nb_2Cl_6(SMe_2)_3$
	8	Dodecahedral	$K_5[Nb(CN)_8]$
Nb^{+4} (d^1)	6	Octahedral	$[Nb(Cl)_6]^{2-}$
	7	Distorted pentagonal bipyramidal	K_3NbF_7
	7	Capped octahedron	$NbCl_4(PMe_3)_3$
	8	Square antiprismatic	$Nb(\beta\text{-dike})_4$
	8	Dodecahedral	$K_4Nb(CN)_8 \cdot 2H_2O$
	8	π Complex	Cp_2NbMe_2
Nb^{+5} (d^0)	4	Tetrahedral	$ScNbO_4$
	5	Trigonal bipyramidal	$NbCl_5$ (g)
	5	Distorted tetragonal pyramid	$Nb(NMe_2)_5$
	5	Square pyramidal	$[Nb(NMe_2)_5]$
	6	Octahedral	$NbOCl_3$
	6	Trigonal prismatic	$[Nb(S_2C_6H_4)_3]^{-}$
	7	Distorted pentagonal bipyramidal	$NbO(S_2CNEt_2)_3$
	7	Capped Trigonal prismatic	$[NbF_7]^{2-}$
	8	Bicapped trigonal prismatic	$[Nb(trop)_4]^{+}$
	8	Dodecahedral	$[Nb(O_2)_4]^{3-}$
	8	Square antiprismatic	$[NbF_8]^{3-}$

2.1.2 Uses

Niobium has a variety of useful properties; not only for the chemical industry, but also for the steel-, nuclear energy- and electronics industries. In most of the applications where tantalum or niobium can be used, tantalum is at present preferred because of its lower cost and due to the fact that it is slightly more resistant to chemical corrosion than niobium.

Table 2.3: Uses of niobium.[5]

Niobium Product	Application	Benefits
Niobium oxide	- Camera lenses. - Coating on glass for computer screens. - Ceramic capacitors. - Manufacture of lithium niobate for surface acoustic wave filters.	- High index of refraction. - High dielectric constant. - Increase light transmittance.
Niobium carbide	Cutting tool compositions.	High temperature deformation and controls grain growth.
Niobium powder	Niobium capacitors for electronic circuits.	High dielectric constant, stability of oxide dielectric.
Niobium metal	Chemical processing equipment.	Corrosion resistance.
Ferro-niobium	Niobium additive to high strength low alloy steel and stainless steel.	Weight reduction and increased strength and toughness due to grain refining.
Niobium-titanium and niobium-tin alloys	Superconducting magnetic coils in magnetic resonance imagery (MRI).	Very low electrical resistance of alloy wire at low temperatures.

Niobium has good high temperature strength and when alloyed with other metals it has improved strength at high temperatures. Ferro-niobium is a mixture of iron and niobium and is used as an additive to improve the strength and corrosion resistance of steel. High purity ferroniobium is used in superalloys for applications as heat-resisting and combustion equipment such as jet engine and missile components.[6]

[5] D. L. Kepert, *The Early Transition Metals*, Academic Press, London, 142, 1972.
[6] D. J. Soisson, J. J. McLafferty, J. A. Pierret, *Ind. Eng. Chem.,* **53**, 11, 861, 1961.

Ferroniobium acts as a grain refiner to increase tensile strength at additions as low as 0.02 wt %. Normal usage is 0.03 – 0.1 wt %.[7]

Addition of niobium to zirconium increases the mechanical strength and corrosion resistance of the metal. The main reason for the addition of niobium to zirconium is for use in the cladding of nuclear fuel rods. This is due to the low thermal-neutron cross section of both metals (Nb, 1.15 barn; Zr, 0.184 barn). The fuel rods need to be cladded to prevent the leakage or corrosion of the rods into the reactor itself. A Zr – 1 wt % Nb alloy has been used as primary cladding in Canada and a Zr – 2.5 wt % Nb alloy has been used to replace Zircaloy-2 as the cladding in Candu-PHW (pressurized hot water) and has led to a 20 % reduction in wall thickness of cladding.[8]

Superconductivity is a term used to describe the lack of electrical resistance at very low temperatures and it is displayed by niobium and many of its alloys. This makes the alloys of great interest for electronic devices, power generation and other applications. Niobium-titanium alloys are used for most superconducting devices due to the ease of its conversion into magnet wire, which is its most common application. Where the use of higher magnetic fields is necessary, niobium-tin alloys are used. The intermetallic nature of this alloy makes production difficult and improved methods of fabrication should lead to wider use. Niobium becomes superconducting at 9.15 K, Nb-Ti at 9.5 K and Nb-Sn at 18 K.[7]

Niobium oxide is the intermediate product used in the manufacturing of high-purity niobium metal, ferro-niobium, nickel niobium and niobium carbide. The leading applications of high purity niobium oxide (> 99.9 %) are ceramics and optical glass. In the field of electro ceramics, niobium based perovskites are expected to exceed the traditional titanate/zirconate based ceramics because of their lower sintering temperature. Classic examples of ceramics comprising of niobium are [$Pb_3MgNb_2O_9$], [$Pb_3NiNb_2O_9$] and [Pb_2FeNbO_6]. When the silica in glass is replaced by niobium oxide the refractive index is increased. This means that thinner and lighter lenses can be produced for the same focal length. It is also a very important material for the electronics industry.

[7] Kirk-Othmer, *Encyclopedia of Chemical Technology*, 5th Ed., Wiley and Sons, New Jersey, 610, 2007.
[8] B. A. Cheadle, W. J. Langford, R. I. Coote, *Nucl. Eng. Int.*, 50, **24**, 289, 1979.

2.2 Separation of Nb and Ta

2.2.1 Marignac Process

The Marignac process[9], developed in 1866, is considered to be the first industrial separation process for the two metals. The process is based on the difference in solubility of the fluoride complexes of tantalum and niobium. It involves the addition of an excess of potassium fluoride to the hydrofluoric acid solutions of the metal ores to precipitate complex fluorides of the two metals. The potassium tantalum fluoride, K_2TaF_7, is only sparingly soluble in dilute hydrofluoric acid (HF), whereas the potassium niobium oxyfluoride, K_2NbOF_5, has very high solubility. Potassium niobium fluoride, K_2NbF_7, is not formed in this process as it is only stable in concentrated HF. The Marignac process has been replaced by other industrial processes because only the purity of the tantalum produced, was adequate. The purity of niobium produced by this process was unsatisfactory due to the presence of titanium in the mineral concentrate.

2.2.2 Solvent Extraction

The U.S. Bureau of Mines and Ames Laboratory of Iowa State University developed the solvent extraction process in 1950.[10,11] This process utilises the extractant, methyl isobutyl ketone (MIBK), for the separation of niobium and tantalum. The solvent extraction is ideal for large-scale operations and satisfactorily for the production of pure niobium compounds. It is also relatively simple when compared to Marignac's process.

Industrial separation processes involve the use of various acids in combination with HF and a choice of four solvents, either tributyl phosphate (TBP), MIBK, cyclohexanone (CHN) or 2-octanol (2-OCL). Some of these combinations have been reported in the literature, eg; HF-nitric acid (HNO_3)-MIBK[12] and HF-hydrochloric acid (HCl)-MIBK[13]. Although these combinations involve different chemicals, they all still

[9] T. Okada, *Manufacturing of Special Niobium Oxides for Optical and Ceramic Applications,* 2000.
[10] Japan Mining Industry Association, "*Study Report of High-purity Rare Metals"*, 1991
[11] J. R. Werning, K. B. Higbie, J. T. Grace, B. F. Speece, H. L. Gilbert, *Industrial and Engineering Chemistry*, **46**, 4, 644, 1954.
[12] C. H. Faye, W. R. Inman, *Research Report MD210*, Dept. Mines and Technical Surveys, Ottawa, Canada, 1956.
[13] J. R. Werning, K. B. Higbie, J. T. Grace, B. F. Speece, H. L. Gilbert, *Ind. Eng. Chem.*, **46**, 644, 1954.

work on the same principal, varying only in terms of the back-extraction of either niobium or tantalum.

The ores are finely ground and dissolved in HF. The acidity is adjusted to greater than 8 M with sulphuric acid (H_2SO_4) in order to dissolve the accompanying elements such as iron, manganese and titanium along with the niobium and tantalum. After removal of the remaining insoluble elements like the rare earth metals by filtration, the acid solution is extracted with MIBK.

Initially both niobium and tantalum are extracted into the organic phase while most of the impurities remain in the aqueous phase. This organic phase is then mixed with a new aqueous phase containing 3 M H_2SO_4. The niobium is back extracted into the aqueous phase due to the lower acidity of the aqueous phase. The back extracted aqueous niobium is again re-extracted with MIBK to remove any traces of tantalum that could be present. This ensures complete separation of niobium (aqueous phase) and tantalum (organic phase).

To precipitate niobium oxide hydrate from the aqueous phase, ammonia is added and the niobium oxide hydrate is removed by filtration. The niobium oxide obtained after drying of the filtrate is of high purity.

2.2.3 Current Research

There is a need to develop novel aqueous and organic systems for the separation of niobium and tantalum. The main goal is to move away from the use of HF or at the very least limit the use of it to very small quantities. A great deal of research has been done in this regard, but up to date no separation process with industrial application could be developed that excluded the use of HF completely.

Most techniques use liquid-liquid extraction, but a few use a supported liquid membrane with the use of various extractants and mineral acid media. The separation of niobium and tantalum in a chloride medium with the use of TBP and Alamine 336 as carrier through a supported liquid membrane was reported by Campderrós *et al*.[14,15] This technique delivered about 55 % extraction of niobium.

[14] M. E. Campderrós, J. Marchese, *J. Membr. Sci.*, **164**, 205, 2000.
[15] M. E. Campderrós, J. Marchese, *Hydrometallurgy*, **61**, 89, 2001.

Buachuang *et al*.[16] reported the separation of tantalum and niobium from dilute hydrofluoric media through a hollow fibre supported liquid membrane (HFSLM). Quaternary ammonium salt diluted in kerosene was used as a carrier. The best conditions were 0.3 M HF, 3 % (v/v) ammonium salt diluted in kerosene and 0.2 M of stripping solution ($NaClO_4$).

2.3 Purification

Three types of impurity elements are considered in the purification of niobium:

- Impurity elements with a higher vapour pressure than Nb. These elements can easily be removed by electron beam melting or high vacuum arc melting.

- Refractory impurity metals with a similar vapour pressure as Nb can only be removed by chemical or physical methods. These methods utilise the difference in kinetic behaviour and thermodynamic properties of the impurity element. Suitable methods are sublimation, electrolysis, distillation, etc.

- The removal of interstitial impurity elements involves high temperature annealing treatments in gas and high vacuum atmospheres.

Niobium oxide (Nb_2O_5) is the starting material for the production of other niobium compounds, such as lithium niobate ($LiNbO_3$) and niobium chloride ($NbCl_5$). Niobium oxide can be reduced with carbon in a two-step reaction, known as the Balke-process.[7] The first step is the formation of the carbide. The oxide is mixed with a stoichiometric amount of carbon black, placed in a carbon vessel and heated in vacuum to 1800 ℃:

$$Nb_2O_5 + 7\ C \rightarrow 2\ NbC + 5\ CO \qquad (\mathbf{2.1})$$

[16] D. Buachuang, P. Ramakul, N. Leepipatpiboon, U. Pancharoen, *J. Alloys Compd.*, 509, 9549, 2011.

The carbide is then remixed with a stoichiometric amount of oxide and then reheated to 2000 ℃ under reduced pressure:

$$5\ NbC + Nb_2O_5 \rightarrow 7Nb + 5\ CO \qquad (\mathbf{2.2})$$

The product is then hydrated, crushed and rehydrated to a powder. All of the carbon and most of the oxygen is removed by high temperature sintering. The powder is then compacted by electron-beam or arc melting.[17]

The powders of niobium can also be produced by the reduction of niobium oxide with magnesium, or by the reduction of potassium niobium heptafluoride with sodium.[18] The latter reaction is carried out in an iron vessel filled with alternating layers of K_2NbF_7 and oxygen free sodium:

$$K_2NbF_7 + 5\ Na \rightarrow Nb + 2\ KF + 5\ NaF \qquad (\mathbf{2.3})$$

The reaction is performed under an argon or helium atmosphere and the sodium (in excess) drives the reaction to completion. The excess sodium is leached with alcohol and the potassium and sodium fluorides are extracted with water. The metal powder is leached with hydrochloric acid to remove iron contamination from the vessel.

2.4 Chemistry of Niobium

Niobium reacts with most non-metals to give products which are frequently interstitial and nonstoichiometric. Most of niobium's chemistry is confined to the +5 oxidation state, as this is the most studied oxidation state.

2.4.1 Oxides

Niobium pentoxide (Nb_2O_5) is relatively stable and difficult to reduce. Concentrated HF is the only acid that can attack Nb_2O_5 and it also dissolves in fused alkali hydrogen sulphate, carbonate and hydroxide. Extensive polymorphism is displayed by Nb_2O_5, based on octahedrally coordinated niobium atoms. High temperature reduction of Nb_2O_5 with hydrogen gives NbO_2 and further reduction produces NbO. NbO_2 has a distorted rutile structure and NbO has a cubic structure.[2]

[17] H. Stuart, O. de Souza Paraiso, R. de Fuccio, *Iron Steel,* **11**, 1980
[18] F. Perfect, *Trans. Metall. Soc.,* AIME 239, 1282, 1967.

Niobium oxide surfaces exhibit extraordinary catalytic properties which find application in the petroleum, petrochemical and pollution control industries. The preparation, physical-, chemical- and catalytic properties of niobium oxide surfaces was investigated by Deng *et al*.[19] They found that the catalytic activity of the niobium oxide surface was dependent on the preparation process as well as to the Nb=O bond.

2.4.2 Halides

All possible halides of niobium(V) are known and preparations of lower valent halides usually start with the pentahalide. Niobium is unique in forming pentaiodides, a property only shared by tantalum and protactinium.[16] The known halides of niobium and tantalum are listed in Table **2.4**. It is important to note that only niobium forms the tetrafluoride and tri-iodide complexes. In the lower oxidation states, niobium and tantalum form a number of generally nonstoichiometric cluster compounds in which the metal has non-integral oxidation states.

Table 2.4: Halides of niobium and tantalum.[4]

Oxidation state	Fluorides	Chlorides	Bromides	Iodides
+3	NbF_3 TaF_3	$NbCl_3$ $TaCl_3$	$NbBr_3$ $TaBr_3$	NbI_3 -
+4	NbF_4 -	$NbCl_4$ $TaCl_4$	$NbBr_4$ $TaBr_4$	NbI_4 TaI_4
+5	NbF_5 TaF_5	$NbCl_5$ $TaCl_5$	$NbBr_5$ $TaBr_5$	NbI_5 TaI_5

All the niobium pentahalides can be prepared by direct addition of the halogen to the heated metal. They are all relatively volatile, hydrolysable solids and the metals reach octahedral coordination by means of halide bridges. NbF_5 is a tetramer whereas the bromides and chlorides are dimers.

[19] H. T. Deng, K. P. Kerns, A. W. Castleman Jnr, *J. Phys. Chem.*, **100**, 13386, 1996.

2.4.3 Borides

A few niobium boride[20] complexes like NbB, NbB_2 Nb_2B, Nb_3B and Nb_3B_4 have been described in literature. The monoboride and the diboride complexes are the only borides that melt completely. NbB_2 decomposes at the melting point to form NbB and boron.[21] The most familiar methods of preparation of niobium borides is sintering, hot-pressing and remelting of powdered mixtures of niobium or niobium hydride with elemental boron.[22]

2.4.4 Carbides

Two phases of niobium carbide are known, Nb_2C and the monocarbide NbC. The monocarbide is the only phase of industrial importance. It melts at 3600 °C without decomposition. It is found primarily in combination with TaC in 10, 20 or 50 wt % NbC, and is used to improve the properties of cemented carbides.[23] Industrial preparation utilizes carbon (CH_4) and Nb_2O_5 as starting materials. The initial reaction begins at 675 °C but temperatures of 1800 – 2000 °C are needed for completion of the reaction.[7]

2.4.5 Nitrides

Nitrogen has a high bond energy (941 kJ/mol) and requires high temperatures for activation.[24] At these elevated temperatures the Nb-N bonds in ionic/covalent nitrides become less stable and entropic effects favour lower nitrogen-metal ratios. The synthesis usually involves the reaction of niobium pentachloride with a hydrogen/nitrogen mixture. The main product formed is the mononitride, but other stoichiometries such as Nb_4N_3 and Nb_2N can also be formed, depending on the deposition conditions employed.[25]

[20] C. L. Yeh, W. H. Chen, *J. Alloys Compd.*, **420**, 111, 2006.
[21] F. Fairbrother, *The Chemistry of Niobium and Tantalum*, Elsevier, New York, 34, 1976.
[22] P. M. McKenna, *Ind. Eng. Chem.*, **28**, 767, 1936.
[23] H. O. Pierson, *Handbook of Chemical Vapor Deposition*, Elsevier, New York, 241, 1999.
[24] S. T. Oyama, *The Chemistry of Transition Metal Carbides and Nitrides*, Blackie Academic and Proffesional, Glasgow, 154, 1996.
[25] R. Fix, R. G. Gordon, D. M. Hoffman, *Chem. Mater.*, **5**, 614, 1993.

2.4.6 Water absorption

The interaction of water with transition-metal centers is an important subject in especially catalysis. The initial product formed from the reaction is a H-Nb-OH insertion intermediate.[26] The insertion product can either photochemically isomerize to the high-valent H_2-Nb-O isomer or decompose to the metal monoxide and H_2. The later transition metals as well as the lanthanides react with water to predominately give the M(H_2O) complexes, which rearranges to the insertion product under UV-visible light excitation.[27] Extensive studies have been done on the reactions of ionic and neutral transition-metals with water, but the reactions of transition metal oxides have gained much less attention. Recently Zhou *et al.*[28] published a paper on the reactions of niobium monoxides and dioxides with water. They investigated it by making use of matrix isolation infrared spectroscopy and density functional theoretical calculations. Niobium monoxide and dioxide were reacted with water to form the NbO(H_2O) and NbO_2(H_2O) complexes and were characterized to involve bonding interactions between the water, oxygen and niobium. The NbO_2(H_2O) complex isomerized to the more stable $NbO(OH)_2$ complex by means of a hydrogen atom transfer from water to one of the metal dioxide oxygens upon visible light irradiation at 400 – 580 nm. NbO(H_2O) on the other hand, photochemically rearranged to the more stable HNbO(OH) isomer under visible light excitation at 500 – 580 nm.

2.4.7 Silicates

Silicates are compounds containing silicon bearing anions and usually occur as the oxide. Transition metal silicates in octahedral or distorted octahedral framework sites have enjoyed attention because they usually display good thermal stability and other physical and catalytic properties.[29] Three niobium silicate frameworks consisting of a novel silicate unit, [$(Si_8O_{22})^{12-}$], were prepared under mild hydrothermal conditions by Salvadó *et al.*[30] in 2001. More recently a niobium(V) silicate, [$Rb_2(Nb_2O_4)(Si_2O_6)$],

[26] M. F. Zhou, J. Dong, L. N. Zhang, Q. Z. Qin, *J. Am. Chem. Soc.*, **123**, 135, 2001.
[27] J. Xu, X. Jin, M. F. Zhou, *J. Phys. Chem.*, A, **111**, 7105, 2007.
[28] M. Zhou, J. Zhuang, G. Wang, M. Chen, *J. Phys. Chem.*, 115, 2238, 2011.
[29] J. Rocha, M. W. Anderson, *Eur. J. Inorg. Chem.*, 801, 2000.
[30] M. A. Salvadó, P. Pertierra, S. Garcia-Granda, S. A. Khainakov, J. R. Garcia, A. I. Bortun, A. Clearfield, *Inorg. Chem.*, **40**, 17, 4368, 2001.

was prepared by Tasi *et al.*[31] They previously also synthesised $[Rb_4(NbO)_2(Si_8O_{21})]$ which is isotypic to $[Cs_4(NbO)_2(Si_8O_{21})]$ which was prepared by Crosnier *et al.*[32]

2.4.8 Cyclopentadienes

Based on the type of bonding between metals and the cyclopentadienyl moiety, cyclopentadienyl complexes are distinguished into three groups; π-, σ- and ionic complexes. The cyclopentadienyl ligand is usually firmly bound to metals, making the C_5H_5M unit a stable synthetic platform for the development of a wide range of complexes for varied applications. The presence of various functional groups attached to the cyclopentadienyl ligand determines both the electronic and steric properties of the metal centres and alters the reactivity of their complexes.

Numerous niobium complexes have been synthesised using cyclopentadienes and their derivatives as ligands.[33,34,35] Postigo *et al.*[36] published a paper on the synthesis and reactivity of imido niobium complexes containing a functionalized (dichloromethylsilyl)cyclopentadienyl ligand in 2007. The products, imidodichloro- and imidochloroamido-niobium complexes with aminosilylcyclopentadienyl ligands, were isolated by the reaction of $NbCl_5$ with $C_5H_4(SiCl_2Me)(SiMe_3)$ followed by the reaction of the resulting product with lithium amide. In 2010, Sánchez-Nieves *et al.*[37] synthesised neutral and cationic monocyclopentadienyl alkyl niobium complexes with the chemical formula, $[NbCl_3(C_5H_4SiMe_3)(OR)]$ (R = *t*Bu, Si*i*Pr_3, 2,6-$Me_2C_6H_3$).

2.4.9 Phosphates

Phosphates are polyatomic ions with the empirical formula PO_4^{3-} and consist of one phosphorus atom surrounded by four oxygen atoms in a tetrahedral arrangement. Niobium phosphates are generally condensed phases prepared by solid-state reactions or by reactions in fluxes.[38] A wide variety of niobium phosphates have

[31] J. Tasi, P. Tu, T. Chan, K. Lii, *Inorg. Chem.*, **47**, 23, 11223, 2008.
[32] M. P. Crosnier, D. Guyomard, A. Verbaere, Y. Piffard, *Eur. J. Solid State Inorg. Chem.*, **27**, 435, 1990.
[33] M. J. Humphries, M. L. H. Green, R. E. Douthwaite, L. H. Rees, *Dalton Trans.*, 4555, 2000.
[34] J. Sánchez-Nieves, L. M. Frutos, P. Royo, O. Castano, E. Herdtweck, M. E. G. Mosquera, *Inorg. Chem.*, **49**, 10642, 2010.
[35] J. A. Acho, L. H. Doerrer, S. J. Lippard. *Inorg. Chem.*, **34**, 2542, 1995.
[36] L. Postigo, J. Sánchez-Nieves, P. Royo, *Inorg. Chim. Acta*, 360, 1305, 2007.
[37] J. Sánches-Nieves, V. Tabernero, C. Camejo, P. Royo, *J. Organomet. Chem.*, 695, 2469, 2010.
[38] A. Leclaire, M. M. Borel, J. Chardon, B. Raveau, *J. Solid State Chem.*, 111, 26, 1994.

been reported in literature. Recent studies include work done by Lui *et al.*[39] who prepared two new inorganic niobium phosphates, [$KNbP_2O_8$] and [$NbPO_4F_2$], by similar two-step hydrothermal methods.

2.5 Niobium as catalyst

Niobium compounds exhibit unique properties not displayed by the compounds of neighbouring elements in the periodic table. These include stability and strong metal support interaction (SMSI) which are all important for the production of a catalyst. Niobium materials are currently of great importance in heterogeneous catalysis where they are used as catalyst components or are added in small amounts to catalysts. The characterization of niobium compounds is very important when considering their catalytic activity and for the prediction of both their selectivity and activity in various reactions.[40]

Various functions of niobium compounds in heterogeneous catalysis:[41,42]

- Redox Material: One of the main applications of niobium-based catalysis has been in the area of oxidation catalysis. The redox potential of niobia (Nb_2O_5) enhances the redox properties of some metal oxide species (Mo, V, Cr, etc) supported on Nb_2O_5. The addition of niobia to mixed oxide catalysts can result in enhanced activity and selectivity as displayed in the Bi-Nb-O and Nb-Ta systems.[43,44]

- Support Effect: Niobium oxide has been used as an oxide support for numerous metals (Fe, Ru, Re, W, Mo).[45,46] The properties of the niobia are enhanced by the addition of these elements, while its high selectivity is preserved.

[39] G. Lui, J. Wang, L. Wang, *Inorg. Chem. Comm.*, **14**, 1279, 2011.
[40] K. Tanabe, *Catal Today*, **78**, 65, 2003.
[41] I. Nowak, M. Ziolek, *Chem. Rev.*, **99**, 3603, 1999.
[42] M. Ziolek, *Catal. Today*, **78**, 47, 2003.
[43] I. E. Wachs, J. Jehng, G. Deo, H. Hu, N. Arora, *Catal. Today*, **28**, 199, 1996.
[44] A. Morikawa, A. Togashi, *Catal. Today*, **16**, 333, 1993.
[45] M. D. Phadke, E. I. Ko, *J. Catal.*, 100, 503, 1986.
[46] J. Jehng, A. M. Turek, I. E. Wachs, *Appl. Catal.* A, 83, 179, 1992.

- Promoter or Active phase: Interactions that allow the reactants to interact simultaneously with the metal and the promoter are the most relevant to catalysis. When the catalyst consists of metal fragments covered by promoter oxide, some steps in the overall reaction may be catalyzed at the metal-promoter-liquid/gas interphase. A supported metal-promotor interaction has been observed in niobium oxide-promoted Rh/SiO_2 catalysts[47], niobia-promoted Pt/Al_2O_3 catalysts[48], and silica supported $NiNb_2O_6$ catalysts[49].

- Solid Acid Catalyst: Although niobium-containing catalysts were studied in various acid catalysed reactions and their acidity was assessed by various techniques, they have not been widely used as acid catalysts in practise. Datka *et al.*[50] examined the acidic properties of niobium oxide catalysts and found Lewis acidity in the silica-, magnesia-, titania-, and zirconia-supported systems, while Brønsted acid sites were only encountered when the niobia was supported on alumina or silica.

Recent work includes a study by Silva *et al.*[51] on Nb-doped iron oxides that were used as heterogeneous catalysts to oxidize organic compounds in aqueous solutions containing hydrogen peroxide (H_2O_2). The H_2O_2 treatment of the solid catalyst induces important surface and structural changes to the iron oxides, essentially by formation of peroxo-niobium complexes which enhances the catalytic properties of the composite. Research on the catalytic performance of niobium in crystalline and amorphous solids in catalytic oxidation reactions were done by Ziolek *et al.*[52] in 2011. Bulk niobium(v) oxide materials were used as catalysts in the gas phase oxidation of methanol with oxygen, liquid phase oxidation of glycerol with oxygen and the liquid phase oxidation of cyclohexene with H_2O_2. The amorphous materials containing niobium were the most effective catalyst because of the strong interaction between the Nb and H_2O_2. That was not the case for the crystalline catalysts

[47] T. Beutel, V. Siborov, B. Tesche, H. Knözinger, *J. Catal.*, 167, 379, 1997.
[48] T. Hoffer, S. Dobos, L. Guczi, *Catal. Today*, **16**, 435, 1993.
[49] K. Kunimori, H. Shindo, H. Oyanagi, T.Uchijima, *Catal. Today*, **16**, 387, 1993.
[50] J. Datka, A. M. Turek, J. M. Jehng, I. E. Wachs, *J. Catal.*, 135, 186, 1992.
[51] A. C. Silva, R. M. Cepera, M. C. Pereira, D. Q. Lima, J. D. Fabris, L. C. A. Oliveira, *Appl. Catal. B*, **107**, 237, 2011.
[52] M. Ziolek, D. I. Sobczak, M. Trejda, J. Florek, H. Golinska, W. Klimas, A. Wojtaszek, *Appl. Catal. A*, **391**, 194, 2011.

containing niobium as the niobium species promoted the stabilization of the active species loaded.

2.6 β-diketone complexes of niobium

Metal β-diketonates are amongst the most studied coordination compounds and their chemistry has been examined for most of the metals in the periodic table. The ligand forms chelates with the metal and delocalizes the negative charge over a "metallacycle".[53] β-diketones has the potential to be easily derivatized using well-established procedures. The steric and electronic nature of this ligand type may be varied to probe the structure and function of interest.

Variation of the R groups influence the properties displayed by metal β-diketonates and the ability to form higher coordinate species can be achieved by variation of the terminal R groups on the β-diketone. It has been shown that the stepwise incorporation of electron-withdrawing trifluoromethyl groups increases the affinity of the central metal ion for further ligation.[54]

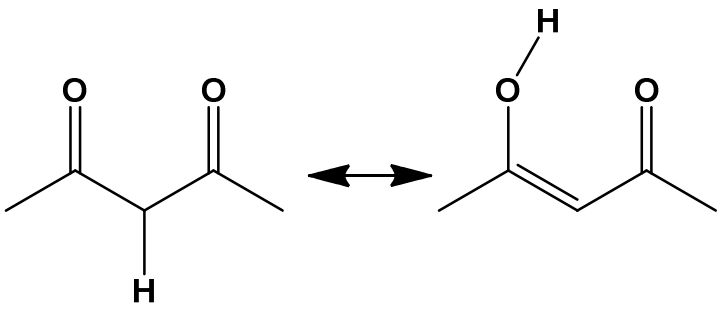

Keto Enol

Figure 2.1: Keto-enol tautomerism in β-diketones.

The simplest β-diketone is acetylacetone (2,4-pentanedione, acacH), which tends to form neutral complexes with niobium. The adopted geometry normally reflects the preferred geometry of the metal ion involved. Slight basic conditions cause deprotonation and the resulting acetylacetone anion readily complexes a range of

[53] R. C. Mehrotra, R. Bohra, D. P. Gaur, *Metal β-diketonates and Allied Derivatives,* Academic Press, London, 1978.
[54] R. van Eldik, K. Bowman-James, *Advances in Inorganic Chemistry,* Academic Press, London, 3, 2006.

metal ions, usually forming a six-membered chelate ring [Fig 2.2]. Acetylacetone is also capable of keto-enol tautomerism; the tautomers exist in equilibrium with each other and structurally they occupy a *syn* conformation and a *cis* configuration [Fig 2.1].[55]

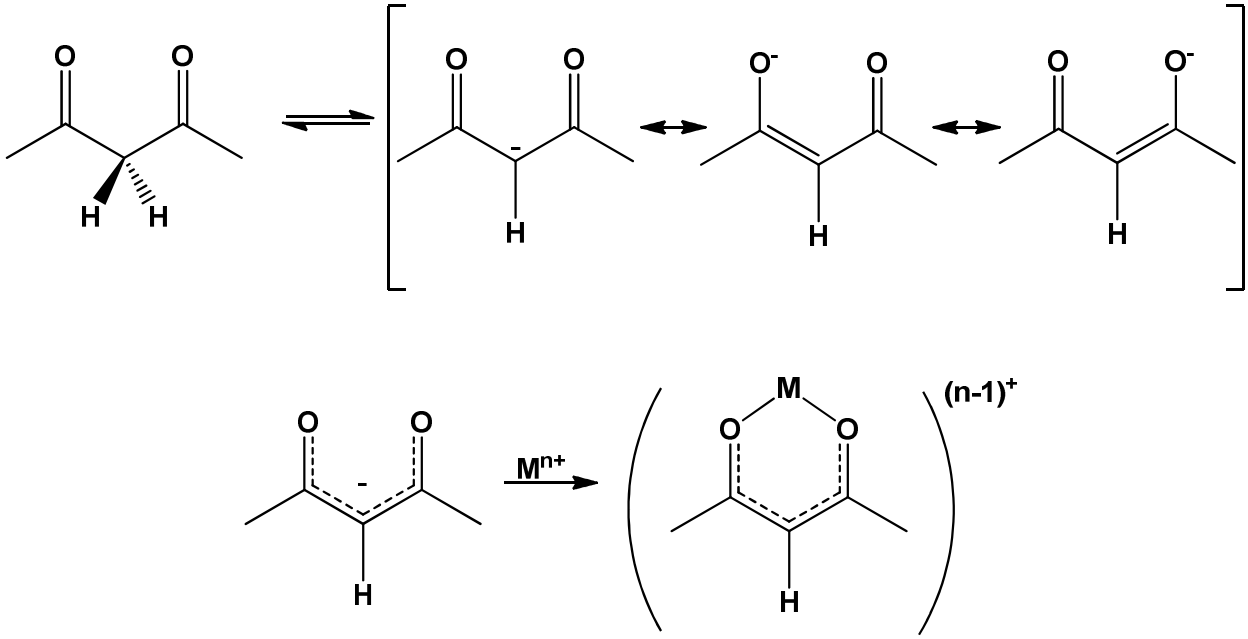

Figure 2.2: Metal complexation by an acetylacetonate anion.

Although acetylacetonate complexes of many metal ions are well known, relatively few compounds have been reported for niobium, especially in the plus five oxidation state.[56]

2.6.1 Tetrakis(β-diketonate) niobium(IV) complexes:

2.6.1.1 [Nb(thd)$_4$]

The first niobium(IV) tetrakis β-diketonate complex to be characterized by X-ray crystallography, was published in 1975 by Pinnavaia *et al*.[57] The aim of the study was to fully characterize the coordination geometry of a tetrakis coordinated tetramethylheptanedionate (thd*)* complex of niobium. The final

[55] D. J. Otway, W. S. Rees Jnr, *Coordination Chemistry Reviews,* **210**, 281, 2000
[56] F. H. Allen, *Acta Cryst*., **B58**, 380, 2002.
[57] T. J. Pinnavaia, B. L. Barnett, G. Podolsky, A. Tulinsky, *J. Am. Chem. Soc.*, **97**, 2712, 1975.

conclusions, with regard to the completed characterization, defined the square antiprismatic properties of the coordination sphere. The average Nb-$O_{(thd)}$ bond distance was determined as 2.13 Å. This set the field for niobium β-diketonate research for the future. Comparisons were made with a similar zirconium complex and were found to be not isomorphous.

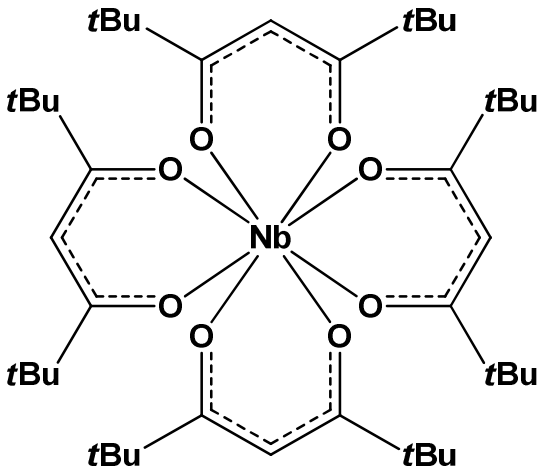

Figure 2.3: Structure of [Nb(thd)$_4$].

2.6.1.2 [Nb(hfacac)$_4$]

In 1998 Calderazzo *et al.*[58] published a structure for the 4-coordinated 1,1,1,5,5,5-hexafluoroacetylacetonato (hfacac) niobium complex. The study involved characterization by means of X-ray crystallography and an investigation into the electronic structure by means of electron paramagnetic resonance (EPR) spectroscopy. Comparison was made between the two similar compounds of niobium and zirconium (M(hfacac)$_4$, M = Nb, Zr). X-ray crystallography revealed that both compounds had a square antiprismatic coordination at the metal with an average M-$O_{(hfacac)}$ bond distance of 2.12 Å for Nb and 2.18 Å for Zr. The EPR investigation obtained the point of symmetry at the paramagnetic centre for both complexes.

[58] F. Calderazzo, U. Englert, C. Maichle-Mossmer, F. Marchetti, G. Pampaloni, D. Petroni, C. Pinzino, J. Strahle, G. Tripepi, *Inorg. Chim. Acta.*, **270**, 177, 1998.

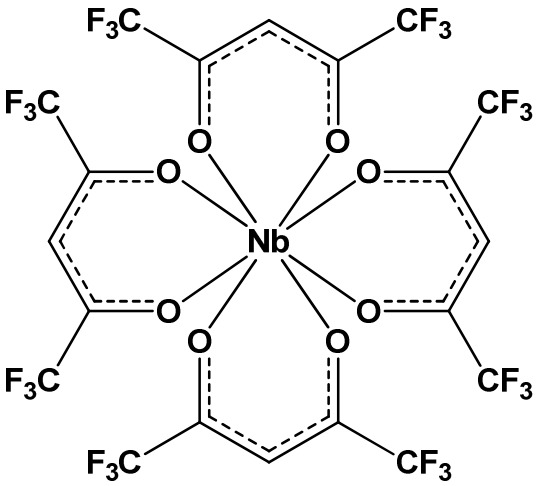

Figure 2.4: Stucture of $[Nb(hfaa)_4]$.

2.6.2 Bis(β-diketonate) niobium(IV) complexes:

2.6.2.1 *trans*-$[NbCl_2(thd)_2]$

In 1985 Cotton *et al.*[59] published a structure in which two thd ligands coordinated *trans* to a Nb(IV) metal centre. The structural characterization showed that the niobium metal centre was in a 6-coordinated state with 4 oxido and 2 chlorido atoms. The examination of the crystals on a diffractometer showed that there were two polymorphic forms present, namely orthorhombic and monoclinic, **1** and **2** respectively. The unit cell volume of **1** was almost twice that of **2** and the abundance of the former type of crystals was roughly twice the latter. The average $Nb\text{-}O_{(thd)}$ bonding distances was determined as 1.99 Å for **1** and 1.98 Å for **2**. The crystals were prepared through sublimation.

[59] F. A. Cotton, M. P. Diebold, W. J. Roth, *Polyhedron,* **4**, 1485, 1985.

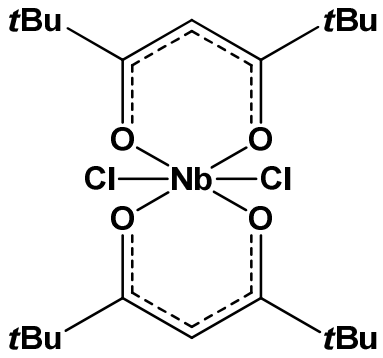

Figure 2.5: Structure of trans-[$NbCl_2(thd)_2$].

2.6.3 Mono(β-diketonate) niobium(V) complexes:

2.6.3.1 *fac*-[Nb(NCS)$(Opr)_3$(dbm)] and *trans*-[$Nb(NCS)_2(OEt)_2$(dbm)]

In 1976 Dahan *et al.*[60,61] published two articles on the structures of 6-coordinated niobium complexes with dibenzoylmethanato (dbm) as bidentate ligand. This was done in order to resolve the stereochemistry of the metal atoms. The X-ray structure of *fac*-[Nb(NCS)$(Opr)_3$(dbm)] was carried out following that of *trans*-[$Nb(NCS)_2(OEt)_2$(dbm)]. The average Nb-$O_{(dbm)}$ bond lengths were determined as 2.09 Å for *fac*-[Nb(NCS)$(Opr)_3$(dbm)] and 2.04 Å for *trans*[$Nb(NCS)_2(OEt)_2$(dbm)]. Both crystals were found to be built up of monomeric molecules and the only intermolecular interactions found were van der Waals contacts. The niobium atoms for both crystals were at the centre of a distorted co-ordination octahedron.

[60] F. Dahan, R. Kergoat, M. Senechal-Tocquer, J. E. Guerchais, *J. Chem. Soc.*, *Dalton Trans*., 2202, 1976.
[61] F. Dahan, R. Kergoat, M. Senechal-Tocquer, J. E. Guerchias, *Acta Cryst.*, **B32**, 1038, 1976.

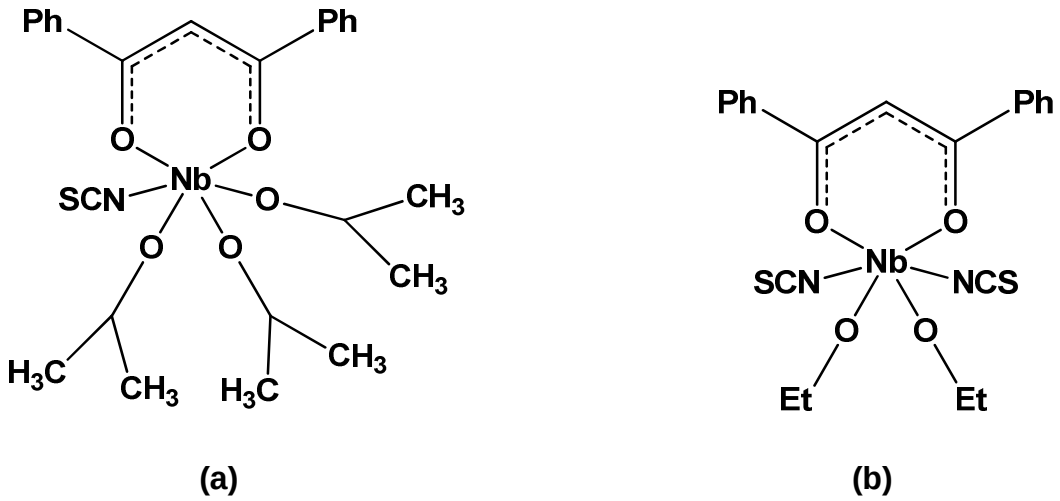

Figure 2.6: Structures of **a**) *fac*-[Nb(NCS)(Opr)$_3$(dbm)] and **b**) *trans*-[Nb(NCS)$_2$(OEt)$_2$(dbm)].

2.6.3.2 [Nb(OEt)$_4$(dbm)]

In 2002 Williams *et al.*[62] published a 6-coordinated niobium complex with dbm as bidentate ligand. The study was aimed at improving the thermal stability of niobium oxide precursors such as [Nb(OEt)$_4$(dbm)]. [Nb(OEt)$_4$(dbm)] is used as starting material in the liquid injection metal-organic chemical vapour deposition (LI-MOCVD) to deposit thin films of niobium oxide. Single-crystal X-ray diffraction (XRD) showed the complex to be mononuclear with a distorted octahedral configuration. The average Nb-O$_{(dbm)}$ bond lengths were determined as 2.13 Å.

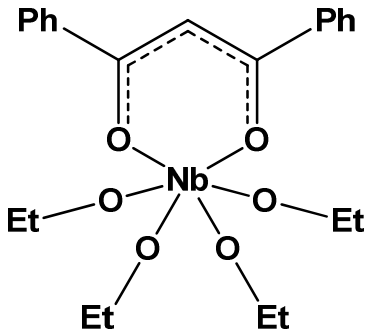

Figure 2.7: Structure of [Nb(OEt)$_4$(dbm)].

[62] P. A. Williams, A. C. Jones, P. J. Wright, M. J. Crosbie, J. F. Bickley, A. Steiner, H. O. Dacies, T. J. Leedham, *Chem. Vap. Deposition.,* **8**, 110, 2002.

2.6.3.3 [$NbCl_3O(ttbd)^-$]

An article of a 6-coordinated niobium complex, with 1,1,1-trifluoro-4-thenoyl-2,4-butanedionato (ttbd) as bidentate ligand, was published by Daran *et al.*[63] in 1979. The crystal structure was determined by single crystal X-ray analysis and was found to be built up of isolated ammonium cations and trichlorooxo-(1,1,1-trifluoro-4-thenoyl-2,4-butanedionato)niobate(V) anions. The niobium atom was at the centre of a distorted coordination octahedron of three chlorido atoms, the chelating diketone and the oxido atom. The niobium-oxygen bond was determined as 1.704 Å and a bond order of two was suggested by Wendling and Röhmer.[64] The average Nb-$O_{(ttbd)}$ bond length with regards to the β-diketone was determined as 2.17 Å.

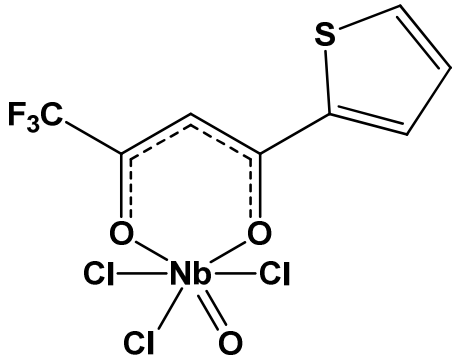

Figure 2.8: Structure of [$NbCl_3O(ttbd)^-$].

2.6.3.4 *trans*-[$NbCl_2(OEt)_2(dbm)$]

Antiñolo *et al.*[65] published an article on the reactivity of alkoxo-niobium(V) compounds towards O,O'-chelate ligands in 2000. The aim of their work was to investigate the synthesis and structural characterisation of *trans*-[$NbCl_2(OEt)_2(dbm)$]. The niobium complex crystallized in the monoclinic spacegroup $P2_1/n$, with one molecule in the asymmetric unit cell. The product was described as a pseudooctahedral Nb(V) complex containing two *trans*-chloride ligands in the axial positions and two *cis*-ethoxide ligands and a β-

[63] J. Daran, Y. Jeannin, J. E. Guerchais, R. Kergoat, *Inorg. Chim. Acta.*, **33**, 81, 1979.
[64] E. Wendling, R. Röhmer, *Bull. Soc. Chim. Fr.*, **1**, 8, 1967.
[65] A. Antiñolo, F. Carrillo-Hermosilla, J. Fernández-Baeza, S. Garcia-Yuste, A. Otero, E. Palomares, A. M. Rodriguez, L. F. Sánchez-Barba, *J. Organomet. Chem.*, **603**, 194, 2000.

diketonate ligand in the equatorial plane. The average Nb-$O_{(dbm)}$ bond length was determined as 2.07 Å.

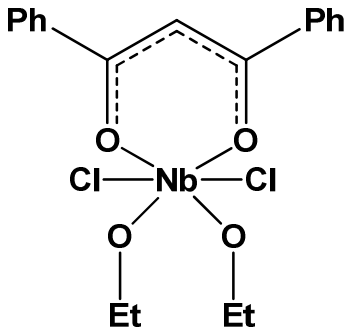

Figure 2.9: Structure of *trans*-[$NbCl_2(OEt)_2$(dbm)].

2.6.4 Bridged niobium β-diketonate complexes:

Formation of metal-metal bonded dimers is common to d^1 metal centres such as Nb(IV) and Ta(IV), especially as their tetrahalide structures.[66]

2.6.4.1 [$Nb_2(\mu\text{-}S_2)_2(acac)_4$] and [$Nb_2(\mu\text{-}S_2)(acac)_4$]

In 1999 Sokolov *et al.*[67] published two crystal structures in their efforts to synthesise niobium clusters with bridging chalcogen atoms. The key stage in this chemistry was the transformation of the inert polymeric NbS_2Cl_2 into soluble salts of $[Nb_2S_4(NCS)_8]^{4-}$ by the reaction with molten KNCS at 180 °C. The Nb(IV) oxidation state is stabilized in dimeric complexes. In their study they investigated the coordination chemistry of these $[Nb_2(\mu\text{-}S_2)_2]^{4+}$ cores with various β-diketone ligands.[68] [$Nb_2(\mu\text{-}S_2)(acac)_4$] crystallized in the triclinic spacegroup $P\bar{1}$ and [$Nb_2(\mu\text{-}S_2)_2(acac)_4$] crystallized in the monoclinic spacegroup *C*2/*c*. The average Nb-$O_{(acac)}$ bond lengths for [$Nb_2(\mu\text{-}S_2)_2(acac)_4$] was determined as 2.14 Å and for [$Nb_2(\mu\text{-}S_2)(acac)_4$] as 2.10 Å. The average Nb-Nb distance for both complexes was determined as 2.89 Å.

[66] M. Sokolov, A. Virovets, V. Nadolinnyi, K. Hegetschweiler, V. Fedin, N. Podberezskaya, V. Fedorov, *Inorg. Chem.*, **33**, 3503, 1994.
[67] M. Sokolov, H. Imoto, T. Saito, V. Fedorov, *Dalton Trans*., 85, 1999.
[68] M. Sokolov, O. Gerascko, A. Virovets, V. Fedorov, K. Hegetschweiler, *Inorg. Chim. Acta*, **271**, 222, 1998.

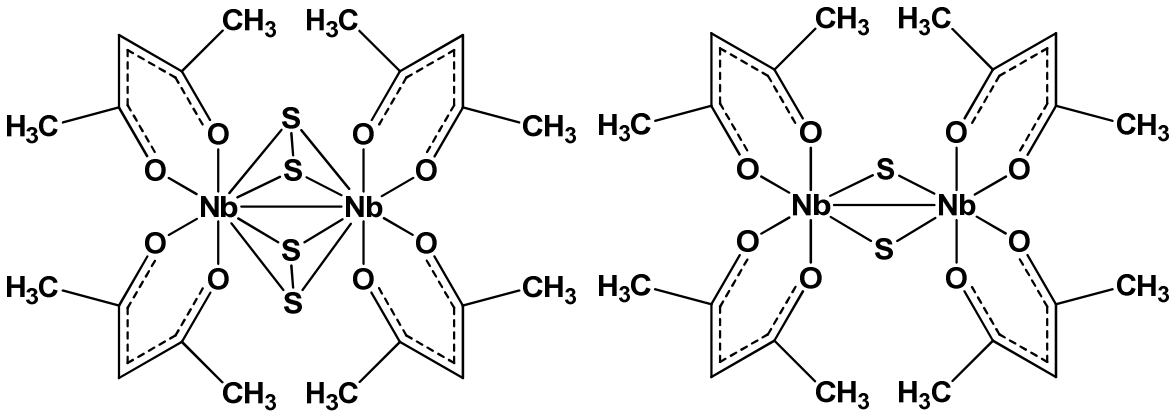

Figure 2.10: Structures of **a**) $[Nb_2(\mu\text{-}S_2)_2(acac)_4]$ and **b**) $[Nb_2(\mu\text{-}S_2)(acac)_4]$.

2.6.4.2 $[Sr_2Nb_2O(thd)_3(OEt)_9(EtOH)_3]$ and $[Sr_2Nb_2O(thd)_3(O^nPr)_9(^nPrOH)_3]$

A paper following the structural transformations of a number of individual single-source precursors on microhydrolysis and traced structural principles in the formation of oligonuclear oxo-alkoxide "clusters" was published in 2008 by Seisenbaeva *et al.*[69] The structures of these products result from a thermodynamically driven self-assembly of metal cations and ligands directed towards the most densely packed cores. The ratio between the metal cations and the cations to bidentate heteroligands, can simply be changed to alter the packing density. The objective was to investigate the heteroleptic metal alkoxide oxcoclusters as molecular models for the sol-gel synthesis of perovskite nanoparticles for bio-imaging applications.

[69] G. A. Seisenbaeva, V. G. Kessler, R. Pazik, W. Strek, *Dalton Trans.*, 3412, 2008.

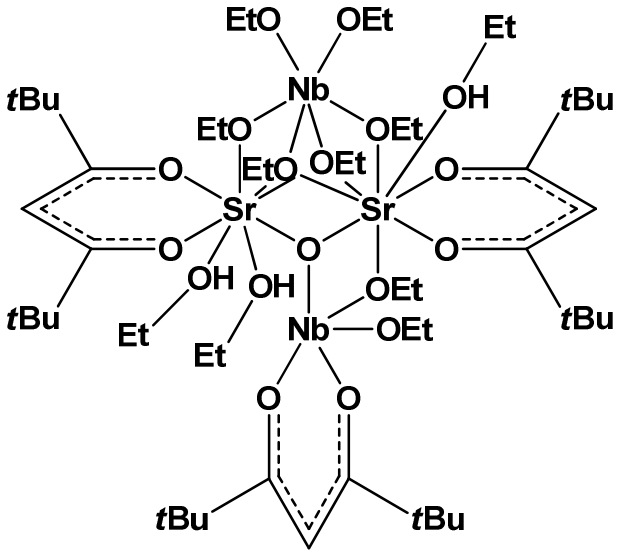

Figure 2.11: Structure of $[Sr_2Nb_2O(thd)_3(OEt)_9(EtOH)_3]$.

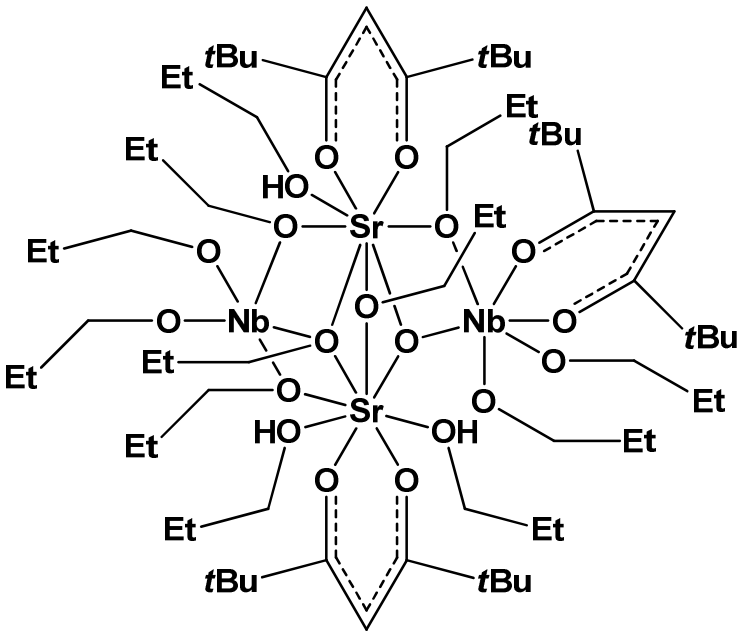

Figure 2.12: Structure of $[Sr_2Nb_2O(thd)_3(O^nPr)_9(^nPrOH)_3$.

2.7 Alkoxides

Specific knowledge of the nature of the species formed in alcoholic solutions of metal ions is essential for the manufacture of the final product. Metal alkoxides have the general formula $M(OR)_x$, where M is the metal with a valence *x* and O is the oxygen atom that connects the alkyl group (R) to the metal at each valence site. Metal alkoxides are usually very reactive species due to the presence of the electronegative alkoxy groups that make the metal atoms susceptible to nucleophilic attack.

The properties of metal alkoxides are mainly determined by the shape and size of the alkyl group (R) as well as by the stereochemistry, valency, atomic radius and coordination number of the metal. Based on the high electronegativity of oxygen, the M-OR bonds are expected to possess fundamental ionic character.

According to Bradley's concept,[70] alkoxides with the lower primary or secondary alkyl groups have a strong tendency towards polymerization, creating coordination polymers $[M(OR)_x]_n$ (where n is the degree of polymerization). The magnitude of polymerization is dependent on the following factors:[71]

- Aggregation increases as the metal atom becomes more electron deficient.

- The larger the size of the metal atom, the greater the tendency to increase the degree of association by forming alkoxo bridges.

- The steric effects of the alkyl substituents. They inhibit aggregation with an increase in steric demand and have been found to be of greater importance than the electronic nature of the substituents in determining the final extent of aggregation.

2.7.1 Preparation of Metal alkoxides

Various methods are available for the preparation of metal alkoxides. The choice of synthesis depends on the ionisation energy of the metal. The less electronegative

[70] D. C. Bradley, *Nature*, 182, 1211, 1958.
[71] D. C. Bradley, R. C. Mehrotra, D. P. Gaur, *Metal Alkoxides,* Academic Press, London, 1978.

metal react spontaneously with alcohols, but other metals need an activation agent or more complex reactions need to be applied. The general methods for synthesis can be summarized as follows[72]:

- Direct reactions of metals with alcohols: This method is the most used one in laboratories. It is based on substitution of the hydroxyl hydrogen by a suitable metal cation, accompanied by intense heat and H_2 evolution

$$M + (1 + x)\ ROH \rightarrow 1/y\ [MOR{\cdot}xROH]_y + 1/2\ H_2 \quad (\mathbf{2.4})$$

(y indicates the degree of polymerization)

- Reactions of metal halides with alcohols: The reaction leads to the substitution of a halide anion by a RO^- group, forming the corresponding alkoxide:

$$MCl_z + (x + y)\ ROH \rightarrow MCl_{z-x}(OR)_x(ROH)_y + x HCl \quad (\mathbf{2.5})$$

- Reactions of metal oxides and hydroxides with alcohols: Metal oxides and hydroxides react with alcohols to form the appropriate alkoxide and water:

$$MO_x + 2x\ ROH \rightarrow M(OR)_{2x} + x\ H_2O \quad (\mathbf{2.6})$$

$$M(OH)_x + x\ ROH \rightarrow M(OR)_x + x\ H_2O \quad (\mathbf{2.7})$$

- Reactions of alcohols with organometallics: These reactions are useful for the synthesis of mono- and mixed-metal alkoxides. The drawback of this reaction is that most organometallics are air/moisture sensitive and complicates the the reaction conditions:

$$MR_2 + R'OH \rightarrow 1/x\ [MOR']_x + RH \quad (\mathbf{2.8})$$

$$MR_3 + R'OH \rightarrow 1/x\ [R_2MOR']_x + RH \quad (\mathbf{2.9})$$

$$R_2MX + M'OR \rightarrow 1/x\ [R_2MOR']_x + M'X \quad (\mathbf{2.10})$$

- Alcohol interchange reactions: The activity of metal alkoxides in the substitution reactions of alkoxo groups is one of their characteristic properties:

$$M(OR)_x + y\ R'OH \rightarrow M(OR)_{x-y}(OR')_y + y\ ROH \quad (\mathbf{2.11})$$

[72] L. John, *Alkoxo Metal Complexes as Precursors for new Oxide Materials*, Faculty of Chemistry, University of Wroclaw, Poland, 72, 2008.

- ❖ Reactions of dialkylamides with alcohols: Dialkylamides, $M(NR_2)_x$ (R = Me, Et, $SiMe_3$), react with alcohols according to the equation below:

$$M(NR_2)_x + x\ R'OH \rightarrow M(OR')_x + x\ R_2NH \qquad (\mathbf{2.12})$$

2.7.2 Niobium alkoxides

Knowledge of niobium and tantalum alkoxides is almost exclusively limited to those in which the metal is in the +5 oxidation state. In solution these alkoxides exist in equilibrium between the monomeric, $M(OR)_x$, and dimeric ,$M_2(OR)_{10}$, forms with the ratio of monomer to dimer depending on the solvent, temperature and on the R group. A few Nb(IV) alkoxide complexes have been reported. Many of these are products of the reduction of $NbCl_5$ in alcohols, though several were prepared by the reaction of alcohols with other Nb(IV) compounds.[73,74]

The process of niobium and tantalum homoleptic alkoxides starts with the metal chlorides. The reaction of niobium pentachloride with alcohol in the presence of ammonia was described by Bradley *et al.*[75] Firstly, the $NbCl_5$ is dissolved in an organic solvent (benzene) then the alcohol is added, resulting in a vigorous reaction. Secondly, an excess of ammonia is added to the reaction mixture. This forms the desired niobium homoleptic alkoxide which is isolated by distillation after ammonium chloride is removed by filtration.

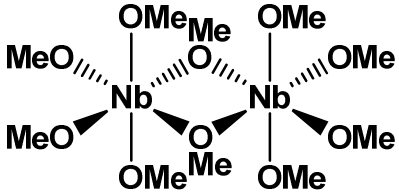

Figure 2.13: Structure of $[Nb(OMe)_5]_2$.

The methoxides and ethoxides of tantalum are more volatile than the niobium counterparts whereas for higher *n*-alkoxides, the reverse is true. With increasing chain length the volatility of both niobium and tantalum alkoxides decrease.

[73] F. A. Cotton, M. P. Diebold, W. J. Roth, *Inorg. Chem.*, **26**, 3323, 1987.
[74] M. Melnik, P. Sharrock, *Can. J. Chem.*, **63**, 57, 1985.
[75] D. C. Bradley, B. N. Chakravarti, W. Wardlaw, *J. Chem. Soc.*, 2381, 1956.

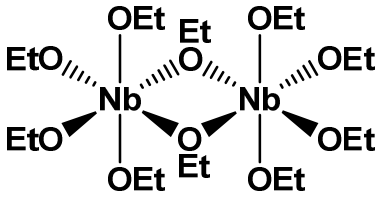

Figure 2.14: Structure of $[Nb(OEt)_5]_2$.

The sensitivity of metal chlorides towards alcohols decreases with the progressing electropositive character of the metal. An exothermic reaction occurs when $NbCl_5$ is added to an alcohol, producing a niobium chloride alkoxide as displayed below[76]:

$$NbCl_5 + 3\ ROH \rightarrow NbCl_2(OR)_3 + 3\ HCl \qquad (\mathbf{2.13})$$

The replacement of the chlorides by the methoxide groups does not proceed to completion without the addition of an activating agent like ammonia. Comprehensive studies have been carried out for $NbCl_5$ complexes with ROH (R = Me, Et, Pr) in the solid state to determine influencing factors and products formed.

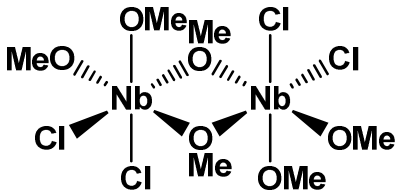

Figure 2.15: Structure of $[NbCl_2(OMe)_3]_2$.

2.7.3 ^{93}Nb-NMR Studies

Karaliota *et al.*[77] found that the molecular constitution of the methanol solutions is dependent on the $NbCl_5$ concentration, the temperature and storage time. ^{1}H-, ^{13}C- and ^{93}Nb-NMR spectroscopy was used to identify the substitution products formed in the solvolysis of $NbCl_5$ by MeOD. The chloro-methoxo complexes contain bridging methoxo groups and act as precursors for the formation of organic products like MeCl and Me_2O. Results confirmed previous reports[78,79] that only $[NbCl_2(OMe)_3]$ is formed in non-polar solvents. Their investigation also indicated that the formation of

[76] C. Sanchez, J. Livage, M. Henry, F. Babonneau, *J. Non-Cryst. Solids*, **100**, p65, 1988.
[77] A. Karaliota, M, Kamariotaki, D, Hatzipanayioti, *Transition Met. Chem.*, **22**, 411, 1997.
[78] L. Hubert-Pfalzgraf, A. Pinkerton, J. Riess, *Inorg. Chem.*, **17**, 663, 1978.
[79] C. Alquier, M. T. Vanderborre, M. Henry, *J. Non-Cryst. Solids*, **79**, 383, 1986.

other $NbCl_{5-x}(OMe)_x$ products is heavily dependent on the storage time of the sample as indicated in Table **2.5**. The number of coordinated MeO groups per metal atom was calculated from the integrals of peaks corresponding to terminal-MeO (MeO-ter) and briging-MeO (MeO-br) using ^{1}H NMR spectroscopy.

In the NMR experiments the ratio MeO-coordinated**/**Nb was calculated as follows, such that α is a percentage and the quantities in the square brackets are the NMR integrals:

$$\mathrm{MeO_{coord}} \,/\, \mathrm{Nb} = \alpha \times (\text{initial moles of MeOD}) \,/\, (\text{moles of Nb})$$

$$\alpha = [\mathrm{MeO_{coord}}]$$

$$= \frac{[\mathrm{MeO{-}ter}] + [\mathrm{MeO{-}br}]}{[\mathrm{MeOD{-}free}]} \times 100 \qquad (\mathbf{2.14})$$

From the ^{1}H NMR spectrum, the number of coordinated MeO groups (terminal and bridging) was calculated per metal atom. As seen in Table **2.5**, the ratio MeO_{coord}/Nb decreases with an increase in $NbCl_5$ concentration. The decrease in MeO_{coord}/Nb is due to the conversion of methoxo groups into Me_2O and MeCl, but the percentage of free methanol remains the same, indicating that the MeCl was derived from the coordinated methoxide groups.

The ^{93}Nb NMR spectra of $NbCl_5$ in MeOD (1.18 M) over time, is displayed in Figure **2.16** (at 4 °C). The two bands at -500 and -850 ppm are assigned to $[NbCl_4(OMe)]$ and $[NbCl_2(OMe)_3]$ respectively.[80,81,82] After considerable time a broad band appeared in the -600 to -800 ppm region with a shoulder on the side at -850 ppm (Figure **2.16**). These resonances were attributed to species with a higher number of oxygens around the Nb centre. After 37 days the solution was heated to 50 °C, then cooled to 25 °C and a band at -1100 ppm was observed. This could be due to the coordination of 5 methoxo groups per Nb centre or the coordination of four methoxo groups and a Nb=O group.

[80] G. R. Lee, J. Crayston, *Dalton Trans.*, 3073, 1991.
[81] R. Idd, H. Spinney, *Inorg. Chem.*, **12**, 1967, 1973.
[82] C. Jameson, D. Pehder, M. Hoch, *Inorg. Chem.*, **27**, 3490, 1988.

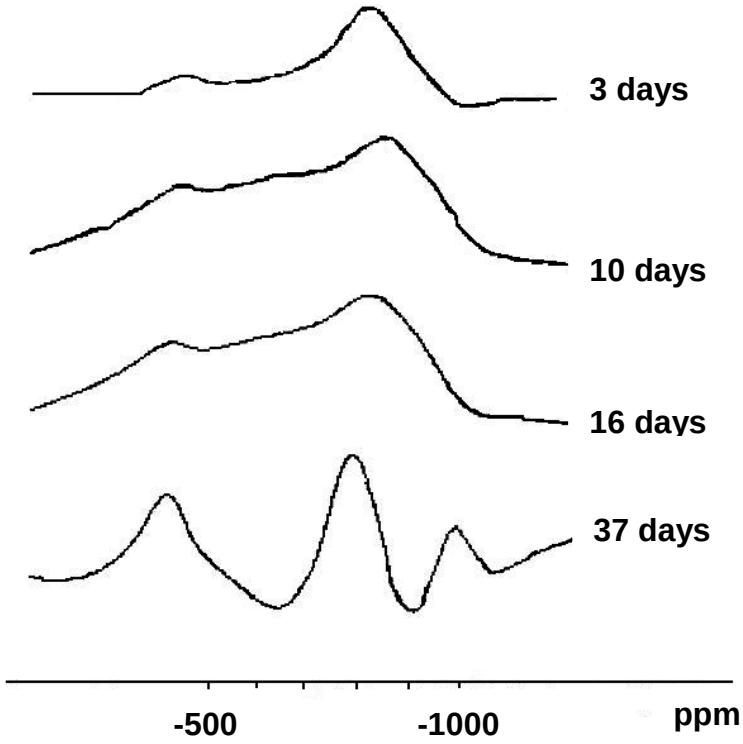

Figure 2.16: ^{93}Nb NMR spectra of a solution of $NbCl_5$ (1.18M) in MeOD run at different storage times.[78]

Table 2.5: The influence of concentration and storage time on the alcoholysis of $NbCl_5$.[78]

Sample $NbCl_5$	Concentration (M)	Time (days)	MeO-coord	MeO-br	MeO-ter	OH (ppm)
1a	0.185	0	-	-	-	5.8
1b		10	5	-	-	5.8
2a	0.85	0	3.1	0.696	2.4	7.9
2b		10	3.2	0.75	2.5	7.8
3a	1.15	0	3.4	1.2	2.4	8.3
3b		12	2.5	0.5	2	7.6
3c		49	1.6	0.16	1.43	7.1
4a	1.18	10	2.8	0.63	2.2	7.8
4b		16	2.7	0.56	2.14	7.7
4c		37	2.3	0.39	1.92	7.4

In 1991 Lee *et al*.[83] published a paper where they used ^{93}Nb- and ^{1}H NMR spectroscopy to investigate the different substitution products of $[NbCl_{5-x}(OMe)_x]$ that forms in the stepwise substitution of $NbCl_5$ by MeOH in non co-ordinating solvents. Their results confirmed Schönherr's *et al.*[84] results that only $[NbCl_2(OMe)_3]$ is formed on adding an excess MeOH to $NbCl_5$ in non-polar solvents.

To validate their results they isolated and characterized $[NbCl_4(OMe)]$, $[NbCl_2(OMe)_3]$ and $[Nb(OMe)_5]$ as reference samples. They did not isolate $[NbCl_3(OMe)_2]$ as it readily disproportionates to form $[NbCl_2(OMe)_3]$ and $[NbCl_4(OMe)]$. This is due to the lower solubility of $[NbCl_4(OMe)]$ and the stability of $[NbCl_2(OMe)_3]$. The coordination of $NbCl_5$ with MeOH in different aromatic solvents was followed by ^{93}Nb NMR and compared to the relative reference peaks. The results are presented in Table **2.6.**

Table 2.6: Assignment of ^{93}Nb NMR signals to $NbCl_{5-x}(OMe)_x$ species.[84]

Solvent	$x = 0$	$x = 1$	$x = 3$	$x = 4$	$x = 5$
Benzene	2.6	-497	-810	-1010	-1160
Toluene	2	-495	-810	-	-1150
Methanol	-0.5	-480	-820	-1015	-1155
Ethanol	-	-470	-830	-1020	-1180
Isopropanol	-	-470	-830	-1025	-1135
Acetonitrile	-	-495 / -560	-850	-	-1160

2.8 Kinetic Studies of Niobium Complexes

Antiñolo *et al*.[85] published a paper in 2000 in which they studied the reaction of niobium alkoxo complexes with different β-diketones. The β-diketones of choice was *t*BuCOCH$_2$CO*t*Bu (Hdpm), PhCOCH$_2$COPh (Hdbm) and acacH. They followed the kinetics of the displacement reaction of $[NbCl_2(OEt)_2(dpm)]$ (complex **1)** and $[NbCl_2(OEt)_2(dbm)]$ (complex **2**) with acacH to give $[NbCl_2(OEt)_2(acac)]$ as seen in Figure **2.17**.

[83] G. R. Lee, J. A. Crayston, *Dalton Trans.*, 3073, 1991.
[84] M. Schönherr, L. Kolditz, *Z. Chem.*, **10**, 72, 1970.
[85] A. Antiñolo, F. Carrillo-Hermosilla, J. Fernández-Baeza, S. Garcia-Yuste, A. Otera, E. Palomares, A. M. Rodriguez, L. F. Sánchez-Barba, *J. Organomet. Chem.*, 603, 194, 2000.

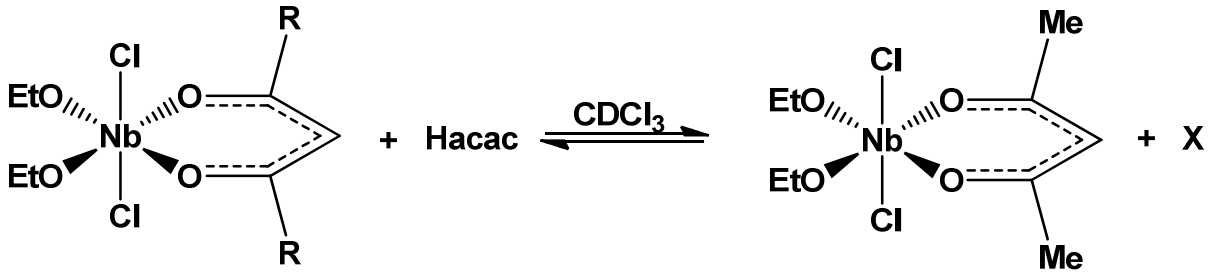

1: R = *t*Bu, X = Hdpm

2: R = Ph, X = Hdbm

Figure 2.17: Displacement reaction of **1** and **2** with Hacac.

Kinetic studies on the exchange processes were carried out by following the reactions as a function of time and temperature by ^{1}H-NMR spectroscopy. The molar ratios for [Hacac]/[Complex **1** or **2**] were varied from 1:1 up to 7:1. They observed a negligible dependence on the rate constant for ratios greater than 4:1. Accordingly a pseudo-first-order dissociative process was proposed with the formation of a pentacoordinated and electronically unsaturated species as the rate-limiting step. The proposed mechanism is displayed in Scheme **2.1**. The calculated values of the *pseudo*-first-order rate constants, k_{app}, at five temperature values are displayed in Table **2.7**.

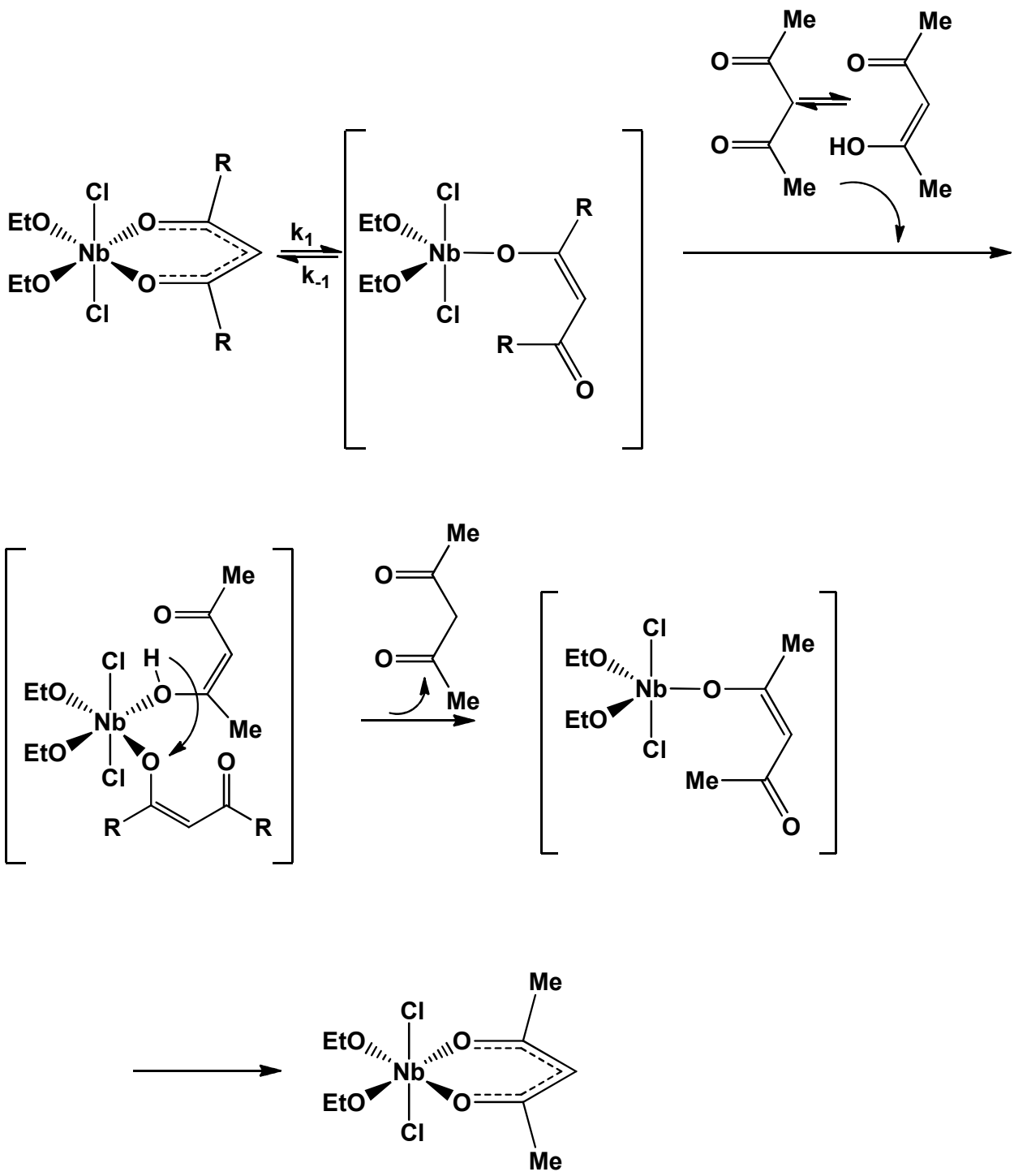

Scheme 2.1: Proposed mechanism on the displacement of **1** and **2** with acacH.[86]

Table 2.7: Kinetic and thermodynamic parameters on the displacement reactions of complex **1** and **2** with Hacac.[86]

Experiment	k_{app} x 10^3 (s^{-1})	T (K)	E_a (kJ.mol^{-1})	$\Delta H^{\ddagger}$ (kJ.mol^{-1})	$\Delta S^{\ddagger}$ (J.mol^{-1}.K^{-1})
1	0.3 ± 0.2 0.6 ± 0.2 1.2 ± 0.2 2.1 ± 0.2 3.1 ± 0.2	293 298 303 308 313	90.3 ± 0.1	87.8 ± 0.1	-11 ± 4
2	0.1 ± 0.2 0.2 ± 0.2 0.5 ± 0.2 0.9 ± 0.2 1.5 ± 0.2	293 298 303 308 313	105.5 ± 0.1	102.9 ± 0.1	31 ± 4

The k_{app} values were fit to the Arrhenius plot, $k_{app} = A_{exp}(-E_a/RT)$, and the E_a values for the two processes were calculated (Table **2.7**). The activation parameters, $\Delta H^{\ddagger}$ and $\Delta S^{\ddagger}$, were determined from the Eyring plot. The differences in the activation energy of the two processes were attributed to the more stable bond between the dbm ligand and the niobium atom in complex **2**, through a delocalized π system due to the phenyl rings of the ligand, than in complex **1** with the dpm ligand

In 2003 Aresta *et al.*[86] published an article on CO_2 insertion into Nb-OR bonds of various $Nb(OR)_5$ (R = Me, Et, allyl) complexes. Their study also included the absorption kinetics of CO_2 insertion into $Nb(OEt)_5$. As mentioned before, the niobium penta-alkoxo complexes are dimeric in the solid state and in solution. They conducted a ^{1}H NMR investigation and found that $[Nb(OEt)_5]_2$ undergoes a dissociation equilibrium in solution. The dissociation equilibrium (K_{eq}) was calculated as 2.07 x 10^{-4}.

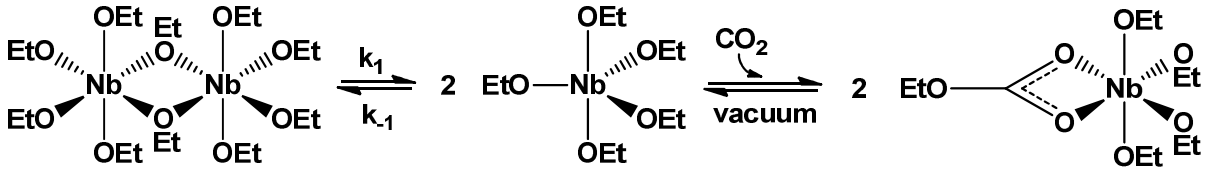

Figure 2.18: Reaction of niobium penta ethoxide with CO_2.

[86] M. Aresta, A. Dibenedetto, C. Pastore, *Inorg. Chem.*, **42**, 10, 3256, 2003.

The hemicarbonate formed in the CO_2 insertion reaction can function as a η^1-monodentate ligand (**a**), a η^2-bidentate ligand (**b**) or a η^2-μ^2 ligand (**c**), bridging two metal centers as displayed in Figure **2.19**:

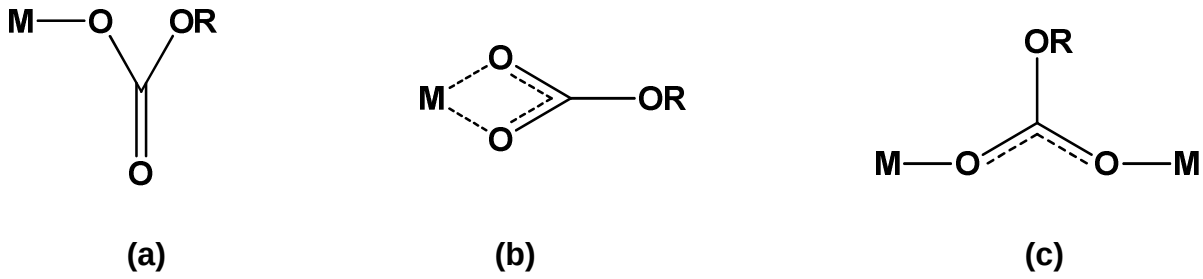

(a) **(b)** **(c)**

Figure 2.19: Mode of bonding of hemicarbonate.

The kinetics of absorption of CO_2 by $[Nb(OEt)_5]_2$ was done in EtOH and benzene that had been saturated with CO_2 in an absorption cell connected to a gas buret. The gas adsorption was monitored for 70 h at 298 K. The reaction was stopped when the CO_2 uptake reached 0.9 mol/(mol niobium) and the product was isolated and confirmed to be $[Nb(OEt)_4(OC(O)OEt)]$.

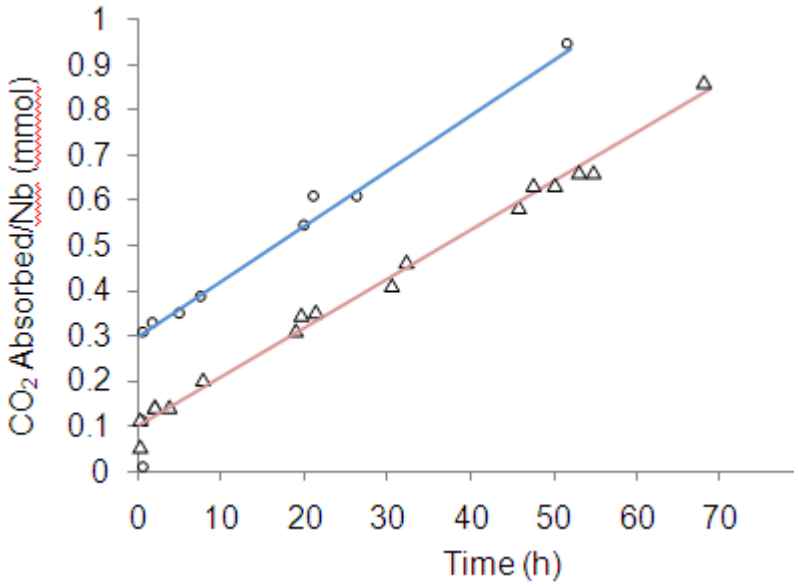

Figure 2.20: Kinetics of absorption of CO_2 by $[Nb(OEt)_5]_2$ in ethanol (blue) and benzene (red).[87]

A slower rate was observed in benzene than in ethanol. The reason for this is that alcohol favours the conversion of the dimer to the monomer.[87] The absorption curves illustrate the fast absorption of CO_2 during the first few minutes, followed by a slow continuous absorption over several hours. This is displayed by both the ethanol and benzene solutions. This supports the hypothesis that the carboxylation of the monomer is faster than the dissociation of the dimer.

$$V_{carb} = k_2[Nb(OEt)_5][CO_2] \qquad (\mathbf{2.15})$$

Second order kinetics was determined for the carboxylation reaction of $[Nb(OEt)_5]_2$ (Eq. **2.15**). k_2 was calculated as 1.19×10^{-1} $l.mol^{-1}.s^{-1}$ for the first part of the absorption curve, that is the carboxylation step. The same value was determined for both the ethanol and benzene solutions. The second part of the curve was used to calculate the dissociation process. The k_1 value in ethanol was determined as 1.15×10^{-5} s^{-1} and that for benzene was determined as 0.97×10^{-5} s^{-1}.

The insertion of CO_2 into the Nb-OEt bond was found to be reversible. The CO_2 was released by the hemicarbonate under vacuum. This was confirmed by the fact that the IR signal due to the carbonate group disappeared and the starting complex ($[Nb(OEt)_5]_2$) was quantitatively regenerated.

2.9 Conclusion

Most of the work done on niobium focuses on the +5 oxidation state. The syntheses of these complexes are complicated due to the metal's affinity to readily form oxides. A few niobium complexes have also been characterized to contain oxo bridges. Relatively few papers have been published on the kinetics of niobium complexes. From literature, it is clear that there is a significant need for research in the separation of niobium and tantalum without the use of HF.

[87] D. C. Bradley, C. E. Holloway, *J. Chem. Soc.*, 219, 1968.

3. Synthesis and Characterisation of Niobium(V) Complexes

Synopsis...

In this chapter the major characterisation techniques employed in this study as well as the detailed synthetic procedures of several metal complexes are described.

oooooooooooooo

3.1 Introduction

All of the niobium complexes synthesized was characterised using various techniques, including nuclear magnetic resonance (NMR), ultraviolet-visible (UV-Vis) and infrared (IR) spectroscopy. Single Crystal X-ray crystallography (XRD) was also used for characterisation when crystals, suitable for this technique, could be isolated. A detailed discussion of the complexes studied by this technique is given separately in Chapter **4**. Brief discussions on these basic techniques are included, as well as some basic principles of chemical kinetics which serves as an introduction to the kinetics addressed in Chapter **5**.

3.2 Nuclear Magnetic Resonance Spectroscopy (NMR)

NMR is a spectroscopic technique that relies on the magnetic properties of the atomic nucleus. When placed in a strong magnetic field, certain nuclei resonate at a particular frequency in the radio frequency range. From the small variations in the resonant frequency, detailed information about the molecular structure in which the atom resides can be obtained.[1]

[1] N. E. Jacobsen, *NMR Spectroscopy Explained,* Wiley and Sons, New Jersey, 1, 2007,

Electrons, neutrons and protons are considered to posses spinning properties and when these spins are paired against each other, the overall spin of the atom can be determined. The rules for determining the overall spin (*I*) of a nucleus are as follows:

i. If the number of protons and neutrons are both even, the nucleus has no spin.
ii. If the number of protons plus the number of neutrons is odd, the nucleus has a half-integer spin (1/2, 3/2, 5/2).
iii. If the number of protons and the number of neutrons are both odd, the nucleus has an integer spin (1, 2, 3).

According to quantum mechanics, a nucleus of spin *I* will have 2*I* + 1 possible orientations.[2] Hence, a nucleus (^{1}H) with spin 1/2 will have 2 possible orientations. When no external magnetic field is applied, the spin orientations are of equal energy. In the presence of a magnetic field, the energy levels are split. Each level has a magnetic quantum number (*m*) as indicated in Figure **3.1**.

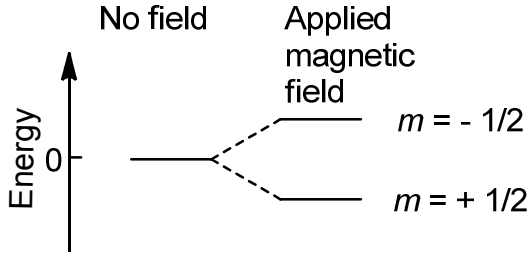

Figure 3.1: Energy levels for a nucleus with spin quantum number 1/2.

The spin state +1/2 has the lowest energy as it is aligned with the applied magnetic field, whereas the –1/2 spin state has higher energy because it is opposed to the applied field. The two spin states are separated by an energy difference, ΔE, which is dependent on the strength of the magnetic field as well as the size of the nuclear magnetic moment. The difference in energy between the levels can be determined from:

$$\Delta E = \frac{\gamma\, h\, B}{2\,\pi} \qquad (\mathbf{3.1})$$

[2] P.J. Hore, *Nuclear Magnetic Resonance*, Oxford University Press, New York, 52, 1995.

with γ = magnetogyric ratio, *h* = Planck's constant and B = strength of the magnetic field at the nucleus. The spinning nucleus generates a small magnetic field which causes it to possess a magnetic moment (*μ*):

$$\mu = \frac{\gamma I h}{2 \pi} \qquad (\mathbf{3.2})$$

The magnetic moment has both magnitude and direction as defined by its axis of spin. In the presence of a magnetic field, the nucleus's axis of spin will precess around the magnetic field. The frequency of this precession is called the Larmor frequency and it is identical to the transition frequency:

$$E = -\mu B \cos\theta \qquad (\mathbf{3.3})$$

where θ is the angle between the direction of the applied field and the axis of nuclear rotation. The angle will change if the nucleus absorbs energy. In a nucleus with a spin 1/2, the absorption of radiation will "flip" the magnetic moment so that it will oppose the applied magnetic field.

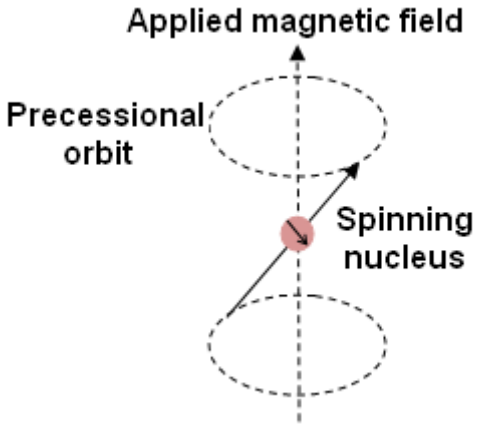

Figure 3.2: Axis of rotation precessing around the magnetic field.

The magnetic field experienced at the nucleus is not equal to the applied magnetic field due to shielding from the electrons around the nucleus. If the electron density around the nucleus is high, the induced field experienced by the nucleus is stronger due to the electrons. The reverse is true if the electron density decreases. Deshielding occurs due to electron withdrawing groups and shielding results from electron donating groups.

The multiplicity of a multiplet is given by the number of equivalent protons in neighbouring atoms plus one (n + 1). Equivalent nuclei do not interact with each other and can only cause splitting of neighbouring protons. The signal splitting is a consequence of indirect spin-spin coupling. The distances between the peaks of a multiplet is called the coupling constant (J) and is measured in hertz (Hz).[3]

3.3 Ultraviolet/visible Spectroscopy (UV/Vis)

The ultraviolet region falls in the range between 190 – 380 nm and the visible region between 380 – 750 nm. Most commercial spectrophotometers cover a spectral range of 185 – 900 nm.[4] Ultraviolet and visible radiation interacts with atoms which causes electronic transitions. The following electronic transitions are possible:

- $\pi \rightarrow \pi^*$
- $n \rightarrow \pi^*$
- $\sigma \rightarrow \sigma^*$
- $n \rightarrow \sigma^*$

A molecule can absorb light and then transfer that energy by promoting electrons to higher energy levels from the ground state (highest occupied molecular orbital – HOMO) to the excited state (lowest unoccupied molecular orbital – LUMO). Three types of molecular orbitals exist, bonding (σ or π), non-bonding (n) and anti-bonding (σ^* or π^*). The electrons are generally present in the bonding orbitals, or non-bonding orbitals if they are lone pairs, and are excited to the anti-bonding orbitals. An absorbance spectrum simply depicts what wavelength of light is absorbed by a sample.

3.4 Infrared Spectroscopy (IR)

IR is used to gather information about the structure of a compound and as an analytical tool to assess the purity of a compound. Infrared refers to that part of the

[3] E. Breitmaier, G. Bauer, *^{13}C NMR Spectroscopy*, Vol 3, Harwood Academic Publishers, London, 3, 1984.
[4] F. Rouessac, A. Rouessac, *Chemical Analysis: Modern Instrumentation Methods and Techniques*, 2nd Ed, Wiley and Sons, New York, 167, 2007.

electromagnetic spectrum between the visible and microwave regions and this area is divided into three regions: near (14 000 – 4 000 cm^{-1}), mid (4 000 – 400 cm^{-1}) and far (400 – 10 cm^{-1}) IR. The technique is based on the vibrations of atoms of a molecule. Important parameters are the frequency (*v*), wavelength (λ, length of 1 wave) and wavenumber ($\bar{\nu}$, number of waves per unit length) and they are related to one another by the following equation[5]. Here, *c* is the speed of light and *n* the refractive index of the medium it is passing through:

$$\bar{\nu} = \frac{\mathrm{v}}{(c/\mathrm{n})} = \frac{1}{\lambda} \qquad (\mathbf{3.4})$$

A spectrum is obtained by passing infrared radiation through a sample and determining the fraction of incident radiation that is absorbed at a specific energy. Radiation is considered as two perpendicular electric and magnetic fields, oscillating in a single plane. This radiation can be regarded as a stream of particles for which the energy (*E*) can be calculated as follows. Where *h* is the Planck constant (*h* = 6.626 x 10^{-34} J.s).

$$E = hv \qquad (\mathbf{3.5})$$

Two important characteristics to the process are the radiation frequency and the molecular dipole moment (μ). The interaction of radiation with molecules involves a resonance condition where the specific oscillating radiation frequency matches the natural frequency of a particular normal mode of vibration. The molecular vibration must cause a change in the dipole moment of the molecule in order for the energy to be transferred from the IR photon to the molecule, via absorption[6].

IR spectroscopy depends on the specific frequencies at which chemical bonds vibrate or rotate. Chemical bonds can be excited by IR radiation to cause bond "stretching" (high energy) or bond "bending" (low energy) vibrations. This stretching or bending of bonds can be classified into various vibrational modes.[7] In the case of stretching, the modes can either be symmetrical or asymmetrical. The modes of bending include rocking, scissoring, wagging and twisting. As a rule, the stretching

[5] B. H. Stuart, *Infrared Spectroscopy: Fundamentals and Applications*, Wiley and Sons, New York, 3, 2004.
[6] D. N. Sathyanarayana, *Vibrational Spectroscopy: Theory and Applications*, New Age International, New Delhi, 44, 2004.
[7] L. D. Field, S. Sternhell, J. R. Kalman, *Organic Structures from Spectra*, 4th Ed, Wiley and Sons, New York, 15, 2007.

vibrations for shorter and stronger bonds generally occur at the higher energy end (shorter wavelength) of the IR spectrum than the longer and weaker bonds. In addition, bonds to lighter atoms also vibrate at a higher energy than bonds to heavier atoms.

3.5 X-Ray Diffraction (XRD)

Most of the knowledge about crystal structures comes from X-ray diffraction. Diffraction is the bending or scattering of a wave as it passes an obstacle. X-rays are a form of electromagnetic radiation and are useful for probing crystalline solids as their wavelengths are in the same range as that of atoms (10^{-10} m).[8] When an X-ray beam is focused on a crystal, the atoms within the crystal scatter the X-rays resulting in a pattern of constructive and destructive interference. Constructive interference results when waves are in phase and reinforce each other, while in destructive interference the waves are out of phase and cancel each other. These scattered beams create a diffraction pattern from which a three-dimensional picture of the electronegativity of the electrons is obtained.

In a crystalline compound all the atoms are arranged in a regular pattern. The repetition of the smallest volume element in three directions describes the crystal. This smallest volume element is known as a unit cell. The dimensions of the unit cell are described by three axes (a, b, c) and the angles between them; alpha, beta and gamma. The directions and planes in a crystal lattice are known as Miller indices (hkl). A given set of planes with indices h, k, l cut the a-axis of the unit cell in h sections, the b axis in k sections and the c axis in l sections. A zero indicates that the planes are parallel to the corresponding axis.[9]

[8] C. Suryanarayana, M. G. Norton, *X-ray Diffraction: A Practical Approach*, Springer, New York, 3, 1998.
[9] B. E. Warren, *X-ray Diffraction*, Courier Dover Publications, New York, 1, 1990.

3.5.1 Bragg's law

Bragg's law[10] defines the conditions under which diffraction occurs and gives the position of a diffracted beam without any reference to its intensity. X-rays are diffracted by "lattice planes" within a crystal. All X-rays reflected from a given plane are in phase after reflection. Neighboring plane X-rays travel different path lengths and are out of phase after reflection. Bragg's law is used to correct phase difference for diffracted rays by two adjacent planes:

$$n\lambda = 2d_{hkl}\sin\theta \qquad (\mathbf{3.6})$$

where n is an integer, λ is the wavelength of the radiation, d_{hkl} is the interplanar spacing of the (hkl) planes and θ is the diffraction angle (Bragg angle).

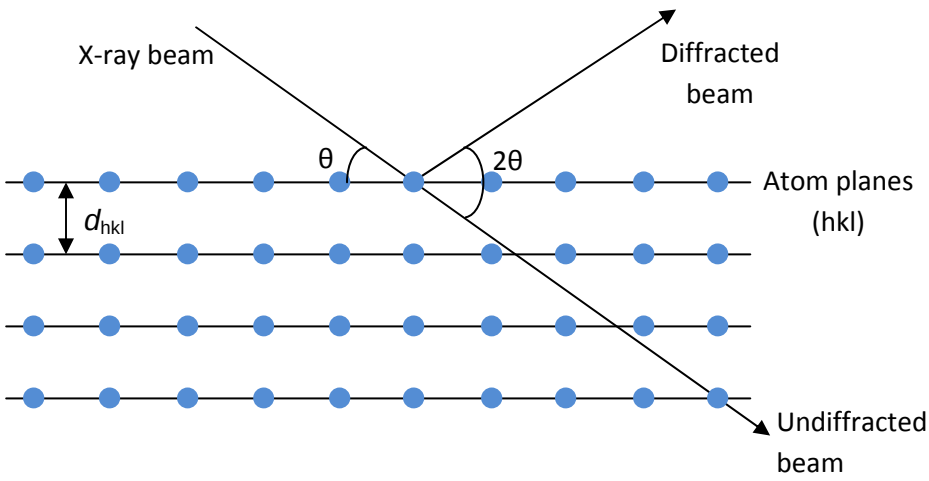

Figure 3.3: Diffraction of X-rays as proposed by Bragg.[11]

There are an infinite number of sets of atom planes within a crystal, and Bragg's law applies to all these. Subsequently, if a crystal is rotated in an X-ray beam, each set of planes will in turn diffract the radiation when the value of sin θ becomes appropriate. The part of the X-ray that is not reflected off the upper atomic plane with angle *θ* can pass on to the following plane and reflect at the same angle. The spacing between these lattice planes is represented as *d* and all X-rays reflected of a given plane are in phase afterwards. The arrangement of the diffracted beams gives

[10] D. Sherwood, J. Cooper, *Crystals, X-ray's and Proteins: Comprehensive Protein Crystallography*, Oxford University Press, New York, 291, 2011.

the diffraction pattern of the crystal. The d_{hkl} values can be obtained when the Bragg equation is applied to the diffraction data.[11]

3.5.2 Structure factor

The structure factor, *F*(hkl), of any diffracted X-ray (hkl) is the quantity that expresses both the amplitude and the phase of that reflection. The intensity of a diffracted beam is directly related to the amplitude of the structure factor, but the phase must normally be calculated by indirect means. In structure determination, phases are estimated and an initial description of the positions and anisotropic displacements of the scattering atoms is deduced. From this initial model, structure factors are calculated and compared with those experimentally observed. Iterative refinement procedures attempt to minimize the difference between calculation and experiment, until a satisfactory fit has been obtained. The total scattering of all atoms in the unit cell is given as:[12]

$$\boldsymbol{F}_{hkl} = \sum_{j=1}^{N} f_j \exp[i2\pi(hx_j + ky_j + lz_j) \quad (\mathbf{3.7})$$

where *fj* = scattering factor of each of the N atoms. This relation may be recast in terms of its amplitude, |*F*(*hkl*)|, and its phase angle, φ(*hkl*) or in terms of its real, *A*, and imaginary, *B* components in the following expressions:[13]

$$\boldsymbol{F}_{hkl} = |\boldsymbol{F}_{hkl}| \exp [i2\pi\, \varphi(hkl)] \quad (\mathbf{3.8})$$

$$\boldsymbol{F}_{hkl} = A + iB \quad (\mathbf{3.9})$$

The set of structure factors for all the reflections (hkl) are the primary quantities necessary for the derivation of the three dimensional distribution of electron density. When considering electron density the structure factor can be written as:

$$\boldsymbol{F}_{hkl} = \int p(x,y,z) \exp [i2\pi(hx_n + ky_n + lz_n)] dV \quad (\mathbf{3.10})$$

[11] R. J. D. Tilley, *Crystals and Crystal Structures*, Wiley and Sons, New York, 114, 2006.
[12] M. F. C. Ladd, R. A. Palmer, *Structure Determination by X-ray Crystallography*, Plenum Press, New York, 36, 1977.
[13] Y. Waseda, E. Matsubara, K. Shinoda, *X-ray Diffraction Crystallography*, Springer, Heidelberg, 109, 2011.

3.5.3 'Phase problem'

In order to form an image from the combined diffracted X-ray beams, 3 factors need to be known; the direction, amplitude and phase of each beam. By identifying the Miller indices of the crystal plane that gives rise to each diffracted beam, the direction of the beam can be specified. The amplitude of the beam can readily be deduced from the measured intensity. There is no practical way to determine the relative phase angles for the diffracted beams and consequently it has to be calculated in an indirect manner.[14]

3.5.3.1 Direct method

The direct method[15] resolves the approximate reflection phases from measured X-ray intensities *via* mathematical formulae. The direct method proves most useful for structures consisting only of light atoms. The Patterson function is used with compounds that contain heavier atoms.

3.5.3.2 Patterson method

The Patterson function, $P(u, v, w)$, is an auto-correlation function of the density.[16] When referring to the Patterson cell, the coordinates are u, v and w with dimensions identical to the real cell. A plot of the Patterson function delivers a map with peaks that correspond to interatomic vectors. The peak heights are proportional to the product of the two atoms between which the vector is found. From this map the position of the atoms relative to one another and the centre of the unit cell can be obtained. The Patterson peaks are a proportional indication of the size of the atoms involved.

$$\boldsymbol{P}_{(u,v,w)} = V^{-1}\sum_{hkl}(F_{hkl})^2 \exp[-i2\pi(hu + kv + lw)] \qquad (\mathbf{3.11})$$

[14] J. Als-Nielsen, D. McMorrow, *Elements of Modern X-ray Physics*, 2nd Ed, Wiley and Sons, West Sussex, 295, 2011.
[15] J. Lima-de-Faria, M. J. Buerger, *Historical Atlas of Crystallography*, Kluwer Academic Publishers, Dordrecht, 93, 1990.
[16] J. Drenth, *Principles of Protein X-ray Crystallography*, 2nd Ed, Springer, New York, 130, 1999.

3.5.4 Least-squares refinement

The least square refinement is a way of comparing the calculated diffraction pattern with the observed diffraction pattern. If the atoms of the model structure are in the approximate correct positions, then there should be a degree of resemblance between the calculated diffraction pattern and the observed one. The calculated structure factor (F_c) is compared to the experimental data (F_0) and described in terms of residual index or R-factor.

$$R = \frac{\Sigma\left||F_0|-|F_c|\right|}{\Sigma|F_0|} \qquad (\mathbf{3.12})$$

The value of the R-factor for a correct and complete crystal structure as determined from well measured experimental data is around 0.02-0.07.[17]

3.6 Chemical Kinetics

Chemical kinetics involves the study of the rate of chemical reactions and the mechanism by which they occur. Chemistry is concerned with the study of molecular structures, equilibria between these structures and the rates at which these structures are transformed into others. Spectrophotometry is often used to follow reaction kinetics as every molecule displays a different and unique absorption spectrum. From the Beer-Lambert law, the relationship of concentration to absorption can be found.[18]

$$\text{Log}_{10} = \frac{I_0}{I_{trs}} = \varepsilon c l = A \qquad (\mathbf{3.13})$$

with I_0 the intensity of the incident monochromatic light, I_{trs} the transmitted intensity, ε the extinction coefficient, c the concentration, l the pathlength and A the absorbance. The total absorbance of a solution is calculated by adding the individual absorbances of each species:

[17] J. P. Gluster, M. Lewis, M. Rossi, *Crystal Structure Analysis for Chemist and Biologists*, Wiley and Sons, New York, 389, 1994.
[18] E. T. Denisov, O. M. Sarkisov, G. I. Likhtenshtein, *Chemical Kinetics: Fundamentals and New Developments*, Elsevier, Amsterdam, 1, 2003.

$$A = \sum_1 \varepsilon cl \quad (\textbf{3.14})$$

In chemical kinetics, the rate constant and reaction mechanism can be influenced by a variety of factors such as temperature, pressure, concentration, homogeneity and sensitivity to air or light. If the system is kept at constant temperature, constant pressure and constant volume, the rate constant are now simply the rate of change in time of any of the reactants or products.

3.6.1 Reaction rate and rate laws

In a closed system, the rate of a chemical reaction can be defined as the change in concentration of a reactant or product per unit of time. The rate is defined as a positive quantity that is unaffected by the component whose concentration change is being measured. For a generalized chemical reaction:

$$a\text{A} + b\text{B} \rightarrow c\text{C} + d\text{D} \quad (\textbf{3.15})$$

The rate can be described as a derivative because the rate changes continually with time. Where t = time and the brackets indicate the concentration of the species:

$$\text{Rate} = \frac{-d[\text{A}]}{dt} = \frac{-d[\text{B}]}{dt} = \frac{d[\text{C}]}{dt} = \frac{d[\text{D}]}{dt} \quad (\textbf{3.16})$$

The negative signs indicate the disappearance of the compounds. In general, the rate of reaction can be a function of the concentration of all the species present in a reaction mixture. Where k is the rate constant and the exponents x and y represent the order of the reaction with regards to the concentration of A and B:

$$\text{Rate} = k[\text{A}]^x[\text{B}]^y \quad (\textbf{3.17})$$

The rate constant (k) is independent of the concentrations A and B, but is influenced by environmental factors such as solvent and temperature changes.

The order of the reaction is determined from the kinetic study and the sum of the exponents (Eq **3.17**) gives the total order of the reaction. Experimentally, great difficulty is experienced in the determination of these values and in order to overcome this problem, *pseudo*-first order conditions are used. Under these

conditions, one of the concentrations remain constant while the other varies, e.g. [A]>>>[B]. This simplifies Equation **3.17** to:

$$\text{Rate} = k_{obs}[A]^x \text{ and then } k_{obs} = k[B]^y \quad (\mathbf{3.18})$$

k_{obs} is the observed *pseudo*-first order rate constant. By varying the concentration of A, the rate constant of the reaction can be determined. The rate law for a second order reaction (where $x = y = 1$) is given by:

$$a[A] + b[B] \underset{k_2}{\overset{k_1}{\rightleftharpoons}} c[C] \quad (\mathbf{3.19})$$

$$\text{Rate} = k_1[A][B] + k_2[A] \quad (\mathbf{3.20})$$

k_{obs} under *pseudo*-first order conditions ([B]>>>[A]) is given by:

$$k_{obs} = k_1[B] + k_2 \quad (\mathbf{3.21})$$

The equilibrium constant for an equilibrium reaction, where k_1 represents the forward reaction and k_2 represents the reverse reaction, is given by:

$$K_{eq} = \frac{k_1}{k_2} \quad (\mathbf{3.22})$$

Integration of Equation **3.22** from t = 0 to t yields Equation **3.23**:

$$\ln\frac{[C]_t}{[C]_0} = k_{obs} \text{ or } [C]_t = [C]_0\, e^{k_{obs}t} \quad (\mathbf{3.23})$$

$[C]_t$ and $[C]_0$ represent the concentration change of the reactant at time = 0 and t respectively. Through the basic principles of the Beer-lambert law, expressing absorbance in terms of concentration, and a bit of mathematical manipulation, Equation **3.23** can be given as:

$$A_t = A_\infty - (A_\infty - A_0)e^{k_{obs}t} \quad (\mathbf{3.24})$$

where A_t = absorbance after time t and A_∞ = absorbance at infinite time (when reaction is complete). Absorbance versus time data can be used in a least-squares fit to give *k*obs for the reaction. The half-life ($t_{1/2}$) for a first order reaction, meaning the time needed for the reactant concentration to decay by 50%, will be:

$$t_{1/2} = \frac{\ln 2}{k_{obs}} = \frac{0.6932}{k_{obs}} \quad (\mathbf{3.25})$$

3.7 Synthesis and Spectroscopic Characterisation of Compounds

3.7.1 Chemicals and Instrumentation

All reagents used for the synthesis and characterisation were of analytical grade and were purchased from Sigma-Aldrich, South Africa, unless otherwise stated. Reagents were used as received, without further purification. All organic solvents were purified and dried according to literature.[19]

All the infrared spectra of the complexes were recorded on a Bruker Tensor 27 Standard System spectrophotometer with a laser range of 4 000 – 370 cm^{-1}, coupled to a computer. All samples were analyzed as solid state species *via* ATR infrared spectrophotometry and all data was recorded at room temperature. No solution or KX (where X = I, Cl, Br) solid salt pellets were utilized since halogen interaction was expected from the solution cell and the KX pellet preparation technique. All ^{1}H and ^{13}C NMR spectra were obtained in CD_3OD on a Bruker 300 MHz nuclear magnetic resonance spectrometer. Chemical shifts are reported relative to tetramethylsilane using the CD_3OD (^{1}H NMR: 3.31 ppm; ^{13}C NMR: 49.1 ppm) peak. All ^{93}Nb NMR spectra were obtained in CD_3OD on a Bruker 600 MHz nuclear magnetic resonance spectrometer. The applicable resonance frequency was located at 146.93 MHz

Elemental analysis could not be performed on the products obtained due to the sensitive nature of these crystals.

3.7.2 Synthetic Procedures

The syntheses of all the niobium compounds were performed under Schlenk conditions due to the air- and moisture sensitive nature of the metal. All product solutions were stored at -21 ℃ for possible crysta llization.

[19] D. D. Perrin, W. L. F. Armarego, *Purification of Laboratory Chemicals*, 3rd Ed., Pergamon Press, 1988.

3.7.2.1 Synthesis of [NbCl(acac)$(OMe)_3$]:

$[NbCl_5]_2$ (0.313 g, 0.58 mmol) was dissolved in methanol (5 ml). One molar equivalent of acacH (0.119 ml, 1.16 mmol) was added and the colourless solution was stirred for 30 minutes. White crystals were obtained from the colourless solution after 16h. **Yield:** 0.193 g (52 %). **IR (cm^{-1}):** ν(C–O) 1057, 1028; ν(C–H) 1343; ν(C=C) 1536. **UV/Vis (λ_{max}):** 323 nm. ε = 216 $cm^{-1}.M^{-1}$. **^{1}H NMR (methanol-*d_4*):** δ = 1.48 (s, 1H), 2.11 (s, 9H), 5.26 (s, 6H). **^{13}C NMR (methanol-*d_4*):** δ = 18.2, 21.6, 141.4, 197.7. **^{93}Nb NMR (methanol-*d_4*):** δ = -931.

3.7.2.2 Synthesis of [Nb(acac)$(OEt)_2(O)]_4$:

$[Nb(OEt)_5]$ (0.291 ml, 1.16 mmol) and one molar equivalent of acacH (0.119 ml, 1.16 mmol) was added together and the colourless solution was stirred for 30 minutes. Methanol (5 ml) was then added to the reaction mixture and again stirred for 30 minutes. A single, large colourless crystal was obtained after 3 weeks. **Yield:** 0.074 g (5 %). **IR (cm^{-1}):** ν(C–O) 1086, 1103; ν(C–H) 1357, 1434. **UV/Vis (λ_{max}):** 321 nm. ε = 443 $cm^{-1}.M^{-1}$. **^{1}H NMR (methanol-*d_4*):** δ = 1.09 (t, 24H), 2.12 (s, 24H), 3.57 (q, 16H). **^{13}C NMR (methanol-*d_4*):** δ = 18.9, 22.4, 25.9, 140.7, 179.8. **^{93}Nb NMR (methanol-*d_4*):** δ = -1108.

3.7.2.3 Synthesis of [NbCl(phacac)$(OMe)_3$] and [$NbCl_2$(phacac)$(OMe)_2$]:

$[NbCl_5]_2$ (0.313 g, 0.58 mmol) was dissolved in methanol (5 ml). One molar equivalent of phacacH (0.1891 g, 1.16 mmol) was added and the yellow solution was stirred for 3 hours. A yellow powder formed which was removed to give a colourless solution. Yellow crystals were obtained after 24h from the colourless solution. **Yield:** 0.256 g (58 %). **IR (cm^{-1}):** ν(C–O) 1106; ν(C–H) 1445; ν(C=C) 1581. **UV/Vis (λ_{max}):** 311 nm. ε = 624 $cm^{-1}.M^{-1}$. **^{1}H NMR (methanol-*d_4*):** δ = 1.59 (s, 1H), 2.19 (s, 3H), 2.32 (s, 3H), 4.95 (s, 9H), 7.17 (m, 3H), 7.52 (m, 3H), 7.94 (dd, 2H). **^{13}C NMR (methanol-*d_4*):** δ = 18.1, 21.6, 127.9, 128.6, 130.3, 144.5, 149.2, 182.8. **^{93}Nb NMR (methanol-*d_4*):** δ = -1076.

3.7.2.4 Synthesis of $[NbCl_4(acac)]$:

$[NbCl_5]_2$ (0.313 g, 0.58 mmol) was dissolved in tetrahydrofuran (5 ml) and formed a yellow solution. One molar equivalent of acacH (0.119 ml, 1.16 mmol) was added and the yellow solution changed colour to orange. The solution was stirred for 1 hour. Small, orange, needle-like crystals were obtained after 24 hours. **Yield:** 0.266 g (69 %). **IR (cm^{-1}):** v(C–O) 1138; v(C–H) 1334. **UV/Vis (λ_{max}):** 269 nm. ε = 482 $cm^{-1}.M^{-1}$. **^{1}H NMR (methanol-*d_4*):** δ = 1.59 (s, 1H), 2.21 (s, 6H). **^{13}C NMR (methanol-*d_4*):** δ = 19.2, 141.4, 179.5. **^{93}Nb NMR (methanol-*d_4*):** δ = -896.

3.7.2.5 Synthesis of $[NbCl_4(hfacac)]$:

$[NbCl_5]_2$ (0.313 g, 0.58 mmol) was dissolved in tetrahydrofuran (5 ml) and formed a yellow solution. One molar equivalent of hfacacH (0.164 ml, 1.16 mmol) was added and the dark yellow solution was stirred for 2 hours. An orange powder was obtained after 24h. **Yield:** 0.185 g (39 %). **IR (cm^{-1}):** v(C–O) 1033; v(C=C) 1603. **UV/Vis (λ_{max}):** 205 nm. ε = 386 $cm^{-1}.M^{-1}$. **^{1}H NMR (methanol-*d_4*):** δ = 1.67 (s, 1H). **^{13}C NMR (methanol-*d_4*):** δ = 123.4, 141.2, 180.2. **^{93}Nb NMR (methanol-*d_4*):** δ = -911.

3.7.2.6 Synthesis of $[NbCl(trop)(OMe)_3]$:

$[NbCl_5]_2$ (0.313 g, 0.58 mmol) was dissolved in tetrahydrofuran (8 ml). Tropolone (0.1417 g, 1.16 mmol) was added and the reaction mixture was stirred for 2 hours. A yellow precipitate formed and the tetrahydrofuran was removed in vacuo. The precipitate was partially dissolved in methanol (5 ml) and the remaining precipitate turned white. The yellow methanol solution was collected and the remaining precipitate was dissolved in toluene (6 ml) forming a colourless solution. After 48 hours the methanol solution formed a yellow powder and the toluene solution formed a white powder. The white powder obtained from the toluene solution was determined as the uncoordinated tropolone ligand. Further characterization was done on the yellow powder. **Yield:** 0.111 g (28 %). **IR (cm^{-1}):** v(C–O) 1172; v(C–H) 1323, 1401; v(C=C) 1519, 1522. **UV/Vis (λ_{max}):** 388 nm. ε = 443 $cm^{-1}.M^{-1}$. **^{1}H NMR (methanol-*d_4*):** δ = 5.18 (s, 9H), 6.84 (s, 1H), 7.47 (s, 5H). **^{13}C NMR (methanol-*d_4*):** δ = 17.8, 53.9, 106.4, 126.6, 127.5, 130.9, 131.1, 183.2. **^{93}Nb NMR (methanol-*d_4*):** δ = -964.

3.7.3 Discussion

A limited amount of structural information of niobium(V) mono coordinated to O,O'-bidentate complexes is available. Crystals suitable for X-ray crystallography were obtained for the first three synthesis reactions at -21.0 ℃ ([NbCl(acac)(OMe)$_3$], [Nb(acac)(OEt)$_2$(O)]$_4$, [NbCl(phacac)(OMe)$_3$] and [NbCl$_2$(phacac)(OMe)$_2$]). These reactions were also duplicated with an increase in the molar equivalents of ligand added, from two to five, but only the mono coordinated bidentate complexes were formed every time. All of the synthesized crystals decomposed quickly when exposed to air and elevated temperatures above 0 ℃. Selected crystals had to be synthesized repeatedly before stable enough samples could be collected for analysis on the X-Ray diffractometer. Subsequently, elemental analysis could not be performed due to the sensitive nature of the products. This was also confirmed by ^{1}H NMR of the products before and after environmental exposure.

The ^{1}H NMR results for [NbCl(phacac)(OMe)$_3$] and [NbCl$_2$(phacac)(OMe)$_2$] seems confusing at first glance, however two crystal structures were obtained from the same crystal. Hence two different species were observed on the ^{1}H and ^{13}C NMR spectrums. This is an extremely rare occurrence and is discussed in more detail in Chapter **4** (Section **4.5**).

The last three synthesis reactions ([NbCl$_4$(acac)], [NbCl$_4$(hfacac)] and [NbCl(trop)(OMe)$_3$]) either formed powders or crystals that were not suitable for analysis on the X-Ray diffractometer. Several attempts were made to recrystallize the products, but to no avail.

3.7.4 Conclusion

Four new niobium(V) complexes containing O,O'-bidentate ligands have been obtained and successfully characterized with IR, as well as ^{1}H-, ^{13}C- and ^{93}Nb NMR. The crystallographic characterisation of these crystals are discussed in detail in the next chapter.

4. Crystallographic Characterisation of Niobium(V) β-Diketonato Complexes

Synopsis...

A detailed discussion on the crystallographic characterisation of three novel crystal structures are given. Specific emphasis is placed on the structural properties of these complexes.

oooooooooooooo

4.1 Introduction

In this chapter the solid state characterisation of selected niobium(V) complexes containing O,O'-bidentate ligands is presented. The crystallographic structure determination of (acetylacetonato-κ^2-O,O')chloridotrimethoxidoniobium(V) (**1**), tetrakis(acetylacetonato-κ^2-O,O')octakis(etoxy)tetrakis(μ^2-oxo)tetraniobium(V) (**2**) and the two structures that were obtained from the same crystal, (1-phenyl-1,3-butanedionato-κ^2-O,O')chloridotrimethoxidoniobium(V) and (1-phenyl-1,3-butane-dionato-κ^2-O,O')dichloridodimethoxidoniobium(V) (**3a** and **3b**) are presented in detail. Positional parameters and all bond distances and angles are given in the supplementary data (Appendix **A**).

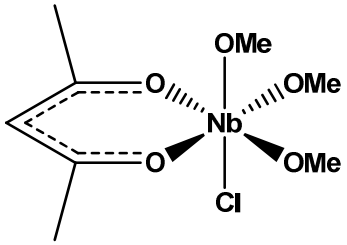

1

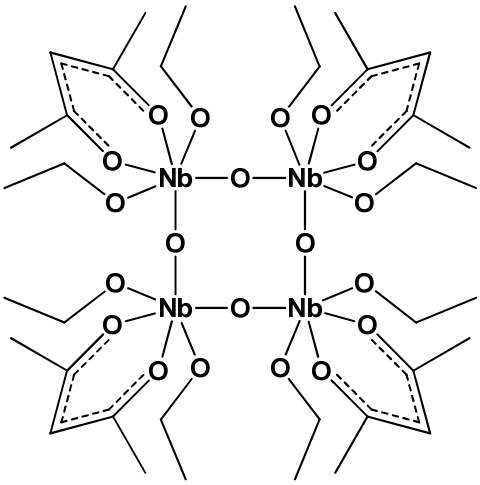

2

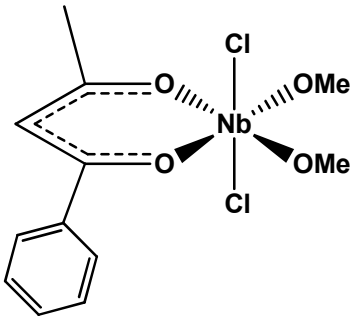

3a

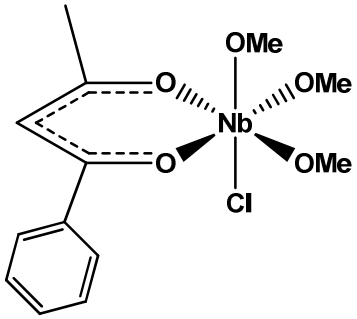

3b

Figure 4.1: Graphical representation of the niobium(V) crystal structures obtained: **1**) [NbCl(acac-κ^2-O,O')$(OMe)_3$], **2**) [Nb(acac-κ^2-O,O')$(OEt)_2(\mu^2$-O)]$_4$, **3a**) [$NbCl_2$(phacac-κ^2-O,O')$(OMe)_2$] and **3b**) [NbCl(phacac-κ^2-O,O')$(OMe)_3$]. (phacac = 1-phenyl-1,3-butane-dionate)

4.2 Experimental

The X-ray intensity data was collected on a Bruker X8 ApexII 4K Kappa CCD area detector diffractometer, equipped with a graphite monochromator and Mo*Kα* fine-focus sealed tube (λ = 0.71073 Å, T = 100(2) K) operated at 2.0 kW (50 kV, 40 mA). The initial unit cell determinations and data collections were done by the SMART[1] software package. The collected frames were integrated using a narrow-frame integration algorithm and reduced with the Bruker SAINT-Plus and XPREP software

[1] Bruker SMART-NT Version 5.050. *Bruker AXS Inc. Area-Detector Software Package;* Madison, WI, USA, 1998.

packages[2] respectively. Analysis of the data showed no significant decay during the data collection. Data was corrected for absorption effects using the multi-scan technique SADABS[3], and the structure was solved by the direct methods package SIR97[4] and refined using the WinGX[5] software incorporating SHELXL.[6] The final anisotropic full-matrix least-squares refinement was done on F^2. The methine, methylene and aromatic protons were placed in geometrically idealized positions (C–H = 0.93 – 0.98 Å) and constrained to ride on their parent atoms with $U_{iso}(H) = 1.2 U_{eq}(C)$. Non-hydrogen atoms were refined with anisotropic displacement parameters. The graphics were done using the DIAMOND[7] program with 50% probability ellipsoids for all non-hydrogen atoms.

[2] Bruker SAINT-Plus Version 6.02 (including XPREP), *Bruker AXS Inc. Area-Detector Integration Software*, Madison, WI, USA, 1999.

[3] Bruker SADABS Version 2004/1. *Bruker AXS Inc. Area Detector Absorption Correction Software,* Madison, WI, USA, 1998.

[4] A. Altomare, M.C. Burla, M. Camalli, G.L. Cascarano, C. Giacovazzo, A. Guagliardi, A.G.G. Moliterni, G. Polidori, R. Spagna, *J. Appl. Cryst.*, 1999, **32**, 115.

[5] L.J. Farrugia, *J. Appl. Cryst.*, 1999, **32**, 837.

[6] G.M. Sheldrick, SHELXL97. *Program for crystal structure refinement,* University of Göttingen, Germany, 1997.

[7] K. Brandenburg & H. Putz; *DIAMOND*, Release 3.0e, Crystal Impact GbR, Bonn, Germany, 2006.

Table 4.1: General X-ray crystallographic data and refinement parameters of [NbCl(acac-κ^2-O,O')$(OMe)_3$] (**1**), [Nb(acac-κ^2-O,O')$(OEt)_2(\mu^2$-O)]$_4$ (**2**) and the two structures from the same crystal, [NbCl(phacac-κ^2-O,O')$(OMe)_3$] and [$NbCl_2$(phacac-κ^2-O,O')$(OMe)_2$] (**3**).

Crystallographic data	1. [NbCl(acac-κ^2-O,O')$(OMe)_3$]	2. [Nb(acac-κ^2-O,O')$(OEt)_2(\mu^2$-O)]$_4$	3. [NbCl(phacac-κ^2-O,O')$(OMe)_3$] and [$NbCl_2$(phacac-κ^2-O,O')$(OMe)_2$]
Empirical formula	C_8 Cl_1 H_{16} Nb_1 O_5	C_{36} H_{68} Nb_4 O_{20}	$C_{12.45}$ $H_{16.35}$ $Cl_{1.55}$ Nb_1 $O_{4.45}$
Formula weight (g mol-1)	320.57	1192.54	385.06
Crystal system	Orthorhombic	Monoclinic	Monoclinic
Temperature (K)	100 (2)	180(2)	180(2)
Space group	*Pbca*	$P2_1/c$	$P2_1/c$
a, b, c (Å)	12.296(4), 12.915(4), 15.470(5)	13.907(5), 12.662(4), 21.354(5)	15.307(4), 11.972(5), 8.371(5)
α, β, γ (°)	90, 90, 90	90, 136.982(13), 90	90, 95.432(5), 90
Volume (Å^3)	2456.7(16)	2565.4(15)	1527.1(12)
Z	8	2	4
ρ_{calc} (g cm^{-3})	1.733	1.544	1.675
μ(mm^{-1})	1.20	0.938	1.068
F(000)	1296	1216	776
Crystal Colour	Pale-yellow	Colourless	Yellow
Crystal morphology	Cuboid	Cuboid	Cuboid
Crystal size (mm)	0.19x0.30x 0.36	0.48x0.32x0.27	0.21x0.27x0.39
θ range (°)	2.64 to 28.35	3.22 to 28.00	2.98 to 27.9 9
Completeness (%)	99.70	99.90	99.90
Limiting indices	-12<=h<=16 -14<=k<=17 -18<=l<=20	-18<=h<=18 -16<=k<=16 -25<=l<=28	-20<=h<=17 -15<=k<=15 -9<=l<=11
Reflections collected	28601	42149	18563
Independent reflections	3083	6191	3686
R_{int}	0.0301	0.0322	0.0322
Refinement method	Full-matrix least-squares on F^2	Full-matrix least-squares on F^2	Full-matrix least-squares on F^2
Data / restraints / parameters	3083 / 0 / 141	6191 / 1 / 275	3686 / 0 / 195
Goodness-of-fit on F^2	1.155	1.056	1.065
Final R indices [I>2sigma(I)]	R1 = 0.0228 wR2 = 0.0678	R1 = 0.0385 wR2 = 0.0910	R1 = 0.0578 wR2 = 0.1422
R indices (all data)	R1 = 0.0302 wR2 = 0.0714	R1 = 0.0467 wR2 = 0.0988	R1 = 0.0784 wR2 = 0.1613
Largest diff. peak and hole (e.Å^{-3})	1.108 and -0.803	2.434 and -1.318	2.616 and -1.760

4.3 Crystal Structure of [NbCl(acac-κ^2-O,O')$(OMe)_3$].

4.3.1 Introduction

Pale-yellow crystals of the title compound were obtained as described in Paragraph **3.7.2.1**. The [NbCl(acac-κ^2-O,O')$(OMe)_3$] complex crystallized in the orthorhombic space group *Pbca*, with eight molecules per unit cell. The structure and numbering scheme of [NbCl(acac-κ^2-O,O')$(OMe)_3$] is illustrated in Figure **4.2**, while the most important bond distances and angles are reported in Table **4.2** and Table **4.3**, respectively.

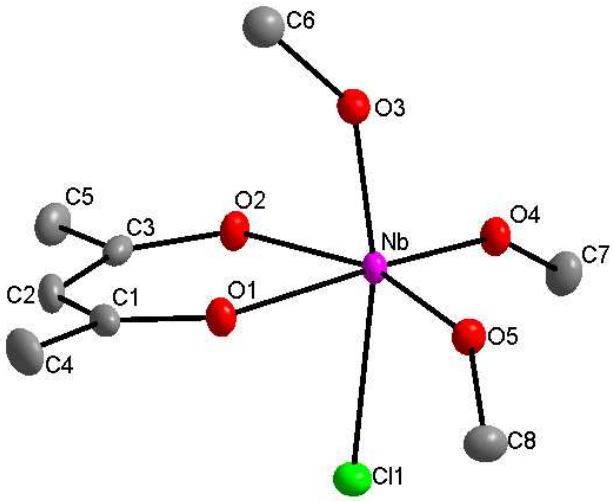

Figure 4.2: Molecular structure of [NbCl(acac-κ^2-O,O')$(OMe)_3$] showing the atom numbering system. Hydrogen atoms have been omitted for clarity. Displacement ellipsoids are drawn at the 50% probability displacement level.

The molecular structure of [NbCl(acac-κ^2-O,O')$(OMe)_3$] consists of a Nb(V) metal centre, coordinated to two oxygen atoms of the chelating acetylacetonate ligand, three oxygen atoms from the methanolate groups and one chloride ligand.[8]

[8] L. Herbst, R. Koen, A. Roodt, H. G. Visser, *Acta Cryst.*, **E66**, m801, 2010.

Table 4.2: Selected bond lengths for [NbCl(acac-κ^2-O,O')$(OMe)_3$].

Atoms	Bond length (Å)	Atoms	Bond length (Å)
Nb – O1	2.109 (2)	O1 – C1	1.282 (3)
Nb – O2	2.085 (2)	O2 – C3	1.289 (3)
Nb – O3	1.879 (3)	O3 – C6	1.416 (3)
Nb – O4	1.864 (1)	O4 – C7	1.414 (3)
Nb – O5	1.862 (2)	O5 – C8	1.419 (2)
Nb – Cl1	2.470 (1)	C1 – C2	1.397 (3)

Table 4.3: Selected bond angles for [NbCl(acac-κ^2-O,O')$(OMe)_3$].

Atoms	Bond angles (°)	Atoms	Bond angles (°)
O1 – Nb – O2	80.74 (6)	O4 – Nb – Cl1	88.76 (5)
O1 – Nb – O4	170.09 (6)	O1 – Nb – Cl1	84.06 (5)
O2 – Nb – O5	163.63 (6)	C1 – C2 – C3	123.71 (2)
O2 – Nb – O3	88.43 (7)	Nb – O1 – C1	133.52 (17)
O3 – Nb – O4	99.45 (7)	Nb – O2 – C3	133.86 (17)
O4 – Nb – O5	100.76 (9)	Nb – O3 – C6	141.75 (16)
O3 – Nb – Cl1	167.55 (6)	Nb – O5 – C8	144.13 (16)

A distorted octahedral geometry is displayed by [NbCl(acac-κ^2-O,O')$(OMe)_3$], with Nb–O distances in the range of 1.862 (2) – 2.109 (2) Å and the Nb–Cl distance of 2.470 (1) Å. The O–Nb–O angles vary between 80.74 (6) and 170.09 (6) °, while the *trans* Cl– Nb–O angle is 167.55 (6)°. All the bond distan ces and angles are similar to other relevant niobium(V) structures.[9,10,11,12]

Enolate type delocalization behaviour is found in the acac bidentate ring. The O1–C1 and O2–C3 bond distances are of similar order (1.282 (3) and 1.289 (3) Å), but are longer than the average C=O bond distance of 1.22 Å and shorter than a single C–O bond distance of 1.43 Å. The three carbon atoms in the acac backbone also have

[9] M. Sokolov, A. L. Gushchin, S. V. Tkachev, D. Y. Naumov, P. Nunez, P. Gili, J. G. Platas, V. P. Fedin. *Inorg. Chim. Acta*, **358**, 2371, 2005.
[10] M. Sokolov, H. Imoto, T. Saito, V. Fedorov, *J. Chem. Soc. Dalton Trans.*, 85, 1999.
[11] A. Antinolo, F. Carrillo-Hermosilla, J. Fernandez-Baeza, A. Otero, E. Palomares, A. M. Rodriguez, L. F. Sanchez-Barba, *J. Organomet. Chem.*, **603**, 194, 2000.
[12] F. Dahan, R. Kergoat, M. C. Senechal-Tocquer, J. E. Guerchais, *J. Chem. Soc. Dalton Trans.*, 2202, 1976.

longer bonds (C1–C2, C2–C3 = 1.397 (3), 1.387 (3) Å) than expected for an average C=C bond (1.34 Å) but shorter than a single C–C bond of 1.54 Å.[13]

An equatorial plane was constructed through O1, O2, O4 and O5 as indicated in Figure **4.3**. The niobium metal centre is slightly elevated above this plane by 0.143 (2) Å. This further illustrates the distorted octahedral geometry of the molecule.

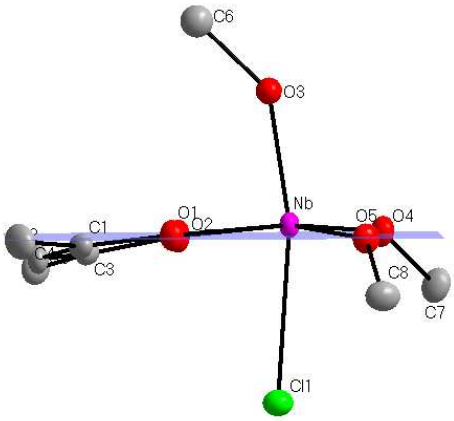

Figure 4.3: Side view of the equatorial plane. Hydrogen atoms have been omitted for clarity. Displacement ellipsoids are drawn at the 50% probability displacement level.

A similar tantalum crystal structure has been obtained by Davies *et al.*[14] by using the same experimental procedure as for [NbCl(acac-κ^2-O,O')$(OMe)_3$]. The tantalum complex, [$TaCl_2$(acac-κ^2-O,O')$(OMe)_2$], also exhibits a distorted octahedral coordination about the metal centre, but is non-isomorphous to the corresponding niobium complex described here. The tantalum complex contains two chlorido ligands that occupy *trans* axial positions while the methoxido and acetylacetonato ligands are coordinated in the equatorial positions.

[13] J. C. Kotz, P. Treichel, G. C. Weaver, *Chemistry and Chemical Reactivity*, 6th Ed, Thomson Learning Inc., 420, 2006.
[14] H. O. Davies, T. J. Leedham, A. C. Jones, P. O'Brien, A. J. P. White, D. J. Williams, *Polyhedron*, **18**, 3165, 1999.

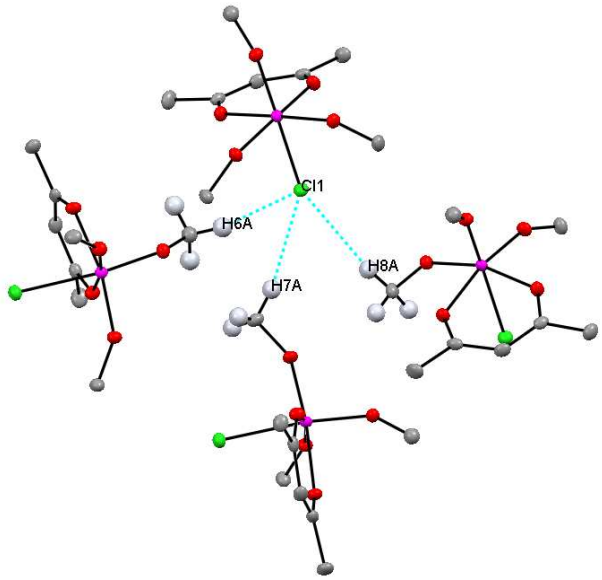

Figure 4.4: Intermolecular short contacts found between [NbCl(acac-κ^2-O,O')$(OMe)_3$] molecules.

There are no classical hydrogen bonds observed in the structure. However, the structure is stabilized by intermolecular C–H···Cl interactions (Figure 4.4). Each chloride atom is involved in three short contacts that afford additional stability to the crystal (Table **4.4**). Similar C–H···Cl bonds have also been observed in other complexes.[15,16]

Table 4.4: Intermolecular interactions observed in [NbCl(acac-κ^2-O,O')$(OMe)_3$] complexes.

Interaction	Bond length (Å)
Cl1···H6A^h	2.912 (3)
Cl1···H7A^i	2.882 (4)
Cl1···H8A^j	2.908 (2)

Symmetry operations: ^{h} [0.5-x, 0.5+y, z]; ^{i} [-x, 0.5+y, 1.5-z]; ^{j} [-0.5+x, y, 1.5-z]

[15] I. Caracelli, *Z. Kristallogr.*, **219**, 273, 2004.
[16] P. K. Thallapally, A. Nangia, *Cryst. Eng. Comm.*, **27**, 1, 2001.

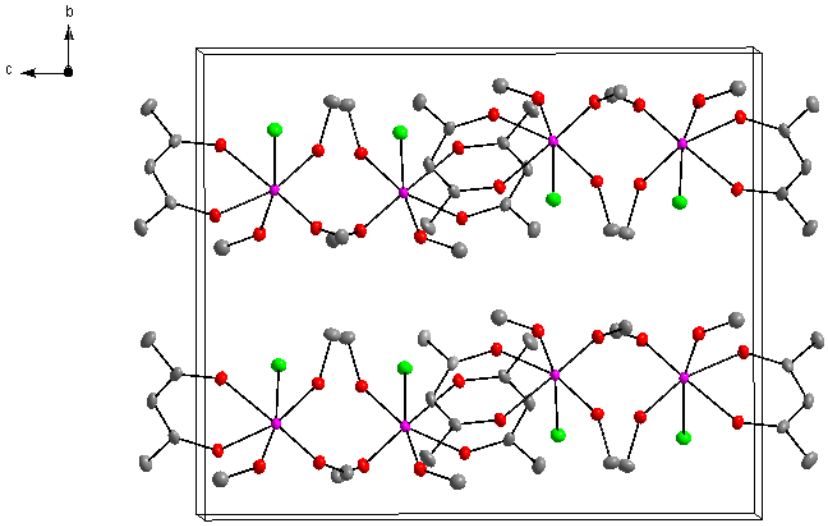

Figure 4.5: Packing of [NbCl(acac-κ^2-O,O')$(OMe)_3$] along the a-axis.

Molecular packing within the unit cell (Figure **4.5**) shows a "head-to-head" arrangement of [NbCl(acac-κ^2-O,O')$(OMe)_3$] complexes along the a-axis. No π-stacking is observed.

The largest differential peak was 1.108 e.Å^{-3}, 0.72 Å from H4B and the deepest hole -0.803 e.Å^{-3}, 0.89 Å from Nb1.

4.4 Crystal structure of [Nb(acac-κ^2-O,O')$(OEt)_2(\mu^2$-O)$]_4$.

4.4.1 Introduction

Colourless crystals of [Nb(acac-κ^2-O,O')$(OEt)_2(\mu^2$-O)$]_4$ were obtained as described in Section **3.7.2.2**. The complex crystallized in the monoclinic space group $P2_1/c$ with two independent molecules in the unit cell. The asymmetric unit of the title tetranuclear niobium(V) complex contains two Nb(V) atoms, two bridging O atoms, two acetylacetonate and four ethanolate ligands (Figure **4.6**). The rest of the tetranuclear unit is generated through an inversion centre. Each Nb(V) atom is six-coordinated by the bridging O atoms, two ethanolate and one chelating acetylacetonate ligands.[17]

[17] L. Herbst, H. G. Visser, A. Roodt, T. J. Muller, *Acta Cryst.*, **E67**, m1669, 2011.

The Nb–O distances vary between 1.817 (2) and 2.201 (2) Å and the O–Nb–O angles vary between 78.88 (8) and 102.78 (9) °, illustrating the significant distorted octahedral geometry around the metal centre. All bond lengths and angles are within normal ranges of these kinds of complexes.[18,19,20,21]

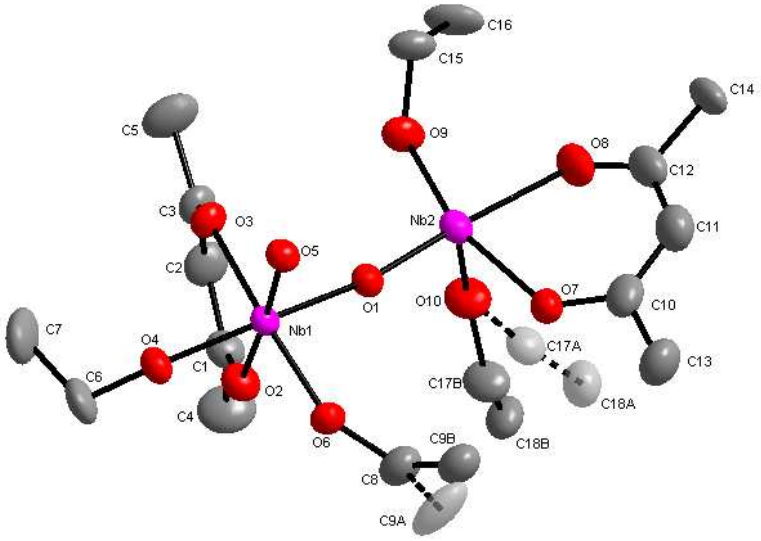

Figure 4.6: The asymmetric unit of [Nb(acac-κ^2-O,O')(OEt)$_2$(μ^2-O)]$_4$ with disorder showing numbering scheme. Hydrogen atoms have been omitted for clarity. Displacement ellipsoids are drawn at the 50% probability displacement level.

The [Nb(acac-κ^2-O,O')(OEt)$_2$(μ^2-O)]$_4$ complex formed a square, cage like structure with oxygen as bridging atoms between the Nb atoms. The O1–Nb1–O5 and the O5–Nb2–O1^i (i = 2-x, 1-y, 1-z) bond angels are 97.12 (10) ° and 93.53 (10) ° respectively. The Nb1–O1, O1–Nb2, Nb1–O5 and O5–Nb2^i bond lengths are 2.020 (2) Å, 1.817 (2) Å, 1.820 (2) Å and 2.015 (2) Å respectively, therefore the Nb1 to Nb2 interatomic distance is 3.837 Å and that of the the Nb$_1$ to Nb$_2^i$ is 3.835 Å. This makes an almost perfect square with the 4 sides equal in length and the angles only slightly larger than 90 °.

[18] F. A. Cotton, W. J. Diebold, W. J. Roth, *Inorg. Chem.*, **24**, 3509, 1985.
[19] F. A. Cotton, W. J. Diebold, W. J. Roth, *Inorg. Chem.*, **26**, 3323, 1987.
[20] B. Ooi, I. Sotofte, *Inorg. Chim. Acta*, **357**, 3780, 2004.
[21] N. Steunou, C. Bonhomme, C. Sanchez, J. Vaisserman, L. G. Hubert-Pfalzgraf, *Inorg. Chem.*, **37**, 901, 1998.

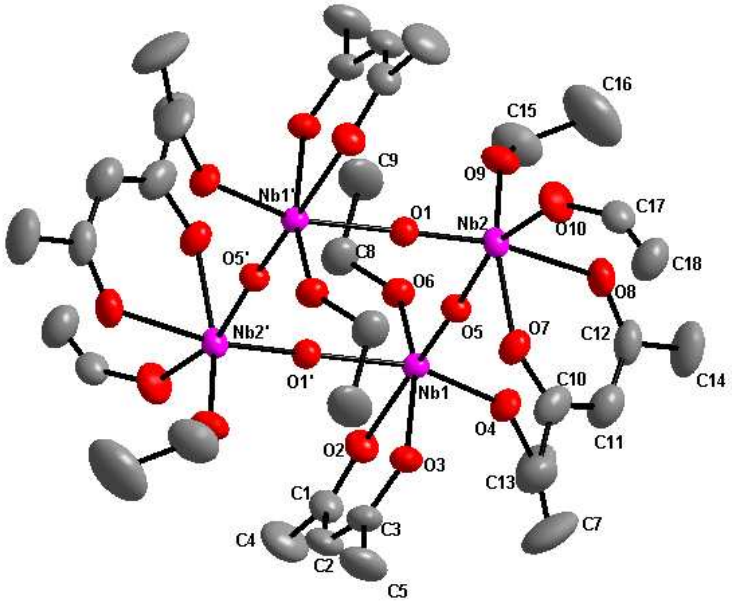

Figure 4.7: Molecular structure of the complete [Nb(acac-κ^2-O,O')$(OEt)_2(\mu^2$-O)]$_4$ tetrameric unit as generated by symmetry showing numbering scheme. Hydrogen atoms and some atom labels have been omitted for clarity. Displacement ellipsoids are drawn at the 50% probability displacement level. [*i* = 2-x, 1-y, 1-z]

A plane was constructed through the four Nb atoms, as displayed in Figure **4.8**. The bridging oxygen, O5, is positioned just above the plane by 0.015 (6) Å, while O1 was elevated above the plane by 0.092 (4) Å.

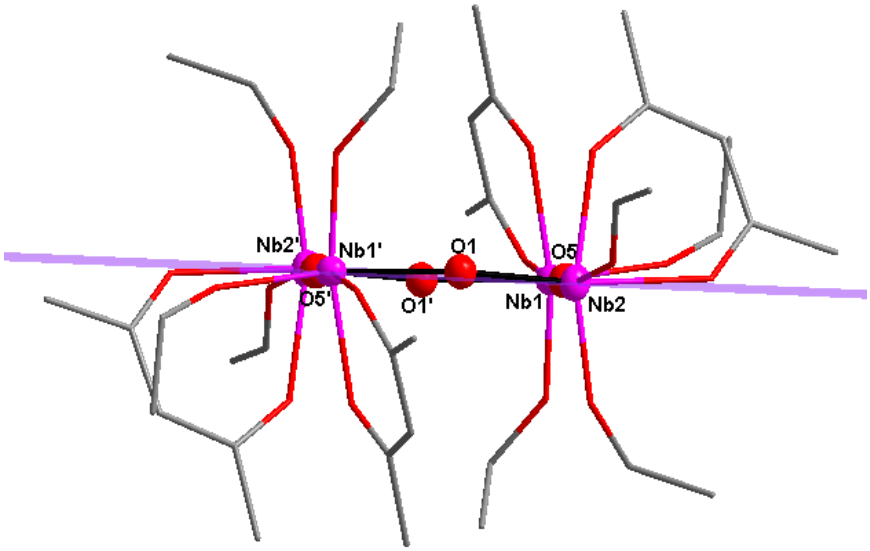

Figure 4.8: A side view of the plane through Nb_1, Nb_2, Nb_1' and Nb_2'. Hydrogen atoms have been omitted for clarity.

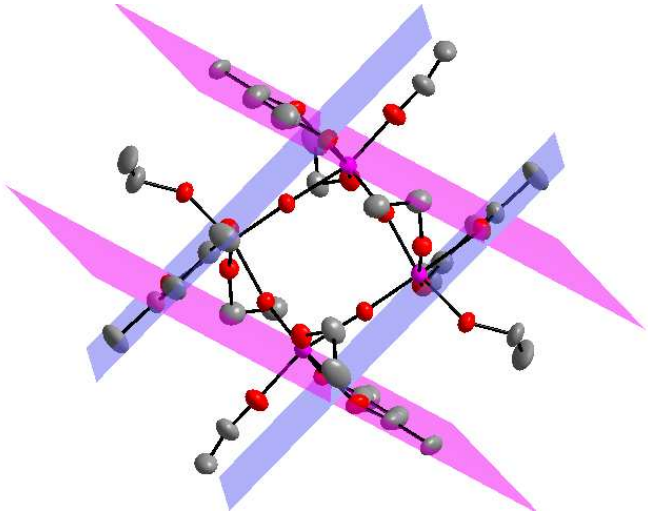

Figure 4.9: A view of the planes constructed through the coordinated acetylacetonate ligands.

Planes constructed through the four-coordinated acac ligands form a square that encloses the niobium "cage". Due to symmetry, the opposing planes are parallel to each other, forming a perfect parallelogram as displayed in Figure **4.9**.

The bite angles of the acac ligands are very similar at 80.03 (10) ° for O2–Nb1–O3 and 79.04 (11) ° for O7–Nb2–O8. The Nb–O bond lengt hs differ from 2.197 (2) Å for Nb1–O2 and 2.088 (2) Å for Nb1–O3, whereas that of Nb2–O7 and Nb2–O8 is 2.091 (3) Å and 2.201 (3) Å, respectively. This is a common phenomenon for acac type of ligands[8], where the metal-oxygen bond of the bidentate ligand differs significantly in bond length. The rest of the Nb–O bond lengths range from 1.817 (2) Å to 2.201 (3) Å (Table **4.5**). All the *trans* O–Nb–O angels deviate from 180 ° by between 9 and 19 °. The *trans* O–Nb1–O angles range from 161.84 (10) to 171.85 (10) ° while the *trans* O–Nb2–O angles range from 162.89 (11) to 169.62 (10) °. From this it can be seen that the *trans* O–Nb2–O angle around Nb2 has a smaller range than the *trans* O–Nb1–O angle around Nb1 (Table **4.6**).

Table 4.5: Selected bond lengths for [Nb(acac-κ^2-O,O')$(OEt)_2(\mu^2$-O)$]_4$.

Atoms	Bond length (Å)	Atom	Bond length (Å)
Nb1 – O1	2.020 (2)	Nb2 – O1	1.817 (2)
Nb1 – O2	2.197 (2)	Nb2 – O7	2.091 (3)
Nb1 – O3	2.088 (2)	Nb2 – O8	2.201 (3)
Nb1 – O4	1.894 (1)	Nb2 – O9	1.880 (3)
Nb1 – O5	1.820 (2)	Nb2 – O10	1.893 (2)
Nb1 – O6	1.879 (2)	$Nb2^i$ – O5	2.015 (3)

[i = 2-x, 1-y, 1-z]

Table 4.6: Selected bond angles for [Nb(acac-κ^2-O,O')$(OEt)_2(\mu^2$-O)$]_4$.

Atoms	Bond angles (°)	Atoms	Bond angles (°)
Nb1 – O1 – Nb2	170.22 (13)	O1 – Nb2 – $O5^i$	93.53 (10)
Nb1 – O5 – $Nb2^i$	177.27 (13)	O10 – Nb2 – $O5^i$	163.11 (12)
O5 – Nb1 – O1	97.12 (10)	O9 – Nb2 – O7	162.89 (11)
O4 – Nb1 – O1	161.84 (10)	O1 – Nb2 – O8	169.62 (10)
O6 – Nb1 – O3	163.66 (10)	O7 – Nb2 – O8	79.04 (11)
O5 – Nb1 – O2	171.85 (10)	C1 – O2 – Nb1	129.84 (19)
O3 – Nb1 – O2	80.03 (10)	C10 – O7 – Nb2	133.40 (16)

[i = 2-x, 1-y, 1-z]

The crystal structure displays a 55:45 positional disorder at one of the ethoxy groups, C17 and C18, as well as a 72:28 positional disorder at C9. There is no hydrogen interaction or π-π stacking observed in the crystal structure. The molecules pack in a sheet-like arrangement, forming channels when viewed in the direction of the a-axis (Figure **4.10**).

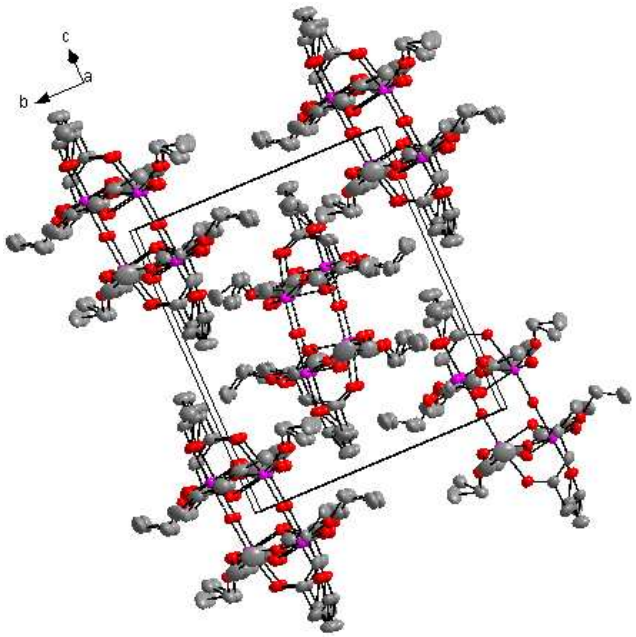

Figure 4.10: An illustration of the molecular packing of the [Nb(acac-κ^2-O,O')$(OEt)_2$ (μ^2-O)]$_4$ as viewed along the a-axis. Hydrogen atoms have been omitted for clarity. Displacement ellipsoids are drawn at the 50% probability displacement level.

The largest differential peak was 2.434 e.Å^{-3}, 0.81 Å from Nb2 and the deepest hole -1.318 e.Å^{-3}, 0.67 Å from Nb2.

4.5 Crystal structure of [NbCl(phacac-κ^2-O,O')$(OMe)_3$] and [$NbCl_2$(phacac-κ^2-O,O')$(OMe)_2$].

4.5.1 Introduction

The title complexes were prepared and crystallized according to the procedure described in Section **3.7.2.3**. Yellow crystals suitable for X-ray diffraction were obtained. The complex crystallized in the monoclinic space group $P2_1/c$, with four molecules per unit cell. The structure and numbering scheme of [NbCl(phacac-κ^2-O,O')$(OMe)_3$] and [$NbCl_2$(phacac-κ^2-O,O')$(OMe)_2$] is illustrated in Figure **4.11**, while the most important bond distances and angles are reported in Table **4.7** and Table **4.8**, respectively. The two molecular structures were obtained from the same crystal.

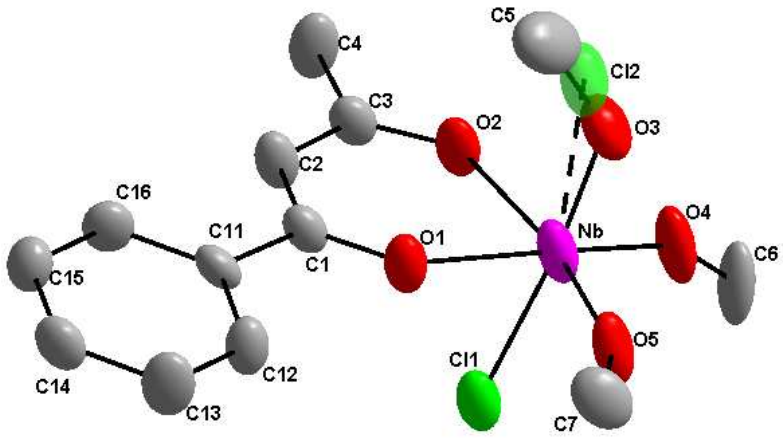

Figure 4.11: Molecular structure of [NbCl(phacac-κ^2-O,O')$(OMe)_3$] and [$NbCl_2$(phacac-κ^2-O,O')$(OMe)_2$] showing the atom numbering system. Hydrogen atoms have been omitted for clarity. Displacement ellipsoids are drawn at the 50% probability displacement level.

The molecular structure of [NbCl(phacac-κ^2-O,O')$(OMe)_3$] consists of a Nb(V) metal centre bonded to two O atoms of the phacac ligand, three O atoms from the methanolato groups and one chlorido ligand, whereas [$NbCl_2$(phacac-κ^2-O,O')$(OMe)_2$] consists of a Nb(V) metal centre bonded to two O atoms of the bidentate ligand and only two O atoms from the methanolato groups and two chlorido ligands. The crystal structure displays a 54:46 substitutional disorder between Cl2 and the O3–C5 methoxy group (Figure **4.11**). This indicates the simultaneous crystallization of [NbCl(phacac-κ^2-O,O')$(OMe)_3$] and [$NbCl_2$(phacac-κ^2-O,O')$(OMe)_2$]. These results could not be confirmed by elemental analysis as the crystals rapidly decompose with exposure to air.

The complex displays a slightly distorted octahedral geometry with the Nb–O distances in the range 1.830 (2) – 2.094 (3) Å and Nb–Cl distances of 2.432 (2) and 2.412 (8) Å. The *trans* angles, Cl1–Nb–O3 and Cl1–Nb–Cl2 are 171.85 (10) and 163.87 (11) ° respectively. Comparison of the two c rystal structures indicate more significant distortion from octahedral geometry is observed in the dichlorido analogue. This is clearly demonstrated by the O1–Nb–O3 and O1–Nb–Cl2 angles of 94.30 (8) and 84.83 (16) ° respectively.

Table 4.7: Selected bond lengths for [NbCl(phacac-κ^2-O,O')$(OMe)_3$] and [$NbCl_2$(phacac-κ^2-O,O')$(OMe)_2$].

Atoms	Bond length (Å)	Atom	Bond length (Å)
Nb – O1	2.094 (3)	Nb – Cl2	2.412 (8)
Nb – O2	2.077 (3)	O1 – C1	1.276 (6)
Nb – O3	1.830 (2)	O2 – C3	1.281 (5)
Nb – O4	1.837 (4)	O3 – C5	1.491 (8)
Nb – O5	1.839 (4)	O4 – C6	1.402 (8)
Nb – Cl1	2.432 (2)	O5 – C7	1.404 (6)

Table 4.8: Selected bond angles for [NbCl(phacac-κ^2-O,O')$(OMe)_3$] and [$NbCl_2$(phacac-κ^2-O,O')$(OMe)_2$].

Atoms	Bond angles (°)	Atoms	Bond angles (°)
O1 – Nb – O3	94.30 (8)	O4 – Nb – O3	92.70 (8)
O1 – Nb – O4	170.27 (17)	O4 – Nb – O5	101.22 (17)
O1 – Nb – O2	80.65 (13)	O5 – Nb – O1	85.23 (15)
O2 – Nb – O3	88.80 (8)	O1 – Nb – Cl2	84.83 (16)
O2 – Nb – O4	92.76 (16)	O1 – Nb – Cl1	84.42 (12)
O3 – Nb – O5	92.50 (7)	O3 – Nb – Cl1	171.85 (10)
O3 – Nb – O2	80.03 (10)	Cl1 – Nb – Cl2	163.87 (11)

The distortion in the two molecules are further illustrated in Figures **4.12** and **4.13**. A plane was constructed through O1, O2, C1 and C3 of the phacac ligand (purple) as well as through C11, C12, C13, C14, C15 and C16 of the phenyl ring (pink) on C1, as indicated in Figure **4.12**. The dihedral angle between the phenyl ring and the acetylacetone backbone is -7.33 (8) °.

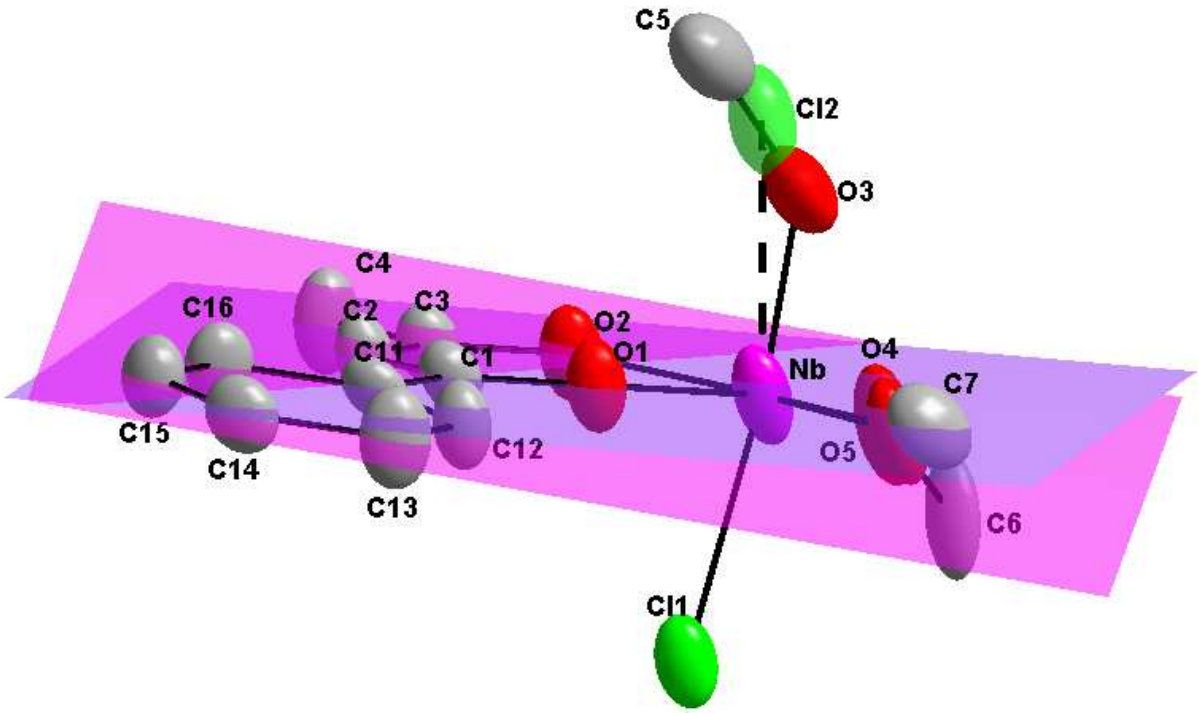

Figure 4.12: The phacac plane constructed through O1, O2, C1 and C3 (purple) illustrating the angle of the phenyl ring (pink) at C_1.

A plane was constructed through O1, O2, O4 and O5 as indicated in Figure **4.13**. The niobium metal centre is slightly elevated above this plane by 0.071 (4) Å. This illustrates the distorted octahedral geometry of the molecule.

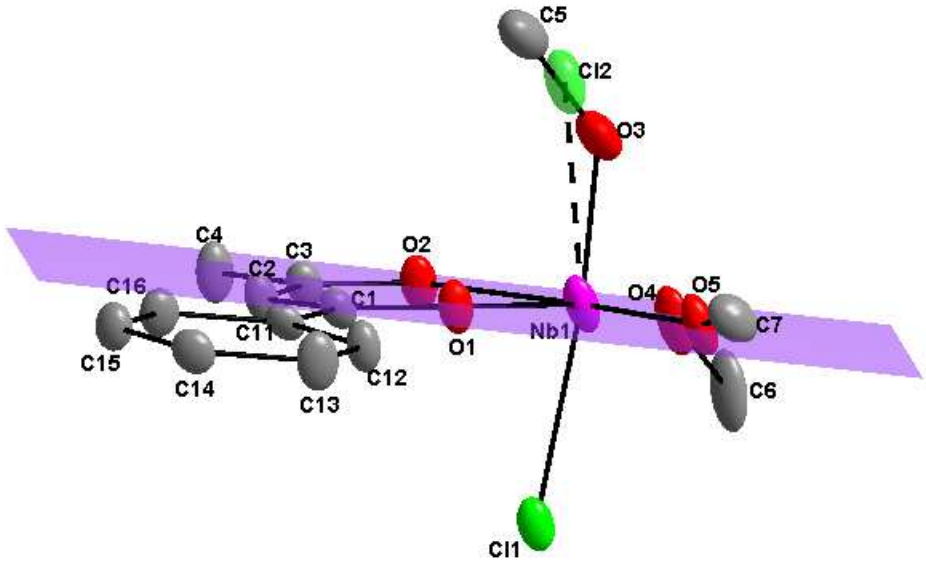

Figure 4.13: Side view of the equatorial plane through O_1, O_2, O_4 and O_5.

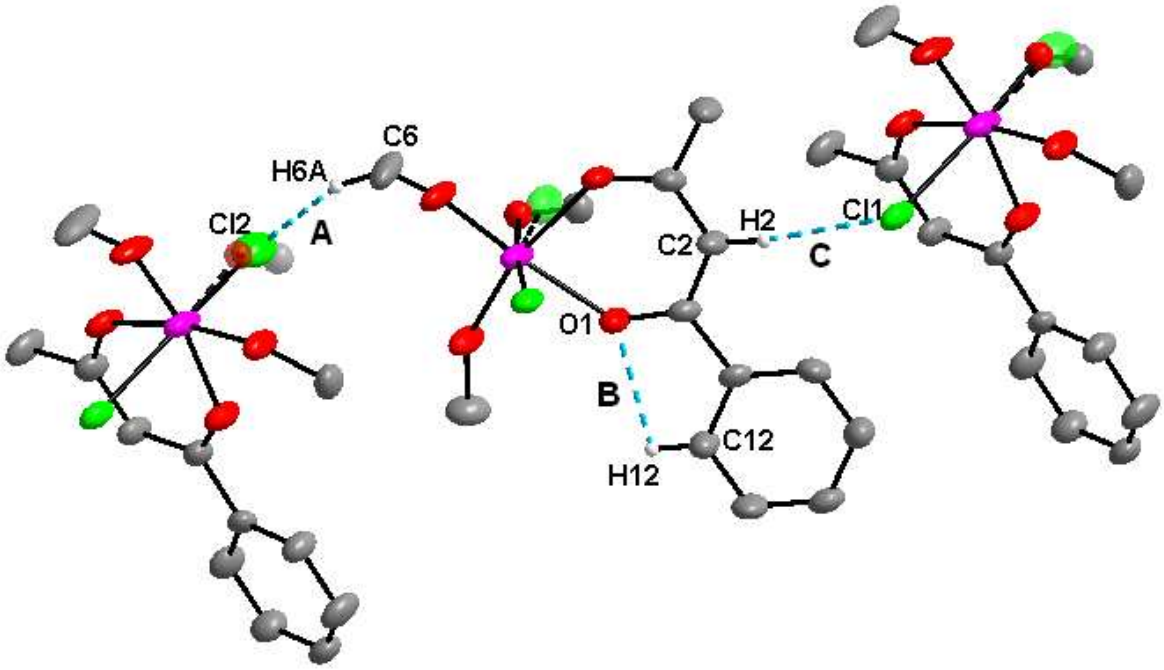

Figure 4.14: Inter- and intramolecular hydrogen interactions found between the [NbCl(phacac-κ^2-O,O')$(OMe)_3$] and [$NbCl_2$(phacac-κ^2-O,O')$(OMe)_2$] molecules. Only applicable hydrogen atoms with relevance to hydrogen bond interactions are indicated.

Inter- and intramolecular hydrogen bonding are illustrated in Figure **4.14**. Intramolecular bonding exists between O1 and H12 (**B**) with a donor-acceptor (D-A) bond distance of 2.742 (6) Å, while intermolecular bonding occurs between Cl2 and H6A (**A**) with a D-A distance of 3.611 (8) Å. An intermolecular interaction also exists between Cl1 and H2 (**C**) with a D-A distance of 3.655 (5) Å. A complete list of hydrogen bonds is given in Table **4.9**.

Table 4.9: Hydrogen bonds for [NbCl(phacac-κ^2-O,O')$(OMe)_3$] and [$NbCl_2$(phacac-κ^2-O,O')$(OMe)_2$].

Interaction	D-H···A	D-H (Å)	H···A (Å)	D···A (Å)	< D-H···A (°)
A	C6^k, H6A^k, Cl2^l	0.958 (3)	2.809 (6)	3.611 (8)	142.04 (4)
B	C12^k, H12^k, O1^k	0.933 (4)	2.423 (2)	2.742 (6)	100.10 (3)
C	C2^k, H2^k, Cl1^m	0.927 (3)	2.768 (4)	3.655 (5)	158.92 (6)

Symmetry operations: ^{k} [x, y, z]; ^{l} [x, 0.5-y, -0.5+z]; ^{m} [x, -0.5-y, 0.5+z]

Molecular packing within the unit cell (Figure **4.15**) shows a "head to tail" arrangement of the [NbCl(phacac-κ^2-O,O')$(OMe)_3$] and [$NbCl_2$(phacac-κ^2-O,O')$(OMe)_2$] complexes when viewed along the b-axis.

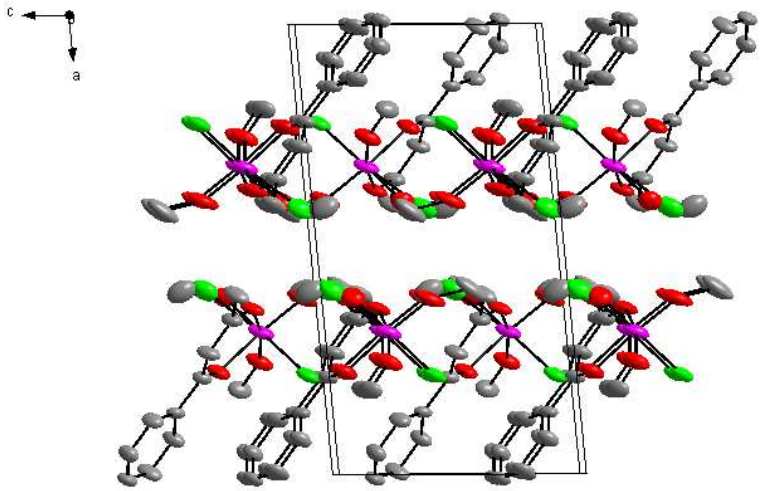

Figure 4.15: Complexes of [NbCl(phacac-κ^2-O,O')$(OMe)_3$] and [$NbCl_2$(phacac-κ^2-O,O')$(OMe)_2$] displaying a sheet-like "head to tail" crystal packing along the b-axis. Hydrogen atoms have been omitted for clarity. Displacement ellipsoids are drawn at the 50% probability displacement level.

The largest differential peak was 2.616 e.Å^{-3}, 0.93 Å from Nb1 and the deepest hole -1.761 e.Å^{-3}, 0.80 Å from Nb1.

4.6 Conclusion

During the course of this project, three novel Nb(V) organometallic complexes have been synthesized and characterised. Two of these structures have already been published.[8,17] Comparative research for Nb(V) and Ta(V) structures are aimed at finding significant coordinative differences for these two metals with similar type ligands, in this case β-diketonate species. As discussed throughout this chapter, comparisons of novel compounds with literature sources have been established.

In general, it was observed that these mono-substituted β-diketonate complexes of Nb(V) finally crystallize in a distorted octahedral coordination polyhedron, which is also described in literature.[14,22,23,24] Furthermore, these complexes were found to crystallize in the absence of any solvent or counter ions in the unit cell.

As a general comparison from this work, it is observed that β-diketonate ligands chelate to the metal centre in a flat plane, with no bending of either the ligand backbone or at the O,O'-coordination sites. This occurs with an average O–Nb–O bite angle of 80.5 (1) °. Additionally, the Nb–O bond distances are never equal for any of these moieties, as from literature, even in cases where symmetrical β-diketonate ligands are utilized.[23,24]

Table 4.10: Nb–O bond distances with regards to β-diketonate coordination.

Complex	$Nb–O_1$ (Å)	$Nb–O_2$ (Å)
$[NbCl(acac-\kappa^2\text{-}O,O')(OMe)_3]$	2.109 (2)	2.085 (2)
$[Nb(acac-\kappa^2\text{-}O,O')(OEt)_2(\mu^2\text{-}O)]_4$	2.197 (2)	2.088 (2)
$[NbCl(phacac-\kappa^2\text{-}O,O')(OMe)_3]$ and $[NbCl_2(phacac-\kappa^2\text{-}O,O')(OMe)_2]$	2.094 (3)	2.077 (3)

Only four other niobium "cage" structures, similar to the $[Nb(acac-\kappa^2\text{-}O,O')(OEt)_2(\mu^2\text{-}O)]_4$ complex, have been reported in literature.[18,19,20,21] These structures all display relative significant differences in terms of the bridging coordination of the niobium metal centres.

[22] P. Werndrup, M. Verdenelli, F. Chassagneux, S. Parola, V. G. Kessler, *J. Mater. Chem.*, **14**, 344, 2004.
[23] P. A. Williams, A. C. Jones, P. J. Wright, M. J. Crosbie, J. F. Bickley, A. Steiner, H. O. Davies, T. J. Leedham, *Chem. Vap. Deposition*, **8**, 3, 110, 2002.
[24] A. Antiñolo, F. Carrillo-Hermosilla, J. Fernández-Baeza, S. Garcia-Yuste, A. Otero, E. Palomares, A. M. Rodriguez, L. F. Sánchez-Barba, *J. Organomet. Chem.*, **603**, 194, 2000.

According to our knowledge the phenomenon of two crystal structures, NbCl(phacac-κ^2-O,O')$(OMe)_3$] and [$NbCl_2$(phacac-κ^2-O,O')$(OMe)_2$], obtained from a single complex crystal is exceptional and unmarked by other niobium complexes.[25]

The remaining chlorido ligands present after solvent coordination are always in axial positions[14,26] in the final solid state structures, with a Nb–Cl bond length averaging 2.438 (3) Å. This value compares well with that reported in literature as 2.43 Å.[27] In addition, the substitute methoxide ligands are directly indicative of the importance of reaction solvent choice. In cases where tailoring reaction conditions around a specific solvent used for synthesis, this characteristic of niobium complex formation bears potentially significant impact on novel structure design.

The next chapter will cover a detailed discussion on the reaction mechanism for the formation of [NbCl(acac-κ^2-O,O')$(OMe)_3$]. ^{93}Nb NMR is also included and plays an integrate part in the identification of the niobium starting material and allows postulation of the possible reaction intermediate(s).

[25] F. H. Allen, *Acta Cryst*., **B58**, 380, 2002.
[26] J. D. Wilkins, M. G. B. Drew, *J. Organomet. Chem.*, **69**, 111, 1974.
[27] N. Prokopuk, C. S. Weinert, V. O. Kennedy, D. P. Siska, H. Jeon, C. L. Stern, D. F. Shriver, *Inorg. Chim. Acta*, **300**, 951, 2000.

5. Formation kinetics of $[NbCl(acac)(OMe)_3]$

Synopsis...

A complete discussion of the reaction kinetics as well as the reaction mechanism of the formation of $[NbCl(acac)(OMe)_3]$ is given. The use of ^{93}Nb NMR is also included as this was used to identify the nature of the niobium halide starting reagent.

oooooooooooooo

5.1 Introduction

Chemical kinetics comprises the study of the rates of chemical reactions, which involves the precise measurement of the variation of concentrations of the reacting species with time. These measurements are conducted in such a way that a certain aspect of the chemical reaction may be studied, such as the influence of temperature, concentration and pressure variation on the reaction time, or the catalytic effect of one species involved in the reaction pathway.

An important aim of this project was to identify and clarify the ligand coordination mechanism for niobium and O,O'-bidentate ligands. A few general trends have been observed in this study:

- The coordination of only one acac moiety to niobium(V) even in the presence of an excess of acacH.
- Several chlorido ligands are immediately substituded by solvents like methanol upon dissolution of $[NbCl_5]_2$ which creates some doubt of the true identity of the starting complex in the reaction with acacH.

The process of mathematical prediction of reaction rate conditions is discussed along with the observations from the kinetic experiments. It is important to note that the available literature on the reactions of niobium(V) is very limited which highlights the importance of this study.

5.2 Experimental procedures

5.2.1 Kinetic experiments

All reagents and chemicals were of analytical grade. $[NbCl_5]_2$ and acacH were used as received from Sigma Aldrich and the solvent (MeOH) was dried and distilled prior to use. Kinetic measurements were performed on Varian Cary 50 Conc UV/Vis (slower reactions) or Applied Photophysics Stopped-flow (fast reactions) spectrophotometers. Temperature control of the reaction solutions was maintained to within ± 0.1 ˚C by means of a circulating water bath system.

The kinetics involve time resolved scanning of a sample over a range of preset wavelengths to determine absorption changes in this range. The sample in this case would be a mixture of a metal complex solution and a ligand solution with known concentrations. The software program Scientist[1] from Micromath was used to fit, *by mathematical calculations*, the data to selected kinetic equations for single step reactions as discussed below in Section **5.3** and in Chapter **3**.

Stability tests of the reagent solutions were the first examinations performed in the kinetic study. The solutions were scanned for a longer period of time than the studied reactions occur, to establish that the reagents themselves do not undergo changes such as decomposition, polymerisation or coordination while in solution, since these additional reactions would significantly complicate the nature of the kinetics. Solutions of $[NbCl_5]_2$ and acacH in methanol were monitored for ± 3 days, signifying no noteworthy decomposition or interaction between the solvent and starting reagents.

Reaction solutions were prepared to comply with *pseudo* first-order conditions. The metal solution was prepared throughout to maintain a final concentration of 2.5×10^{-5} M ($[NbCl_5]_2$ in MeOH), whereas the ligand solution was prepared as a stock solution of 5×10^{-3} M final concentration and dilution was carried out across a series of 5 solutions with minimum final concentration of 5×10^{-4} M (acacH in MeOH). Fresh solutions were prepared for separate days of kinetic experiments. Even though stability of solutions were confirmed for *ca.* 24 hour periods, it was considered unwise to utilize solutions older than that time.

[1] MicroMath Scientist for Windows. Version 2.01. Copyright © 1986 – 1995, MicroMath Inc.

5.2.2 ^{93}Nb NMR

All ^{93}Nb NMR spectra were obtained in CD_3OD on a Bruker 600 MHz nuclear magnetic resonance spectrometer using a TBI 600 MHz S3 5 mm broadband probe. Although ^{93}Nb is quadrupolar (I = 9/2; Q = -0.22 x 10^{-28} m^2) the broadness of the lines are compensated for by a wide niobium(V) chemical shift range (δ = -1500 – 500) and good sensitivity (^{1}H = 1; ^{93}Nb = 0.48).[2] The specific resonance frequency for ^{93}Nb NMR is 146.93 MHz.

As discussed in Section **2.7.2**, niobium(V) chloride forms various niobium(V)-chloro-methoxo species when dissolved in methanol. By controlling the reaction conditions, it is possible to isolate a single niobium(V)-chlorido-methoxido species.[3,4,5] The formation of different species is dependent on the $[NbCl_5]_2$ concentration, storage time and temperature. Experimental work done by Karaliota *et al*.[3] also indicated that at low niobium concentrations, 0.185 M and lower, no bridging methoxides can be observed and the niobium(V)-chlorido-methoxido species exists as a monomer in solution.

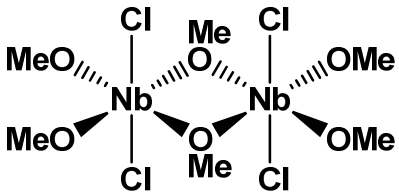

Figure 5.1: $[NbCl_2(OMe)_3]_2$ that exists as a dimer in solutions at 0.185 M and above.[3]

In order to accurately predict the mechanism of any reaction, the correct molecular structure of the starting materials have to be known. Subsequently, a 0.1 M sample of $[NbCl_5]_2$ in deuterated MeOH was prepared for NMR studies, similar to that conducted by Lee *et al.*[4]

The results from our NMR study are presented in Figure **5.2** and will be discussed in the following paragraphs. Only one niobium signal was observed at -822 ppm, that

[2] J. Mason, *Multinuclear NMR*, Plenum Press, New York, 493, 1987.
[3] A. Karaliota, M, Kamariotaki, D, Hatzipanayioti, *Transition Met. Chem.*, **22**, 411, 1997.
[4] G. R. Lee, J. Crayston, *Dalton Trans.*, 3073, 1991.
[5] M. Schönherr, L. Kolditz, *Z. Chem.*, **10**, 72, 1970.

corresponds to one species, possibly $[NbCl_2(OMe)_3(MeOH)]$ (**a**). This will be discussed in detail later in this section. In a second experiment an excess of acacH (0.2 M) was added to the solution in (**a**) and an immediate peak shift to -931 ppm, as shown in (**b**), was observed. The reaction sample was scanned over 24 hours in order to investigate the probability of new species being formed. However, we did not observe the formation of new peaks or the shift of the existing peak which would indicate new species.

In another experiment, crystals of the product, which have been characterized and reported in Chapter **4.3**, was dissolved in deuterated MeOH and the spectrum (**c**) was obtained. It is clear from Figure **5.2** that the spectra for (**b**) and (**c**) are similar, indicating that the final product of the reaction between a solution of $[NbCl_5]_2$ in MeOH and excess acacH is similar to the solution of $[NbCl(acac)(OMe)_3]$.

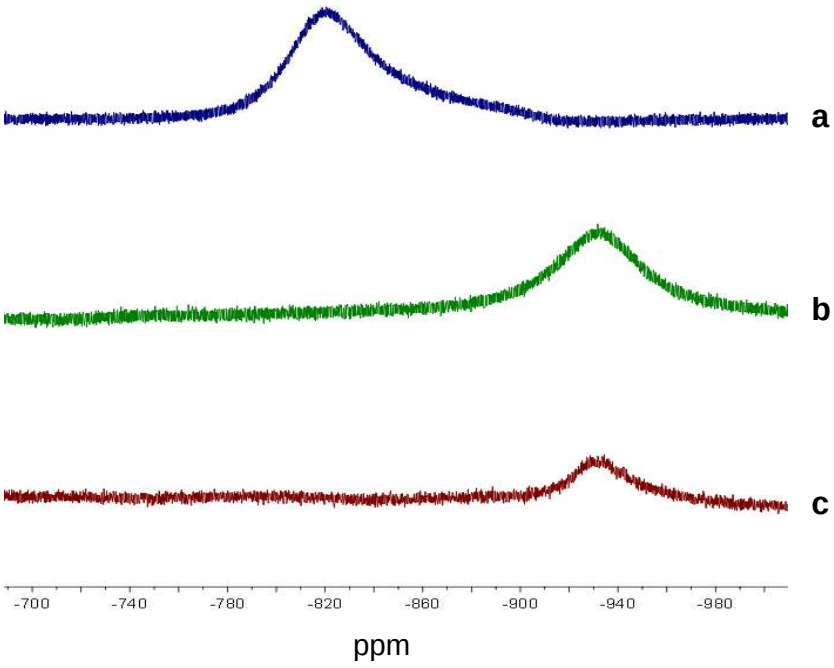

Figure 5.2: ^{93}Nb NMR of (**a**) the niobium(V) starting material, $[NbCl_2(OMe)_3(MeOH)]$, (**b**) the product formed when Hacac is added to $[NbCl_2(OMe)_3(MeOH)]$ and (**c**) $[NbCl(acac)(OMe)_3]$.

Our results expand on the work performed by Lee *et al*.[4] and several important points can be derived from this. Lee and co-workers[4] examined the ^{93}Nb NMR signals for different $NbCl_{5-x}(OMe)_x$ species in various solvents (Table **5.1**) in order to determine the number of coordinated methoxido species in solution. A comparison

of our results to that listed in Table **5.1** indicates the presence of three-coordinated methoxido ligands under our conditions.

Table 5.1: Assignment of ^{93}Nb NMR signals to $[NbCl_{5-x}(OMe)_x]$ species.[4]

Solvent	*x* = 0	*x* = 1	*x* = 3	*x* = 4	*x* = 5
Benzene	2.6	-497	-810	-1010	-1160
Toluene	2	-495	-810	-	-1150
Methanol	-0.5	-480	-820	-1015	-1155
Ethanol	-	-470	-830	-1020	-1180
Isopropanol	-	-470	-830	-1025	-1135
Acetonitrile	-	-495 / -560	-850	-	-1160

x = number of coordinated methoxido species

Further experiments by Lee *et al*.[4] and others[3,5] indicated that there are no bridged (polymeric) niobium species in solution at metal concentrations below 0.185 M. Under our conditions in the kinetic studies, the final metal concentration after mixing is 5 x 10^{-5} M, much lower than these conditions. It is therefore postulated here that the starting material in our kinetic studies is in fact a mono-nuclear niobium complex, $[NbCl_2(OMe)_3(MeOH)]$. The presence of a coordinated methanol solvento species in the niobium coordination sphere is the most obvious choice since the concentration of methanol under our conditions is in the region of 25 M and since charge balance is maintained in this manner. This bridge splitting by coordinating solvents have also been illustrated for platinum(II) chloride olefin complexes.[6]

Another aspect that is important to note here is that there is seemingly only one reaction observed under the conditions of the NMR experiment when excess of acacH is added to $[NbCl_2(OMe)_3(MeOH)]$. Later paragraphs would show that there are in fact two reactions in this process which are only observed under conditions where the concentrations of the starting materials are much lower.

[6] M. R. Plutino, S. Otto, A. Roodt, L. I. Elding, *Inorg. Chem*., **38**, 1233, 1999.

5.3 Results and Discussion

5.3.1 Proposed Reaction Scheme

The following reaction scheme is presented for the reaction between $[NbCl_2(OMe)_3(MeOH)]$ and acacH. According to Scheme **5.1** the reaction involves a fast initial reaction where acacH substitutes the labile coordinated MeOH to form an intermediate species which undergoes ring-closure in a second, slower, rate-determining step. The validation of this scheme will be done in a stepwise manner in the following paragraphs.

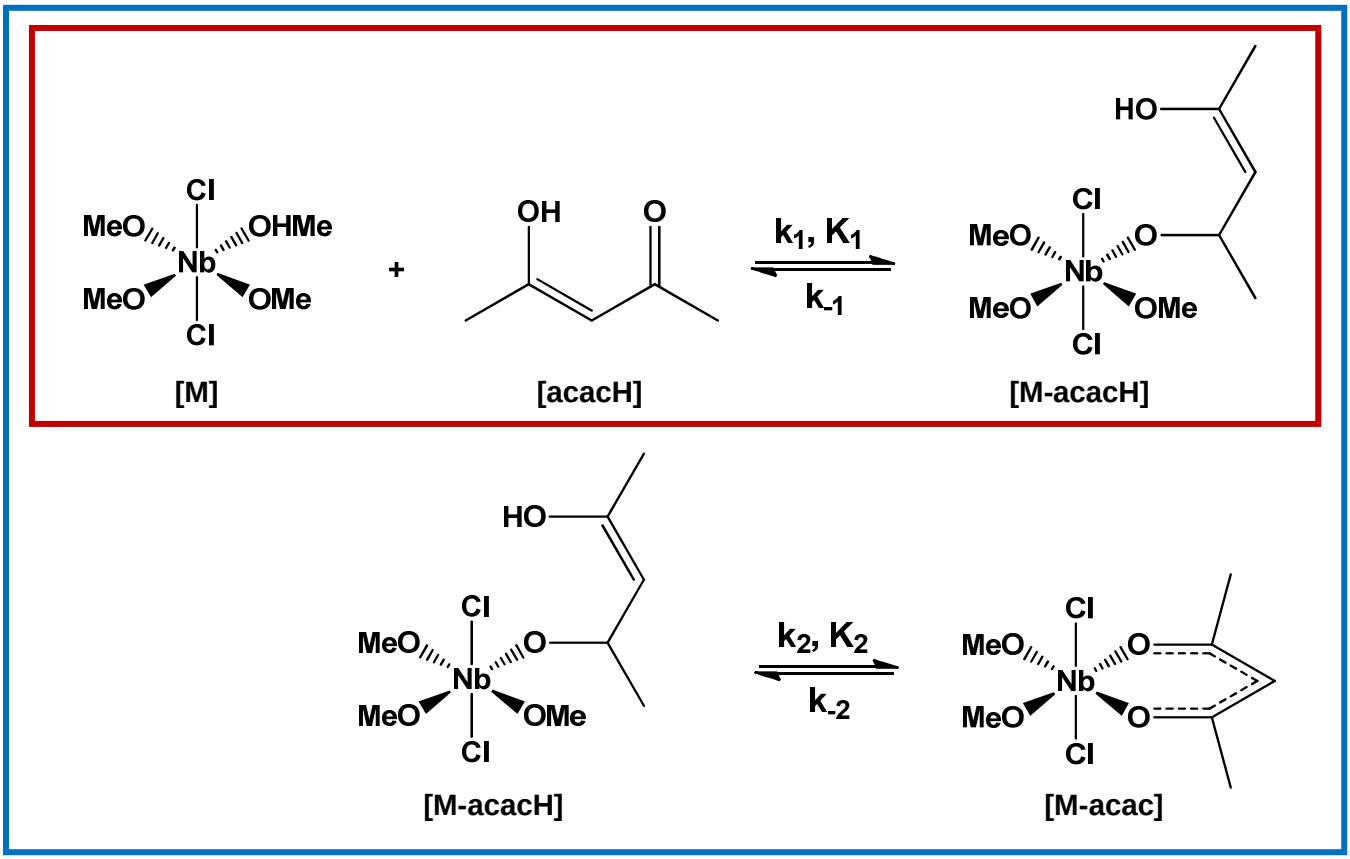

Scheme 5.1: The proposed reaction scheme for the formation of $[NbCl(acac)(OMe)_3]$. Two reactions are observed, the fast first reaction in red and the slower second reaction in blue.

5.3.2. Stepwise analysis of the reaction scheme

The postulation of the complete reaction mechanism (Scheme **5.1**) was based on the following detail:

- The correct identification of the niobium starting material $[NbCl_2(OMe)_3(MeOH)]$ was done with ^{93}Nb NMR. This was discussed in detail in Section **5.2.2**.

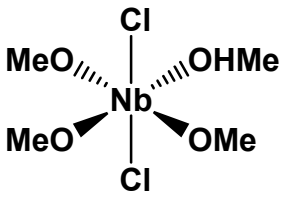

Figure 5.3: Predicted niobium(V) starting reagent in solution.

- The formation of the final product is well-defined as indicated by the successful characterisation by means of IR, UV/Vis, X-Ray diffraction, ^{1}H-, ^{13}C- and ^{93}Nb NMR.

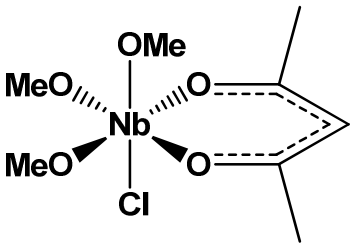

Figure 5.4: The formation product, $[NbCl(acac)(OMe)_3]$, on which the kinetic study is based.

- Preliminary experiments indicated at least 2 consecutive reaction steps – one fast and one slow reaction, see Figure **5.5**. In this experiment, the reaction between $[NbCl_2(OMe)_3(MeOH)]$ and acacH in MeOH was followed at 25.0 ^{o}C. In the initial absorbance *vs* wavelength scans of $[NbCl_2(OMe)_3$ (MeOH)] is indicated in red. When adding acacH to this solution a fast step is observed with peak formation at 323 nm. This is indicated by the red arrow. The second, slower step (blue arrow) involved the disappearance of the peaks at 276 and 323 nm.

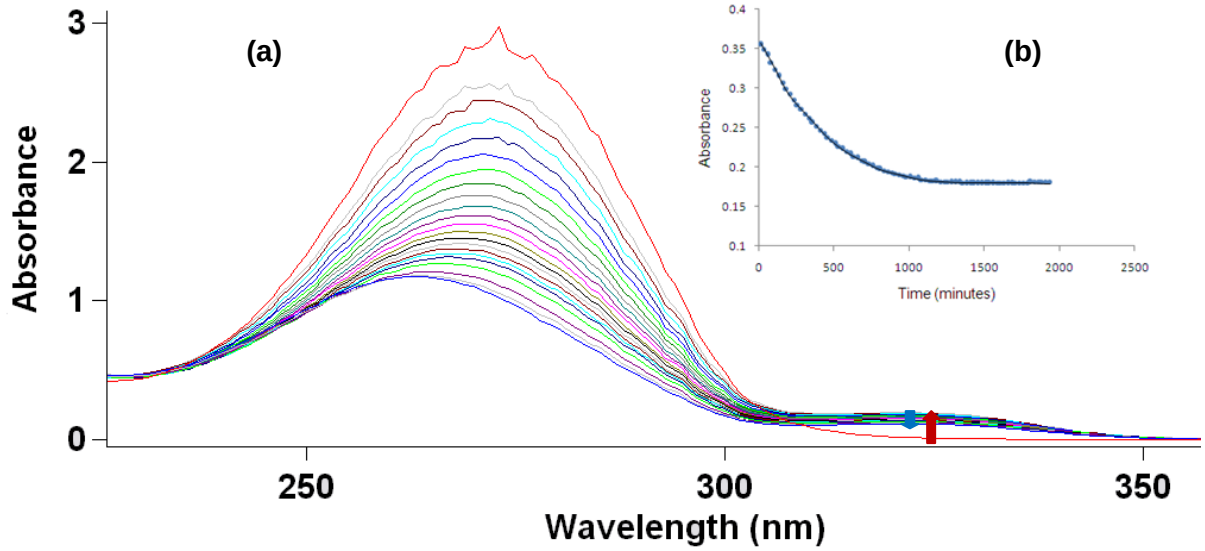

Figure 5.5: Typical UV/Vis spectra of $[NbCl_2(OMe)_3(MeOH)]$ (5×10^{-5} M) and [acacH] (5×10^{-4} M) in MeOH (Δt = 30 min); (**a**) spectrum of absorbance versus a range of wavelengths, and (**b**) a graph of absorbance versus time at 323 nm. T = 25.0 ℃

- In order to verify that the observed, fast reaction involves only one reaction step, as opposed to two or more consecutive steps, the preliminary experimental data was fitted to mathematical models representing a one-step *pseudo* first-order (Eq. **5.1**) and a two-consecutive-step *pseudo* first-order (Eq. **5.2**) reaction, respectively (see Figure **5.6**):

$$A_{obs} = A_1 - (A_1 - A_0)e^{(-k_{obs}.t)} \quad (\mathbf{5.1})$$

$$A_{obs} = (A_0 - B_0)e^{(-k_{obs1}.t)} + (B_0 - B_1)e^{(-k_{obs2}.t)} + B_1 \quad (\mathbf{5.2})$$

with A_{obs} = the observed absorbance, A_0 and B_0 = the initial absorbance for the first and second steps, A_1 and B_1 = the final absorbance for the first and second steps, respectively, and $k_{obs1/2}$ = the observed rate constant for each step.

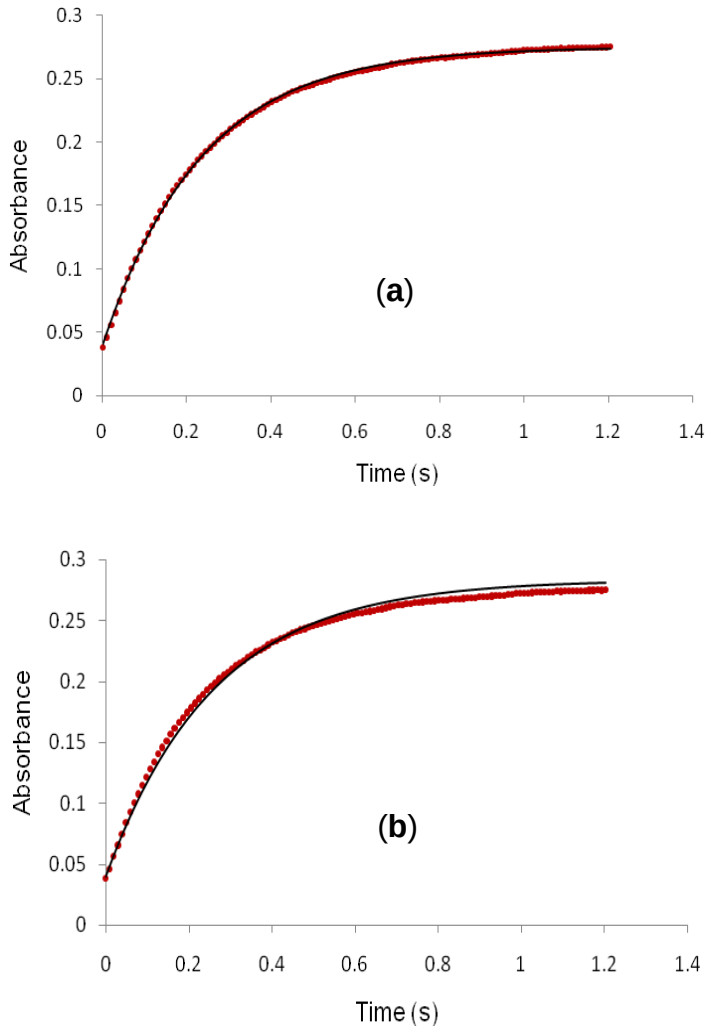

Figure 5.6: Photo-Multiplier data of $[NbCl_2(OMe)_3(MeOH)]$ (5×10^{-5} M) and [acacH] (5×10^{-4} M) in MeOH fitted to (**a**) a one-step *pseudo* first-order reaction model and (**b**) a two-consecutive-step *pseudo* first-order mathematical model at 35.0 °C and λ = 330nm.

It is clear from Figure **5.6** that the data fits the first model better, indicating a one-step *pseudo* first-order reaction.

❖ Preliminary experiments indicated that plots of k_{obs} *vs* [acacH] for the reactions observed on the stopped-flow apparatus yield straight lines, whereas similar plots for the slower, second reaction yield non-linear results.

5.3.3 Derivation of the rate law

The following rate law can be derived from Scheme **5.1**:

$$\text{Rate}=\frac{d\left(\text{M-acac}\right)}{d\text{t}}=k_2\left[\text{M-acacH}\right]-k_{-2}\left[\text{M-acac}\right] \qquad (\mathbf{5.3})$$

The definition of K_1 yields the following equation:

$$K_1=\frac{\left[\text{M-acacH}\right]}{\left[\text{M}\right]\left[\text{acacH}\right]} \qquad (\mathbf{5.4})$$

The total niobium species at any time in solution, M_{tot}, is defined by:

$$M_{tot}=\left[\text{M}\right]+\left[\text{M-acacH}\right] \qquad (\mathbf{5.5})$$

By substituting (**5.4**) in (**5.5**) the following equation is obtained:

$$M_{tot}=\frac{\left[\text{M-acacH}\right]}{K_1\left[\text{acacH}\right]}+\left[\text{M-acacH}\right]$$

$$=\left(\frac{1}{K_1\left[\text{acacH}\right]}+1\right)\left[\text{M-acacH}\right]$$

$$=\left(\frac{1+K_1\left[\text{acacH}\right]}{K_1\left[\text{acacH}\right]}\right)\left[\text{M-acacH}\right]$$

$$\left[\text{M-acacH}\right]=\frac{M_{tot}.K_1.\left[\text{acacH}\right]}{1+K_1\left[\text{acacH}\right]} \qquad (\mathbf{5.6})$$

Substitution of (**5.6**) in (**5.3**) yields:

$$\text{Rate}=\frac{k_2.K_1.\left[M_{tot}\right]\left[\text{acacH}\right]}{1+K_1\left[\text{acacH}\right]}-k_{-2}\left[\text{M-acac}\right] \qquad (\mathbf{5.7})$$

Under *pseudo*-first order conditions with [acacH] >>> [M_{tot}], the following equation for the observed rate, k_{obs}, can be obtained:

$$k_{obs} = \frac{k_2 K_1 [acacH]}{1 + K_1 [acacH]} + k_{-2} \qquad (\mathbf{5.8})$$

5.3.4 Discussion

The following conclusions are made from Scheme **5.1** and the derived rate law (Eq. **5.8**):

- The fast, first reaction (observed on the stopped-flow apparatus) can be attributed to the formation of the Nb-acacH intermediate, $[Nb(Cl)_2(OMe)_3(acacH)]$. When this fast reaction (k_1 path) is considered in isolation, the following simple, reversible equation can be derived:

$$k_{obs} = k_1 [L] + k_{-1} \qquad (\mathbf{5.9})$$

  It follows from Equation **5.9** that plots of k_{obs} *vs* [acacH] should be linear with the slope = k_1 and the intercept = k_{-1}. The equilibrium constant, K_1, is defined by Equation **5.10**:

$$K_1 = \frac{k_1}{k_{-1}} \qquad (\mathbf{5.10})$$

- The fact that the slower observed reaction, producing the chelated final acac complex, yielded non-linear plots for k_{obs} *vs* [acacH], indicates that the results obtained here account for the overall reaction, requiring the data to be fitted to the overall rate law (Eq. **5.8**). The values of k_2, k_{-2} and K_1 should be obtained from fits of k_{obs} vs [acacH]. The equilibrium constant, K_2, can be determined from Equation **5.11**:

$$K_2 = \frac{k_2}{k_{-2}} \qquad (\mathbf{5.11})$$

The Stopped-flow data (fast) obtained at four different temperatures was fitted to Equation **5.9** and the UV/Vis data (slow reaction) was fitted to Equation **5.12**. The results are illustrated in Figures **5.7** and **5.8** respectively.

$$k_{obs} = \frac{k_2 K_1 [L]}{1 + K_1 [L]} + k_{-2} \qquad (\mathbf{5.12})$$

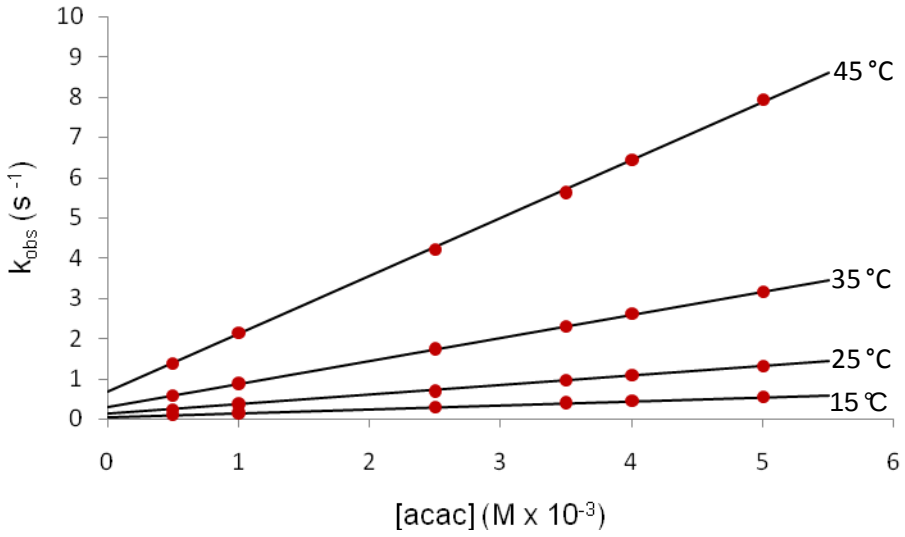

Figure 5.7: Plot of k_{obs} *vs* [acacH] for the fast reaction between $[NbCl_2(OMe)_3(MeOH]$ and [acacH] in MeOH at different temperatures, [Nb] = 5 x 10^{-5} M, λ = 330 nm.

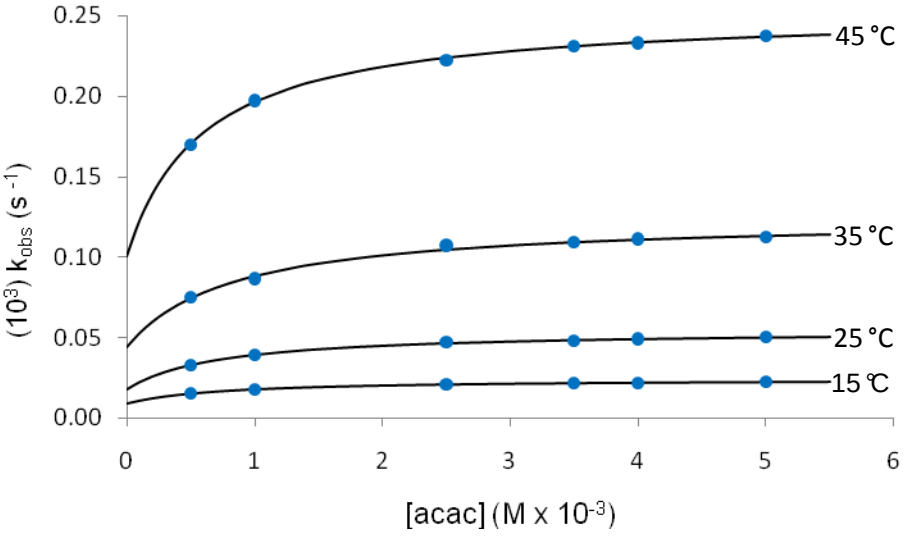

Figure 5.8: Plot of k_{obs} *vs* [acac] for the slow reaction between $[NbCl_2(OMe)_3(MeOH)]$ and [acacH] in MeOH at different temperatures, [Nb] = 5 x 10^{-5} M, λ = 310 nm.

The values of k_1, k_{-1} and K_1 (first reaction) obtained from fits of the data to Equation **5.9** are given in Table **5.2**. Similarly, the values for the rate constants k_2 and k_{-2}, together with the values obtained for the stability constant for the first step, K_1, from fits of the data to Equation **5.12** are also given in Table **5.2**.

Table 5.2: Rate constants for both the fast and slow reactions.

Rate Constants	15 ℃	25 ℃	35 ℃	45 ℃
Fast Reaction				
k_1 ($M^{-1}s^{-1}$)[a]	96 (2)	237 (4)	574 (6)	1440 (15)
k_{-1} (s^{-1})[a]	0.051 (6)	0.12 (1)	0.29 (4)	0.66 (6)
K_1 (M^{-1})[b]	1882 (216)	1975 (201)	1979 (273)	2181 (235)
Slow Reaction				
k_2 (s^{-1})[c]	1.51 (8) x 10^{-5}	3.7 (3) x 10^{-5}	8.0 (9) x 10^{-5}	15.1 (9) x 10^{-5}
k_{-2} (s^{-1})[c]	0.91 (8) x 10^{-5}	1.8 (4) x 10^{-5}	3.9 (8) x 10^{-5}	10.1 (8) x 10^{-5}
K_1 (M^{-1})[c]	1356 (231)	1403 (379)	1213 (604)	1695 (303)
K_2 [d]	1.6 (2)	2.0 (5)	2.1 (6)	1.5 (2)

[a] Fig. **5.7**, Eq. **5.9**; [b] Fig. **5.7**, Eq. **5.10**; [c] Fig. **5.8**, Eq. **5.12**; [d] Fig. **5.8**, Eq. **5.11**

It is clear from Table **5.2** and Figures **5.9** and **5.10** that the fits of the rate data are representative of the rate law, indicating specifically that the equilibrium constant for the fast, first reaction (although with large esd's) agrees quite well with the second observed reaction which describes the total process.

Figure **5.9** and Figure **5.10** shows the Eyring plots of the data in Table **5.2**, to yield the activation parameters for the two steps. The Eyring equation is given as:

$$\ln\frac{k}{T} = \frac{-\Delta H^{\neq}}{RT} + \ln\frac{k_B}{h} + \frac{\Delta S^{\neq}}{R} \qquad (\mathbf{5.13})$$

With $\Delta H^{\ddagger}$ = enthalpy of activation, $\Delta S^{\ddagger}$ = entropy of activation, k_B = Boltzmann constant, R = gas constant and h = Planck's constant.

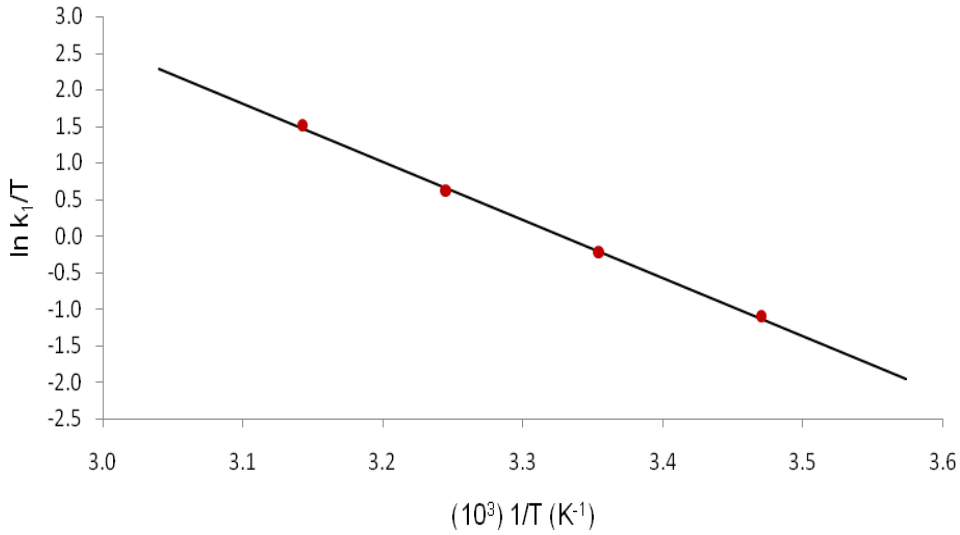

Figure 5.9: Eyring plot, according to Eq. **5.13**, of the k_1 rate constant for the formation of [NbCl(acac)(OMe)$_3$] in a temperature range of 15 – 45 ° C (data in Table **5.2** used).

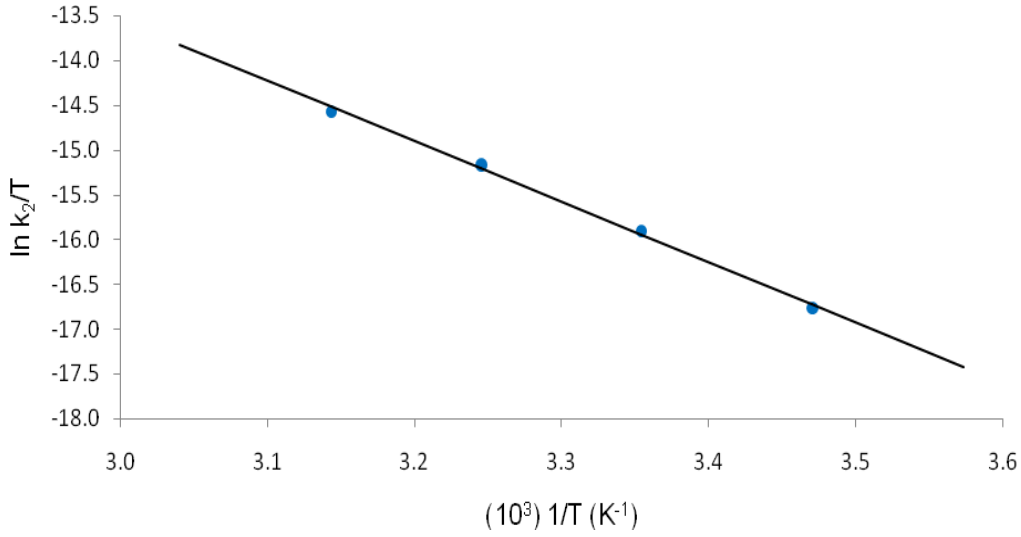

Figure 5.10: Eyring plot, according to Eq. **5.13**, of the k_2 rate constant for the formation of [NbCl(acac)(OMe)$_3$] in a temperature range of 15 – 45 °C (data in Table **5.2** used).

Table 5.3: Determined activation parameters for both the fast and slow reactions.

Reaction	$\Delta H^{\ddagger}$ (kJ.mol^{-1})	$\Delta S^{\ddagger}$ (J.K^{-1}.mol^{-1})
Fast (k_1)	66 (2)	22 (5)
Slow (k_2)	56 (2)	-142 (7)

5.4 Conclusion

The values of K_1 obtained from two separate experiments are the same within experimental error. This is a further indication that the reaction scheme and resulting rate law provides a good understanding of the formation reactions studied here. The value of K_2 is three orders of magnitude smaller than K_1 (e.g. at 25.0 ℃, K_1 = 1975 (201) M^{-1} *vs* K_2 = 2.0 (5) M^{-1}). This is to be expected since the rate-determining ring-closure is slow. Similar examples, where this has been observed, are known for bidentate complexes.[7]

The relative rate of the ring-closure is best illustrated by comparing k_1 to k_2. The rate data cannot be compared simply by looking at the results in Table **5.2**, since the k_2 rate constant is only measured in s^{-1}. The rate constant, k_1 (at 25.0 °C), is converted to a first-order rate constant by multiplying k_1 (237 (4) $M^{-1}s^{-1}$) with [acacH] (0.05 M) and adding k_{-1} (0.12 (1) s^{-1}). When this value of 11.97 (2) s^{-1} is compared with k_2 (3.7 (3) x 10^{-5}), a difference of 6 orders of magnitude is obtained.

The difference between k_2 and k_{-2} is between 1.5 and 2 times at all the temperatures studied. This is also a very good indication of the small value obtained for the equilibrium constant, K_2.

Comparison of the kinetic data obtained for this study with that of the corresponding tantalum study[8] yielded the following:

- Similar rate laws were obtained for both studies, except that no k_{-2} step was observed for the tantalum study.
- The values obtained for the rate constants, k_1 and k_2, of the tantalum study (316 (9) $M^{-1}s^{-1}$; 4.43 (7) x 10^{-5} s^{-1}) was slightly higher than that obtained for the niobium study (237 (4) $M^{-1}s^{-1}$, 3.7 (3) x 10^{-5} s^{-1}) at 25.0 ℃.
- The equilibrium constant, K_1, for both studies are, within experimental error, similar at ± 2000 M^{-1}.

The high positive value obtained for $\Delta S^{\ddagger}$ (k_1), points strongly towards a dissociative type mechanism for the first step, as expected for octahedral substitution reactions.

[7] H. J. van der Westhuizen, R. Meijboom, M. Schutte, A. Roodt, *Inorg. Chem.*, **49**, 20, 9599, 2010.
[8] R. Koen, H. G. Visser, A. Roodt, *M.Sc. Thesis*, University of the Free State, 2012.

However, more information (such as high-pressure kinetic data) is required to make a more reliable conclusion of the type of mechanism. The large negative value obtained for $\Delta S^{\ddagger}$ (k_2) might be misleading. It is expected that a η^1-acac ligand will free rotate quite substantially and that the resulting ring-closure, to form η^2-coordination, could override the observed enthropy for the dissociation of the chlorido ligand, thus resulting in a more ordered transition state for the second step.

6. Evaluation of Study

Synopsis...

A summary of the results obtained and the scientific importance of this M.Sc. study is given, which is followed by some aspects which might be investigated in future.

oooooooooooooo

6.1 Results Obtained

This study was aimed at the investigation and identification of various niobium(V) complexes containing selected O,O'-bidentate ligands that could potentially be used for the selective separation of niobium from tantalum.

Four new complexes were synthesized and successfully characterized by means of single crystal X-ray diffraction. Some unique results were obtained; such as the simultaneous crystallization of $[NbCl_2(phacac\text{-}\kappa^2\text{-}O,O')(OMe)_2]$ and $[NbCl(phacac\text{-}\kappa^2\text{-}O,O')(OMe)_3]$, which is unmarked by any other niobium complexes, and the formation of the "cage"-like structure of $[Nb(acac\text{-}\kappa^2\text{-}O,O')(OEt)_2(\mu^2\text{-}O)]_4$. Only four other similar, "cage"-like structures have been reported in literature. A comparison between the novel $[NbCl(acac\text{-}\kappa^2\text{-}O,O')(OMe)_3]$ complex and the $[TaCl_2(acac\text{-}\kappa^2\text{-}O,O')(OMe)_2]$ complex[1] exhibited significant differences in coordination between the two metal centres. The niobium complex contained only a single chlorido ligand whereas the tantalum analogue contained two coordinated chlorido ligands. In all of the complexes synthesised, the chlorido ligands were always placed in axial positions with an average Nb-Cl bond length of 2.438 (3) Å.

The kinetic study to follow the formation of $[NbCl(acac)(OMe)_3]$ revealed that two reactions occur in methanol as solvent. The initial part of the study involved the correct identification of the niobium(V) starting reagent, as solvent coordination took place to form the corresponding niobium-chlorido-methoxido species. This was done by means of ^{93}Nb NMR. The first, rate determining reaction comprised of the initial mono-coordination of the acacH ligand to the niobium(V) centre and the slow,

[1] R. Koen, *M.Sc. Thesis*, University of the Free State, 2012.

second reaction entailed the ring-closure of the chelating acac ligand to form the final product. When considering the corresponding tantalum study[1] a few differences can be highlighted:

- Within experimental error, similar rate constants were obtained for the fast, first reaction with the Ta reaction only slightly faster than that of the Nb. (Chapter **5**)
- A reverse rate constant, k_{-2}, is observed for the second rate determining step in the niobium reaction, where no reverse reaction is observed for the tantalum reaction.

The comparison of the results obtained in this study with that obtained in the corresponding tantalum study, delivered significant differences, with regards to reaction kinetics and coordination, which could be further exploited to aid in the search towards new, safer techniques for the separation of the two metals.

6.2 Future Research

From the results obtained, various focus areas for future investigations have been identified which could possibly expand on the current available information on niobium. The available information on niobium chemistry, more specifically niobium(V), is limited and focuses mainly on the catalytic activity of the metal and its uses in the alloy industry.[2,3,4]

Future research will include the investigation of the coordination and reaction kinetics of niobium(V) complexes containing various O- and N-donating, bi- and tridentate ligands. Emphasis will also be placed on steric effects as well as electron donating or withdrawing characteristics of the ligands used. Other synthetic routes such as sublimation will also be investigated. ^{93}Nb NMR will be included in future research, as information on this technique is quite limited.

[2] I. Nowak, M. Ziolek, *Chem. Rev.*, **99**, 3603, 1999.
[3] M. Ziolek, *Catal. Today*, **78**, 47, 2003.
[4] D. L. Kepert, *The Early Transition Metals*, Academic Press, London, 142, 1972.

Appendix A

A 1 Supplementary Data for [NbCl(acac)(OMe)$_3$]:

Table 1.1: Atomic coordinates (x 10^4) and equivalent isotropic displacement parameters (Å^2 x 10^3) for [NbCl(acac)(OMe)$_3$]. U(eq) is defined as one third of the trace of the orthogonalized U^{ij} tensor.

Atom	x	y	z	U(eq)
C(1)	2240 (2)	3047 (2)	4597 (2)	16 (1)
C(2)	1434 (2)	2491 (2)	4157 (2)	17 (1)
C(3)	814 (2)	1714 (2)	4534 (2)	15 (1)
C(4)	2957 (2)	3783 (2)	4114 (2)	23 (1)
C(5)	-31 (2)	1161 (2)	4013 (2)	20 (1)
C(6)	3605 (2)	769 (2)	5413 (2)	22 (1)
C(7)	36 (2)	953 (2)	7616 (2)	20 (1)
C(8)	2692 (2)	3880 (2)	7406 (2)	19 (1)
O(1)	2430 (2)	2949 (1)	5408 (1)	16 (1)
O(2)	916 (2)	1421 (1)	5326 (1)	16 (1)
O(3)	2908 (2)	1050 (1)	6097 (1)	16 (1)
O(4)	997 (2)	1158 (1)	7143 (1)	16 (1)
O(5)	2525 (2)	2837 (1)	7154 (1)	16 (1)
Cl(1)	291 (1)	3255 (1)	6411 (1)	18 (1)
Nb(1)	1790 (1)	1982 (1)	6381 (1)	11 (1)

Table 1.2: Bond lengths (Å) for [NbCl(acac)(OMe)$_3$].

Bond	Distance (Å)
C(1)-O(1)	1.282 (3)
C(1)-C(2)	1.400 (4)
C(1)-C(4)	1.496 (4)
C(2)-C(3)	1.389 (4)
C(3)-O(2)	1.288 (3)
C(3)-C(5)	1.496 (4)
C(6)-O(3)	1.410 (3)
C(7)-O(4)	1.414 (3)
C(8)-O(5)	1.418 (3)
O(1)-Nb(1)	2.1088 (18)
O(2)-Nb(1)	2.0846 (18)
O(3)-Nb(1)	1.8790 (19)
O(4)-Nb(1)	1.8643 (18)
O(5)-Nb(1)	1.8616 (18)
Cl(1)-Nb(1)	2.4696 (10)

Table 1.3: Bond angles (°) for [NbCl(acac)(OMe)$_3$].

Bond	Angle (°)
O(1)-C(1)-C(2)	123.7 (2)
O(1)-C(1)-C(4)	116.3 (2)
C(2)-C(1)-C(4)	120.0 (2)
C(3)-C(2)-C(1)	123.7 (2)
O(2)-C(3)-C(2)	123.9 (2)
O(2)-C(3)-C(5)	116.1 (2)
C(2)-C(3)-C(5)	120.0 (2)
C(1)-O(1)-Nb(1)	133.52 (17)
C(3)-O(2)-Nb(1)	133.85 (17)
C(6)-O(3)-Nb(1)	141.75 (17)
C(7)-O(4)-Nb(1)	150.56 (17)
C(8)-O(5)-Nb(1)	144.13 (17)
O(5)-Nb(1)-O(4)	100.76 (9)
O(5)-Nb(1)-O(3)	100.03 (9)
O(4)-Nb(1)-O(3)	99.47 (8)
O(5)-Nb(1)-O(2)	163.65 (8)
O(4)-Nb(1)-O(2)	91.55 (8)
O(3)-Nb(1)-O(2)	88.37 (8)
O(5)-Nb(1)-O(1)	85.76 (8)
O(4)-Nb(1)-O(1)	170.14 (8)
O(3)-Nb(1)-O(1)	86.53 (8)
O(2)-Nb(1)-O(1)	80.74 (8)
O(5)-Nb(1)-Cl(1)	87.49 (7)
O(4)-Nb(1)-Cl(1)	88.75 (6)
O(3)-Nb(1)-Cl(1)	167.55 (6)
O(2)-Nb(1)-Cl(1)	82.03 (6)
O(1)-Nb(1)-Cl(1)	84.13 (6)

Table 1.4: Anisotropic displacement parameters (A^2 x 10^3) for [NbCl(acac)$(OMe)_3$]. The anisotropic displacement factor exponent takes the form: $-2\pi^2[h^2a^{*2}U^{11} + \ldots + 2hka^*b^*U^{23}]$.

Atom	U^{11}	U^{22}	U^{33}	U^{23}	U^{13}	U^{12}
C(1)	18 (1)	16 (1)	13 (1)	4 (1)	5 (1)	4 (1)
C(2)	20 (1)	23 (1)	10 (1)	3 (1)	1 (1)	3 (1)
C(3)	16 (1)	17 (1)	11 (1)	-3 (1)	-1 (1)	5 (1)
C(4)	23 (1)	26 (1)	21 (1)	10 (1)	5 (1)	-1 (1)
C(5)	19 (1)	25 (1)	16 (1)	-4 (1)	-3 (1)	0 (1)
C(7)	20 (1)	22 (1)	17 (1)	0 (1)	4 (1)	-5 (1)
C(8)	18 (1)	16 (1)	24 (1)	-2 (1)	-2 (1)	-2 (1)
O(1)	17 (1)	17 (1)	12 (1)	2 (1)	1 (1)	-2 (1)
O(2)	20 (1)	17 (1)	11 (1)	-1 (1)	-1 (1)	-3 (1)
O(3)	16 (1)	18 (1)	14 (1)	2 (1)	2 (1)	2 (1)
O(4)	19 (1)	18 (1)	13 (1)	2 (1)	3 (1)	-1 (1)
O(5)	19 (1)	15 (1)	15 (1)	-1 (1)	-1 (1)	-2 (1)
Cl(1)	17 (1)	17 (1)	20 (1)	0 (1)	1 (1)	2 (1)
Nb(1)	14 (1)	12 (1)	8 (1)	1 (1)	0 (1)	-1 (1)

Table 1.5: Hydrogen coordinates (x 10^4) and isotropic displacement parameters ($Å^2$ x 10^3) for [NbCl(acac)$(OMe)_3$].

Atom	x	y	z	U(eq)
H(4A)	3471	4106	4517	35
H(4B)	2510	4320	3843	35
H(4C)	3359	3405	3668	35
H(5A)	-389	639	4375	30
H(5B)	315	822	3518	30
H(5C)	-572	1660	3806	30
H(6A)	4075	197	5598	33
H(6B)	4056	1364	5251	33
H(6C)	3171	550	4914	33
H(7A)	127	312	7948	30
H(7B)	-576	875	7215	30
H(7C)	-109	1528	8012	30
H(8A)	3203	3904	7892	29
H(8B)	1997	4186	7581	29
H(8C)	2992	4272	6918	29
H(2)	1310	2590	3620	27

A 2 Supplementary Data for $[Nb(acac)(OEt)_2(O)]_4$:

Table 2.1: Atomic coordinates (x 10^4) and equivalent isotropic displacement parameters ($Å^2$ x 10^3) for $[Nb(acac)(OEt)_2(O)]_4$. U(eq) is defined as one third of the trace of the orthogonalized U^{ij} tensor.

Atom	x	y	z	U(eq)
C(1)	4870 (4)	5567 (3)	2201 (2)	38 (1)
C(2)	5265 (4)	6467 (3)	2725 (3)	44 (1)
C(3)	6286 (4)	6485 (3)	3664 (3)	38 (1)
C(4)	3652 (5)	5633 (4)	1172 (3)	63 (1)
C(5)	6561 (6)	7473 (3)	4160 (3)	60 (1)
C(6)	4761 (5)	3499 (5)	3446 (4)	61 (1)
C(7)	4384 (6)	4361 (6)	3697 (5)	89 (2)
C(8)	7629 (5)	2883 (3)	2820 (3)	49 (1)
C(10)	11001 (4)	4854 (4)	3540 (3)	50 (1)
C(11)	11828 (5)	5714 (4)	3771 (3)	57 (1)
C(12)	11504 (5)	6763 (4)	3767 (3)	47 (1)
C(13)	11352 (5)	3774 (4)	3490 (4)	58 (1)
C(14)	12474 (6)	7643 (4)	4020 (4)	67 (2)
C(15)	9542 (6)	8291 (4)	4375 (4)	67 (1)
C(16)	9432 (9)	9188 (4)	3901 (5)	103 (3)
O(1)	8178 (2)	5172 (2)	3619 (2)	30 (1)
O(2)	5452 (2)	4671 (2)	2530 (2)	38 (1)
O(3)	7048 (2)	5687 (2)	4185 (2)	32 (1)
O(4)	6177 (2)	3559 (2)	3919 (2)	35 (1)
O(5)	9069 (2)	4053 (2)	5149 (2)	29 (1)
O(6)	7517 (2)	3104 (2)	3412 (2)	32 (1)
O(7)	9880 (3)	4925 (2)	3344 (2)	36 (1)
O(8)	10433 (3)	7042 (2)	3562 (2)	43 (1)
O(9)	8764 (3)	7405 (2)	3799 (2)	38 (1)
O(10)	7638 (3)	6257 (2)	2233 (2)	48 (1)
Nb(1)	7421 (1)	4225 (1)	3941 (1)	24 (1)
Nb(2)	9056 (1)	6112 (1)	3525 (1)	28 (1)
C(17A)	7392 (7)	6209 (6)	1478 (5)	38 (1)
C(18A)	7683 (10)	5848 (8)	1185 (7)	57 (1)
C(17B)	6862 (10)	5719 (8)	1397 (6)	48 (1)
C(18B)	6180 (10)	5873 (9)	658 (6)	50 (1)
C(9A)	8381 (18)	1895 (9)	3060 (9)	74 (4)
C(9B)	8990 (20)	2290 (20)	3389 (15)	49 (1)

Table 2.2: Bond lengths (Å) for $[Nb(acac)(OEt)_2(O)]_4$.

Bond	Distance (Å)
C(1)-O(2)	1.267 (4)
C(1)-C(2)	1.398 (6)
C(1)-C(4)	1.504 (5)
C(2)-C(3)	1.369 (5)
C(2)-H(2)	0.93
C(3)-O(3)	1.288 (4)
C(3)-C(5)	1.496 (5)
C(4)-H(4A)	0.96
C(4)-H(4B)	0.96
C(4)-H(4C)	0.96
C(5)-H(5A)	0.96
C(5)-H(5B)	0.96
C(5)-H(5C)	0.96
C(6)-O(4)	1.412 (5)
C(6)-C(7)	1.472 (8)
C(6)-H(6A)	0.97
C(6)-H(6B)	0.97
C(7)-H(7A)	0.96
C(7)-H(7B)	0.96
C(7)-H(7C)	0.96
C(8)-O(6)	1.412 (5)
C(8)-C(9A)	1.462 (8)
C(8)-C(9B)	1.497 (19)
C(8)-H(8A)	0.97
C(8)-H(8B)	0.97
C(10)-O(7)	1.288 (5)
C(10)-C(11)	1.386 (7)
C(10)-C(13)	1.482 (7)
C(11)-C(12)	1.400 (7)
C(11)-H(11)	0.93
C(12)-O(8)	1.257 (5)
C(12)-C(14)	1.512 (6)
C(13)-H(13A)	0.96
C(13)-H(13B)	0.96
C(13)-H(13C)	0.96
C(14)-H(14A)	0.96
C(14)-H(14B)	0.96
C(14)-H(14C)	0.96
C(15)-O(9)	1.413 (5)
C(15)-C(16)	1.454 (8)
C(15)-H(15A)	0.97
C(15)-H(15B)	0.97
C(16)-H(16A)	0.96

C(16)-H(16B)	0.96
C(16)-H(16C)	0.96
O(1)-Nb(2)	1.817 (2)
O(1)-Nb(1)	2.020 (2)
O(2)-Nb(1)	2.197 (2)
O(3)-Nb(1)	2.088 (2)
O(4)-Nb(1)	1.894 (2)
O(5)-Nb(1)	1.820 (2)
O(5)-Nb(2)$^{\#1}$	2.015 (2)
O(6)-Nb(1)	1.879 (2)
O(7)-Nb(2)	2.091 (3)
O(8)-Nb(2)	2.201 (3)
O(9)-Nb(2)	1.880 (3)
O(10)-C(17A)	1.383 (8)
O(10)-C(17B)	1.413 (9)
O(10)-Nb(2)	1.893 (3)
Nb(2)-O(5)$^{\#1}$	2.015 (2)
C(17A)-C(18A)	1.066 (10)
C(17A)-H(17A)	0.97
C(17A)-H(17B)	0.97
C(18A)-H(18A)	0.96
C(18A)-H(18B)	0.96
C(18A)-H(18C)	0.96
C(17B)-C(18B)	1.113 (12)
C(17B)-H(17C)	0.97
C(17B)-H(17D)	0.97
C(18B)-H(18D)	0.96
C(18B)-H(18E)	0.96
C(18B)-H(18F)	0.96
C(9A)-H(9A1)	0.96
C(9A)-H(9A2)	0.96
C(9A)-H(9A3)	0.96
C(9B)-H(9B1)	0.96
C(9B)-H(9B2)	0.96
C(9B)-H(9B3)	0.96

Symmetry transformations used to generate equivalent atoms: $^{\#1}$ -x+2,-y+1,-z+1

Table 2.3: Bond angles (°) for $[Nb(acac)(OEt)_2(O)]_4$.

Bond	Angle (°)
O(2)-C(1)-C(2)	124.6 (3)
O(2)-C(1)-C(4)	116.2 (4)
C(2)-C(1)-C(4)	119.2 (4)
C(3)-C(2)-C(1)	124.5 (3)
C(3)-C(2)-H(2)	117.8
C(1)-C(2)-H(2)	117.8
O(3)-C(3)-C(2)	124.7 (3)
O(3)-C(3)-C(5)	114.9 (3)
C(2)-C(3)-C(5)	120.4 (3)
C(1)-C(4)-H(4A)	109.5
C(1)-C(4)-H(4B)	109.5
H(4A)-C(4)-H(4B)	109.5
C(1)-C(4)-H(4C)	109.5
H(4A)-C(4)-H(4C)	109.5
H(4B)-C(4)-H(4C)	109.5
C(3)-C(5)-H(5A)	109.5
C(3)-C(5)-H(5B)	109.5
H(5A)-C(5)-H(5B)	109.5
C(3)-C(5)-H(5C)	109.5
H(5A)-C(5)-H(5C)	109.5
H(5B)-C(5)-H(5C)	109.5
O(4)-C(6)-C(7)	112.4 (4)
O(4)-C(6)-H(6A)	109.1
C(7)-C(6)-H(6A)	109.1
O(4)-C(6)-H(6B)	109.1
C(7)-C(6)-H(6B)	109.1
H(6A)-C(6)-H(6B)	107.9
C(6)-C(7)-H(7A)	109.5
C(6)-C(7)-H(7B)	109.5
H(7A)-C(7)-H(7B)	109.5
C(6)-C(7)-H(7C)	109.5
H(7A)-C(7)-H(7C)	109.5
H(7B)-C(7)-H(7C)	109.5
O(6)-C(8)-C(9A)	112.0 (4)
O(6)-C(8)-C(9B)	105.7 (9)
C(9A)-C(8)-C(9B)	30.1 (7)
O(6)-C(8)-H(8A)	109.2
C(9A)-C(8)-H(8A)	109.2
C(9B)-C(8)-H(8A)	84.9
O(6)-C(8)-H(8B)	109.2
C(9A)-C(8)-H(8B)	109.2
C(9B)-C(8)-H(8B)	135.7
H(8A)-C(8)-H(8B)	107.9

O(7)-C(10)-C(11)	123.6 (4)
O(7)-C(10)-C(13)	115.2 (4)
C(11)-C(10)-C(13)	121.3 (4)
C(10)-C(11)-C(12)	124.3 (4)
C(10)-C(11)-H(11)	117.8
C(12)-C(11)-H(11)	117.8
O(8)-C(12)-C(11)	124.1 (4)
O(8)-C(12)-C(14)	116.0 (4)
C(11)-C(12)-C(14)	119.9 (4)
C(10)-C(13)-H(13A)	109.5
C(10)-C(13)-H(13B)	109.5
H(13A)-C(13)-H(13B)	109.5
C(10)-C(13)-H(13C)	109.5
H(13A)-C(13)-H(13C)	109.5
H(13B)-C(13)-H(13C)	109.5
C(12)-C(14)-H(14A)	109.5
C(12)-C(14)-H(14B)	109.5
H(14A)-C(14)-H(14B)	109.5
C(12)-C(14)-H(14C)	109.5
H(14A)-C(14)-H(14C)	109.5
H(14B)-C(14)-H(14C)	109.5
O(9)-C(15)-C(16)	113.0 (5)
O(9)-C(15)-H(15A)	109
C(16)-C(15)-H(15A)	109
O(9)-C(15)-H(15B)	109
C(16)-C(15)-H(15B)	109
H(15A)-C(15)-H(15B)	107.8
C(15)-C(16)-H(16A)	109.5
C(15)-C(16)-H(16B)	109.5
H(16A)-C(16)-H(16B)	109.5
C(15)-C(16)-H(16C)	109.5
H(16A)-C(16)-H(16C)	109.5
H(16B)-C(16)-H(16C)	109.5
Nb(2)-O(1)-Nb(1)	170.22 (13)
C(1)-O(2)-Nb(1)	129.9 (2)
C(3)-O(3)-Nb(1)	132.6 (2)
C(6)-O(4)-Nb(1)	144.3 (3)
Nb(1)-O(5)-Nb(2)$^{\#1}$	177.27 (13)
C(8)-O(6)-Nb(1)	142.3 (2)
C(10)-O(7)-Nb(2)	133.4 (3)
C(12)-O(8)-Nb(2)	129.9 (3)
C(15)-O(9)-Nb(2)	139.5 (3)
C(17A)-O(10)-C(17B)	36.6 (4)
C(17A)-O(10)-Nb(2)	143.3 (4)
C(17B)-O(10)-Nb(2)	144.5 (4)
O(5)-Nb(1)-O(6)	101.06 (10)

O(5)-Nb(1)-O(4)	99.36 (11)
O(6)-Nb(1)-O(4)	96.53 (11)
O(5)-Nb(1)-O(1)	97.12 (10)
O(6)-Nb(1)-O(1)	87.70 (10)
O(4)-Nb(1)-O(1)	161.84 (10)
O(5)-Nb(1)-O(3)	92.16 (10)
O(6)-Nb(1)-O(3)	163.66 (10)
O(4)-Nb(1)-O(3)	90.66 (11)
O(1)-Nb(1)-O(3)	81.12 (10)
O(5)-Nb(1)-O(2)	171.85 (10)
O(6)-Nb(1)-O(2)	86.28 (10)
O(4)-Nb(1)-O(2)	83.14 (11)
O(1)-Nb(1)-O(2)	79.50 (10)
O(3)-Nb(1)-O(2)	80.03 (10)
O(1)-Nb(2)-O(9)	102.79 (11)
O(1)-Nb(2)-O(10)	98.99 (12)
O(9)-Nb(2)-O(10)	97.89 (13)
O(1)-Nb(2)-O(5)$^{\#1}$	93.53 (10)
O(9)-Nb(2)-O(5)$^{\#1}$	90.30 (10)
O(10)-Nb(2)-O(5)$^{\#1}$	163.11 (12)
O(1)-Nb(2)-O(7)	93.04 (10)
O(9)-Nb(2)-O(7)	162.89 (11)
O(10)-Nb(2)-O(7)	85.84 (12)
O(5)#1-Nb(2)-O(7)	82.19 (10)
O(1)-Nb(2)-O(8)	169.62 (10)
O(9)-Nb(2)-O(8)	84.44 (12)
O(10)-Nb(2)-O(8)	87.22 (12)
O(5)#1-Nb(2)-O(8)	78.86 (10)
O(7)-Nb(2)-O(8)	79.04 (11)
C(18A)-C(17A)-O(10)	145.8 (8)
C(18A)-C(17A)-H(17A)	100.4
O(10)-C(17A)-H(17A)	100.4
C(18A)-C(17A)-H(17B)	100.4
O(10)-C(17A)-H(17B)	100.4
H(17A)-C(17A)-H(17B)	104.3
C(18B)-C(17B)-O(10)	141.2 (10)
C(18B)-C(17B)-H(17C)	101.7
O(10)-C(17B)-H(17C)	101.7
C(18B)-C(17B)-H(17D)	101.7
O(10)-C(17B)-H(17D)	101.7
H(17C)-C(17B)-H(17D)	104.7
C(17B)-C(18B)-H(18D)	109.5
C(17B)-C(18B)-H(18E)	109.5
H(18D)-C(18B)-H(18E)	109.5
C(17B)-C(18B)-H(18F)	109.5
H(18D)-C(18B)-H(18F)	109.5

H(18E)-C(18B)-H(18F)	109.5
C(8)-C(9A)-H(9A1)	109.5
C(8)-C(9A)-H(9A2)	109.5
C(8)-C(9A)-H(9A3)	109.5
C(8)-C(9B)-H(9B1)	109.5
C(8)-C(9B)-H(9B2)	109.5
C(8)-C(9B)-H(9B3)	109.5

Symmetry transformations used to generate equivalent atoms: #1 -x+2,-y+1,-z+1

Table 2.4: Anisotropic displacement parameters (A^2 x 10^3) for $[Nb(acac)(OEt)_2(O)]_4$. The anisotropic displacement factor exponent takes the form: $-2\pi^2[h^2a^{*2}U^{11} + \ldots + 2hka^*b^*U^{23}]$.

Atom	U^{11}	U^{22}	U^{33}	U^{23}	U^{13}	U^{12}
C(1)	28 (1)	42 (1)	30 (1)	3 (1)	17 (1)	1 (1)
C(2)	42 (2)	39 (2)	41 (2)	13 (2)	28 (2)	18 (2)
C(3)	38 (2)	34 (2)	43 (2)	3 (2)	31 (2)	10 (1)
C(4)	50 (3)	67 (3)	32 (2)	11 (2)	17 (2)	14 (2)
C(5)	73 (3)	41 (2)	54 (3)	5 (2)	43 (3)	22 (2)
C(6)	35 (2)	85 (4)	65 (3)	-1 (3)	37 (2)	-11 (2)
C(7)	51 (3)	138 (6)	96 (5)	-10 (4)	59 (3)	5 (3)
C(8)	60 (2)	44 (2)	53 (2)	-7 (2)	45 (2)	-2 (2)
C(10)	45 (2)	74 (3)	38 (2)	-7 (2)	32 (2)	-4 (2)
C(11)	58 (2)	70 (3)	61 (3)	-6 (2)	49 (2)	-9 (2)
C(12)	51 (2)	57 (2)	41 (2)	-3 (2)	36 (2)	-15 (2)
C(13)	63 (3)	60 (3)	68 (3)	-5 (2)	54 (3)	4 (2)
C(14)	73 (3)	76 (4)	68 (3)	-16 (3)	57 (3)	-37 (3)
C(15)	69 (3)	43 (2)	59 (3)	-10 (2)	37 (3)	-2 (2)
C(16)	125 (6)	41 (3)	83 (4)	-7 (3)	57 (5)	-15 (3)
O(1)	28 (1)	31 (1)	31 (1)	0 (1)	22 (1)	-2 (1)
O(2)	28 (1)	42 (1)	30 (1)	3 (1)	17 (1)	1 (1)
O(3)	33 (1)	31 (1)	32 (1)	2 (1)	24 (1)	7 (1)
O(4)	28 (1)	42 (1)	37 (1)	-2 (1)	24 (1)	-5 (1)
O(5)	24 (1)	31 (1)	26 (1)	1 (1)	17 (1)	0 (1)
O(6)	34 (1)	29 (1)	34 (1)	-3 (1)	25 (1)	-1 (1)
O(7)	37 (1)	41 (1)	39 (1)	-7 (1)	30 (1)	-7 (1)
O(8)	49 (2)	41 (2)	48 (2)	6 (1)	38 (1)	-5 (1)
O(9)	35 (1)	27 (1)	41 (1)	2 (1)	23 (1)	5 (1)
O(10)	44 (1)	56 (2)	28 (1)	4 (1)	21 (1)	-2 (1)
Nb(1)	19 (1)	24 (1)	24 (1)	0 (1)	15 (1)	0 (1)
Nb(2)	25 (1)	30 (1)	24 (1)	3 (1)	16 (1)	-1 (1)
C(17A)	28 (1)	42 (1)	30 (1)	3 (1)	17 (1)	1 (1)
C(18A)	58 (2)	70 (3)	61 (3)	-6 (2)	49 (2)	-9 (2)
C(17B)	44 (1)	56 (2)	28 (1)	4 (1)	21 (1)	-2 (1)

C(18B)	45 (2)	74 (3)	38(2)	-7 (2)	32 (2)	-4 (2)
C(9A)	123 (10)	54 (5)	82 (7)	5 (5)	87 (8)	26 (6)
C(9B)	60 (2)	44 (2)	53 (2)	-7 (2)	45 (2)	-2 (2)

Table 2.5: Hydrogen coordinates (x 10^4) and isotropic displacement parameters ($Å^2$ x 10^3) for $[Nb(acac)(OEt)_2(O)]_4$.

Atom	x	y	z	U(eq)
H(2)	4804	7097	2414	53
H(4A)	3957	5414	908	95
H(4B)	3318	6348	994	95
H(4C)	2906	5180	957	95
H(5A)	6260	7376	4441	89
H(5B)	6050	8049	3732	89
H(5C)	7552	7628	4624	89
H(6A)	4608	2827	3581	73
H(6B)	4146	3526	2790	73
H(7A)	5003	4347	4348	134
H(7B)	3428	4271	3380	134
H(7C)	4475	5026	3529	134
H(8A)	8122	3458	2850	58
H(8B)	6692	2838	2194	58
H(11)	12652	5585	3940	69
H(13A)	11192	3280	3748	87
H(13B)	12325	3748	3830	87
H(13C)	10767	3594	2861	87
H(14A)	11926	8204	3580	100
H(14B)	13121	7378	4020	100
H(14C)	12991	7905	4620	100
H(15A)	10526	8093	4884	80
H(15B)	9207	8498	4627	80
H(16A)	9778	8993	3660	154
H(16B)	9981	9764	4324	154
H(16C)	8463	9401	3407	154
H(17A)	6383	6085	995	45
H(17B)	7488	6949	1414	45
H(18A)	8615	6070	1514	86
H(18B)	7030	6054	553	86
H(18C)	7667	5094	1223	86
H(17C)	7571	5253	1560	58
H(17D)	6265	5262	1364	58
H(18D)	5221	5702	302	75
H(18E)	6488	5444	461	75

H(18F)	6243	6605	575	75
H(9A1)	9319	1944	3673	111
H(9A2)	8427	1770	2639	111
H(9A3)	7892	1323	3026	111
H(9B1)	9740	2693	3931	73
H(9B2)	9170	2185	3040	73
H(9B3)	8916	1621	3563	73

A 3 Supplementary Data for $[NbCl_2(phacac)(OMe)_2]$ and $[NbCl(phacac)(OMe)_3]$:

Table 3.1: Atomic coordinates (x 10^4) and equivalent isotropic displacement parameters ($Å^2$ x 10^3) for $[NbCl_2(phacac)(OMe)_2]$ and $[NbCl(phacac)(OMe)_3]$. U(eq) is defined as one third of the trace of the orthogonalized U^{ij} tensor.

Atom	x	y	z	U(eq)
Nb(1)	6833 (1)	651 (1)	7444 (1)	46 (1)
Cl(1)	7796 (1)	-304 (1)	5738 (2)	43 (1)
Cl(2)	5909 (4)	1104 (4)	9531 (8)	65 (4)
O(3)	6054 (13)	1203 (19)	8770 (40)	56 (4)
C(5)	5930 (20)	1000 (20)	10480 (70)	73 (7)
O(2)	6313 (2)	-931 (3)	7734 (5)	44 (1)
O(1)	7716 (2)	72 (3)	9326 (4)	42 (1)
O(5)	7493 (2)	1936 (3)	7586 (5)	51 (1)
O(4)	6092 (3)	929 (3)	5631 (6)	62 (1)
C(14)	10092 (3)	-1016 (4)	13466 (6)	39 (1)
C(12)	9206 (3)	-52 (4)	11410 (6)	41 (1)
C(11)	8622 (3)	-936 (4)	11254 (6)	31 (1)
C(15)	9518 (3)	-1900 (4)	13341 (6)	41 (1)
C(16)	8785 (3)	-1866 (4)	12232 (7)	42 (1)
C(2)	7293 (3)	-1785 (4)	9703 (7)	41 (1)
C(7)	8115 (4)	2607 (5)	8475 (7)	50 (1)
C(4)	6002 (4)	-2798 (4)	8366 (8)	51 (2)
C(1)	7843 (3)	-864 (4)	10039 (6)	33 (1)
C(13)	9939 (4)	-96 (5)	12510 (8)	51 (1)
C(3)	6555 (3)	-1776 (4)	8605 (7)	38 (1)
C(6)	5869 (5)	905 (5)	3968 (9)	77 (3)

Table 3.2: Bond lengths (Å) for $[NbCl_2(phacac)(OMe)_2]$ and $[NbCl(phacac)(OMe)_3]$.

Bond	Distance (Å)
Nb(1)-O(3)	1.83 (2)
Nb(1)-O(4)	1.837 (4)
Nb(1)-O(5)	1.839 (4)
Nb(1)-O(2)	2.077 (3)
Nb(1)-O(1)	2.094 (3)
Nb(1)-Cl(2)	2.412 (8)
Nb(1)-Cl(1)	2.4319 (17)
O(3)-C(5)	1.49 (8)
C(5)-H(5A)	0.96
C(5)-H(5C)	0.96
C(5)-H(5B)	0.96
O(2)-C(3)	1.281 (6)
O(1)-C(1)	1.276 (6)
O(5)-C(7)	1.404 (6)
O(4)-C(6)	1.402 (8)
C(14)-C(13)	1.368 (8)
C(14)-C(15)	1.374 (7)
C(14)-H(14)	0.93
C(12)-C(13)	1.383 (7)
C(12)-C(11)	1.384 (6)
C(12)-H(12)	0.93
C(11)-C(16)	1.390 (7)
C(11)-C(1)	1.495 (6)
C(15)-C(16)	1.387 (7)
C(15)-H(15)	0.93
C(16)-H(16)	0.93
C(2)-C(3)	1.387 (6)
C(2)-C(1)	1.400 (6)
C(2)-H(2)	0.93
C(7)-H(7B)	0.96
C(7)-H(7A)	0.96
C(7)-H(7C)	0.96
C(4)-C(3)	1.490 (6)
C(4)-H(4C)	0.96
C(4)-H(4A)	0.96
C(4)-H(4B)	0.96
C(13)-H(13)	0.93
C(6)-H(6B)	0.96
C(6)-H(6A)	0.96
C(6)-H(6C)	0.96

Table 3.3: Bond angles (°) for [$NbCl_2(phacac)(OMe)_2$] and [$NbCl(phacac)(OMe)_3$].

Bond	Angle
O(3)-Nb(1)-O(4)	92.7(8)
O(3)-Nb(1)-O(5)	92.5(7)
O(4)-Nb(1)-O(5)	101.22(17)
O(3)-Nb(1)-O(2)	88.8(8)
O(4)-Nb(1)-O(2)	92.76(16)
O(5)-Nb(1)-O(2)	165.87(15)
O(3)-Nb(1)-O(1)	94.3(8)
O(4)-Nb(1)-O(1)	170.27(17)
O(5)-Nb(1)-O(1)	85.23(15)
O(2)-Nb(1)-O(1)	80.65(13)
O(3)-Nb(1)-Cl(2)	10.9(9)
O(4)-Nb(1)-Cl(2)	101.4(2)
O(5)-Nb(1)-Cl(2)	96.95(19)
O(2)-Nb(1)-Cl(2)	82.12(16)
O(1)-Nb(1)-Cl(2)	84.83(16)
O(3)-Nb(1)-Cl(1)	173.1(8)
O(4)-Nb(1)-Cl(1)	87.83(17)
O(5)-Nb(1)-Cl(1)	94.10(14)
O(2)-Nb(1)-Cl(1)	84.29(12)
O(1)-Nb(1)-Cl(1)	84.42(12)
Cl(2)-Nb(1)-Cl(1)	163.87(11)
C(5)-O(3)-Nb(1)	133(2)
O(3)-C(5)-H(5A)	109.5
O(3)-C(5)-H(5C)	109.5
H(5A)-C(5)-H(5C)	109.5
O(3)-C(5)-H(5B)	109.5
H(5A)-C(5)-H(5B)	109.5
H(5C)-C(5)-H(5B)	109.5
C(3)-O(2)-Nb(1)	133.9(3)
C(1)-O(1)-Nb(1)	134.6(3)
C(7)-O(5)-Nb(1)	148.7(4)
C(6)-O(4)-Nb(1)	152.8(5)
C(13)-C(14)-C(15)	120.1(4)
C(13)-C(14)-H(14)	119.9
C(15)-C(14)-H(14)	119.9
C(13)-C(12)-C(11)	120.6(5)
C(13)-C(12)-H(12)	119.7
C(11)-C(12)-H(12)	119.7
C(12)-C(11)-C(16)	118.6(4)
C(12)-C(11)-C(1)	119.1(4)
C(16)-C(11)-C(1)	122.2(4)
C(14)-C(15)-C(16)	120.0(5)
C(14)-C(15)-H(15)	120

C(16)-C(15)-H(15)	120
C(15)-C(16)-C(11)	120.4(4)
C(15)-C(16)-H(16)	119.8
C(11)-C(16)-H(16)	119.8
C(3)-C(2)-C(1)	124.3(5)
C(3)-C(2)-H(2)	117.9
C(1)-C(2)-H(2)	117.9
O(5)-C(7)-H(7B)	109.5
O(5)-C(7)-H(7A)	109.5
H(7B)-C(7)-H(7A)	109.5
O(5)-C(7)-H(7C)	109.5
H(7B)-C(7)-H(7C)	109.5
H(7A)-C(7)-H(7C)	109.5
C(3)-C(4)-H(4C)	109.5
C(3)-C(4)-H(4A)	109.5
H(4C)-C(4)-H(4A)	109.5
C(3)-C(4)-H(4B)	109.5
H(4C)-C(4)-H(4B)	109.5
H(4A)-C(4)-H(4B)	109.5
O(1)-C(1)-C(2)	122.4(4)
O(1)-C(1)-C(11)	116.5(4)
C(2)-C(1)-C(11)	121.2(4)
C(14)-C(13)-C(12)	120.3(5)
C(14)-C(13)-H(13)	119.9
C(12)-C(13)-H(13)	119.9
O(2)-C(3)-C(2)	123.9(4)
O(2)-C(3)-C(4)	116.2(4)
C(2)-C(3)-C(4)	119.9(4)
O(4)-C(6)-H(6B)	109.5
O(4)-C(6)-H(6A)	109.5
H(6B)-C(6)-H(6A)	109.5
O(4)-C(6)-H(6C)	109.5
H(6B)-C(6)-H(6C)	109.5
H(6A)-C(6)-H(6C)	109.5

Table 3.4: Anisotropic displacement parameters ($A^2 \times 10^3$) for $[NbCl_2(phacac)(OMe)_2]$ and $[NbCl(phacac)(OMe)_3]$. The anisotropic displacement factor exponent takes the form: $-2\pi^2[h^2a^{*2}U^{11} + \ldots + 2hka^*b^*U^{23}]$.

Atom	U^{11}	U^{22}	U^{33}	U^{23}	U^{13}	U^{12}
Nb(1)	27 (1)	28 (1)	79 (1)	4 (1)	-21 (1)	-2 (1)
Cl(1)	29 (1)	31 (1)	63 (1)	2 (1)	-18 (1)	-5 (1)
Cl(2)	55 (4)	44 (2)	92 (10)	12 (4)	-19 (4)	5 (2)
O(3)	46 (7)	47 (7)	74 (11)	-3 (8)	-2 (8)	16 (5)
C(5)	68 (14)	44 (10)	110 (20)	-7 (13)	29 (16)	4 (9)
O(2)	25 (2)	34 (2)	69 (2)	8 (2)	-18 (2)	-8 (1)
O(1)	31 (2)	30 (2)	61 (2)	7 (2)	-17 (2)	-7 (1)
O(5)	39 (2)	24 (2)	84 (3)	-1 (2)	-26 (2)	1 (2)
O(4)	37 (2)	36 (2)	105 (3)	10 (2)	-37 (2)	1 (2)
C(14)	25 (2)	42 (3)	48 (3)	-5 (2)	-10 (2)	-2 (2)
C(12)	34 (3)	29 (2)	55 (3)	5 (2)	-14 (2)	-5 (2)
C(11)	17 (2)	32 (2)	44 (2)	-6 (2)	-1 (2)	1 (2)
C(15)	37 (3)	38 (3)	47 (3)	7 (2)	-8 (2)	-3 (2)
C(16)	30 (2)	36 (2)	58 (3)	4 (2)	-4 (2)	-12 (2)
C(2)	27 (2)	25 (2)	66 (3)	2 (2)	-12 (2)	-5 (2)
C(7)	40 (3)	39 (3)	69 (4)	-20 (3)	-5 (3)	-6 (2)
C(4)	40 (3)	35 (3)	74 (4)	10 (2)	-22 (3)	-16 (2)
C(1)	21 (2)	28 (2)	48 (3)	-4 (2)	-5 (2)	-2 (2)
C(13)	37 (3)	41 (3)	71 (4)	5 (3)	-19 (3)	-16 (2)
C(3)	24 (2)	31 (2)	58 (3)	1 (2)	-4 (2)	-5 (2)
C(6)	72 (5)	41 (3)	105 (5)	20 (3)	-60 (4)	-9 (3)

Table 3.5: Hydrogen coordinates ($\times 10^4$) and isotropic displacement parameters ($Å^2 \times 10^3$) for $[NbCl_2(phacac)(OMe)_2]$ and $[NbCl(phacac)(OMe)_3]$.

Atom	x	y	z	U(eq)
H(5A)	6160	280	10800	109
H(5C)	5310	1018	10622	109
H(5B)	6223	1567	11134	109
H(14)	5587	-1042	14203	47
H(12)	9105	578	10768	49
H(15)	9620	-2521	14000	50
H(16)	8401	-2469	12142	50
H(2)	7431	-2447	10252	49
H(7B)	7966	2666	9560	75
H(7A)	8119	3338	8003	75
H(7C)	8686	2276	8469	75
H(4C)	5402	-2612	8486	77
H(4A)	6202	-3349	9150	77

H(4B)	6048	-3090	7309	77
H(13)	1328	501	12600	61
H(6B)	5862	1653	3554	116
H(6A)	5299	576	3743	116
H(6C)	6295	471	3467	116

Appendix B

B 1 Supplementary Data for the formation kinetics of [NbCl(acac)(OMe)$_3$]:

Table B.1: Data collected on the Stopped-flow following the formation reaction of [NbCl(acac)(OMe)$_3$] in MeOH, (λ = 330 nm; [Nb] = 5 x10^{-5} M).

[acac] (M)	15 ℃	25 ℃	35 ℃	45 ℃
	kobs (s^{-1})	kobs (s^{-1})	kobs (s^{-1})	kobs (s^{-1})
0.0005	0.101	0.2389	0.573	1.39
0.001	0.1472	0.3738	0.869	2.151
0.0025	0.2864	0.6977	1.736	4.22
0.0035	0.402	0.969	2.29	5.63
0.004	0.4362	1.083	2.61	6.44
0.005	0.532	1.307	3.152	7.924

Table B.2: Data collected on the CARY following the formation reaction of [NbCl(acac)(OMe)$_3$] in MeOH, (λ = 310 nm; [Nb] = 5 x10^{-5} M).

[acac] (M)	15 ℃	25 ℃	35 ℃	45 ℃
	kobs (x 10^{-5}) (s^{-1})	kobs (x 10^{-5}) (s^{-1})	kobs (x 10^{-5}) (s^{-1})	kobs (x 10^{-5}) (s^{-1})
0.0005	1.52	3.31	7.5	17.03
0.001	1.79	3.92	8.63	19.72
0.0025	2.07	4.71	10.7	22.19
0.0035	2.17	4.8	10.9	23.14
0.004	2.18	4.92	11.1	23.82
0.005	2.24	5.02	11.2	23.66

Table B.3: ln(*k*/T) and 1/T values for both reactions, as used for the Eyring plot.

1/T (K^{-1})	lnk_1/T	lnk_2/T
0.003143	1.5099	-14.5673
0.003245	0.622	-15.164
0.003354	-0.2295	-15.902
0.00347	-1.0991	-16.76